

Towards the Industrial Application of the  
Baeyer-Villiger Monooxygenase MO14 from  
*Rhodococcus jostii*

Benjamin David Summers

Doctor of Philosophy

University of York

Chemistry

September 2014

## Abstract

The Baeyer-Villiger reaction is a key reaction in organic synthesis, due to the utility of the addition of an oxygen atom adjacent to a carbonyl group. This reaction is also useful in an industrial setting and Baeyer-Villiger monooxygenases are often capable of performing this reaction in an exceptionally regio- and enantio-selective manner. This remarkable selectivity means that they are excellent biocatalyst targets for a number of industrially relevant syntheses, including the stereoselective synthesis of lactones and sulfoxides and also the resolution of racemic species, including  $\beta$ -hydroxyketones.

This PhD project focussed on the enzyme MO14, encoded by the gene *ro03437* from the bacterium *Rhodococcus jostii* sp. RHA1. MO14 has previously demonstrated particularly high regio- and enantioselectivity in the conversion of the model BVMO substrate, bicyclo[3.2.0]hept-2-en-6-one. This enzyme, along with several others from the same organism, was selected for study of the activity and MO14 in particular has been singled out due to its remarkable breadth of substrate scope and *S*-selective character.

All of the selected enzymes were tested against a selection of industrially relevant targets, then focus concentrated on MO14, as it demonstrated the most interesting biocatalytic activities. A variety of purification strategies were examined for the purification of MO14, with several potential lines of enquiry identified for the full purification of this enzyme. A study of the transformation of bicyclo[3.2.0]hept-2-en-6-one was conducted, with several variables of the reaction assessed, followed by investigation of the ability of this enzyme to transform a range of prochiral sulfides. As a precursor to industrial applications, a series of scale-up reactions were conducted using MO14 to examine the potential for use on a scale much larger than standard laboratory investigation. Finally, a series of mutants were generated to examine the origin of the exceptional selectivity exhibited by this enzyme.

# Contents

Abstract . . . . .	i
List of Figures . . . . .	vii
List of Tables . . . . .	xii
Acknowledgements . . . . .	xiii
Author's Declaration . . . . .	xiv
<b>1 Introduction</b>	<b>1</b>
1.1 The Chemical Baeyer-Villiger Reaction . . . . .	1
1.1.1 Discovery . . . . .	1
1.1.2 Mechanism . . . . .	2
1.1.3 Mechanistic Details . . . . .	4
1.1.4 Kinetics . . . . .	7
1.1.5 Catalyst Design . . . . .	9
1.1.6 Side Reactions . . . . .	16
1.1.7 Summary . . . . .	18
1.2 The Biological Baeyer-Villiger Reaction . . . . .	18
1.2.1 Discovery . . . . .	18
1.2.2 Mechanism . . . . .	20
1.2.3 Baeyer-Villiger Monooxygenase Structure . . . . .	21
1.2.4 Example Baeyer-Villiger Monooxygenases . . . . .	22

1.2.5	Genetic Modification of Baeyer-Villiger Monooxygenases . . . . .	28
1.2.6	Industrial Application of BVMOs . . . . .	34
1.3	Conclusions . . . . .	36
1.4	Project Aims . . . . .	36
<b>2</b>	<b>Materials and Methods</b>	<b>38</b>
2.1	General Methods . . . . .	38
2.1.1	Agarose gel electrophoresis . . . . .	38
2.1.2	SDS-Polyacrylamide Gel Electrophoresis: . . . . .	39
2.1.3	Transformation of chemically competent <i>E. coli</i> . . . . .	41
2.1.4	DNA Restriction Digest: . . . . .	42
2.1.5	Starter Cultures . . . . .	42
2.1.6	Protein Expression . . . . .	42
2.1.7	Achiral GC Analysis: . . . . .	43
2.1.8	Chiral GC Analysis: . . . . .	45
2.2	Biotransformations . . . . .	45
2.2.1	Plasmid Miniprep . . . . .	45
2.2.2	Cell Stock Production: . . . . .	46
2.2.3	Whole Cell Biotransformations: . . . . .	46
2.2.4	MO14 Sulfide Biotransformations: . . . . .	46
2.3	Purification . . . . .	47
2.3.1	Nickel Ion Affinity Chromatography: . . . . .	47
2.3.2	Ion Exchange Chromatography: . . . . .	49
2.3.3	Sepharose Blue Chromatography: . . . . .	49
2.3.4	Ammonium Sulfate Precipitation: . . . . .	49
2.3.5	Hydrophobic Interaction Chromatography: . . . . .	50
2.3.6	C-terminal Cloning: . . . . .	50

2.3.7	MO14 Degradation Experiment . . . . .	52
2.3.8	Calcium Precipitation Purification . . . . .	53
2.3.9	Codon-Optimised Gene Cloning . . . . .	55
2.3.10	Glutathione-S-transferase Purification . . . . .	57
2.4	Fermentations . . . . .	58
2.5	Mutations . . . . .	58
2.5.1	Site-Directed Mutagenesis . . . . .	59
<b>3</b>	<b>Purification of MO14</b>	<b>60</b>
3.1	Protein Production . . . . .	60
3.2	Chromatographic Purification . . . . .	63
3.2.1	Nickel Ion Affinity . . . . .	63
3.2.2	C-terminal Histidine Tag . . . . .	65
3.2.3	Ion Exchange Chromatography . . . . .	68
3.2.4	Sepharose Blue Purification . . . . .	70
3.2.5	Ammonium Sulfate Precipitation . . . . .	72
3.2.6	Hydrophobic Interaction . . . . .	74
3.3	Column-Free Purification . . . . .	78
3.4	Codon-Optimised Constructs . . . . .	80
3.4.1	Glutathione-S-transferase Purification . . . . .	85
3.5	Conclusions . . . . .	87
<b>4</b>	<b>Biotransformations</b>	<b>88</b>
4.1	Plasmid Preparation . . . . .	88
4.2	Ketone Biotransformations . . . . .	89
4.2.1	Cell Stock Production and Initial Biotransformations . . . . .	89
4.2.2	MO14 Biotransformation of Bicyclo[3.2.0]hept-2-en-6-one . . . . .	94
4.3	MO14 Biotransformation of Sulfides . . . . .	101

4.3.1	Lower Functionality Sulfides . . . . .	103
4.3.2	Halo-substituted Sulfides . . . . .	106
4.3.3	Bulky Substituents . . . . .	110
4.3.4	Heterocyclic Sulfides . . . . .	112
4.4	Conclusions . . . . .	114
<b>5</b>	<b>Fermentations</b>	<b>115</b>
5.1	Method Development . . . . .	116
5.2	Temperature . . . . .	118
5.3	Substrate Concentration . . . . .	123
5.4	Codon-Optimisation . . . . .	125
5.5	Delay of Substrate Addition . . . . .	128
5.6	Conclusions . . . . .	130
<b>6</b>	<b>Mutations</b>	<b>132</b>
6.1	Target Selection . . . . .	132
6.2	Mutant Generation . . . . .	139
6.3	Biotransformations . . . . .	141
6.3.1	Native Cells . . . . .	141
6.3.2	MO14 P441V and MO15 V447P . . . . .	142
6.3.3	MO14 I60V and MO15 V67I . . . . .	143
6.3.4	Double Mutants . . . . .	145
6.4	Conclusions . . . . .	147
<b>7</b>	<b>Conclusions</b>	<b>149</b>
7.1	Conclusions . . . . .	149
7.2	Further Work . . . . .	152
	Appendix . . . . .	154

List of Abbreviations . . . . .	156
References . . . . .	159

# List of Figures

1.1	The first Baeyer-Villiger oxygenations . . . . .	2
1.2	The von Baeyer Mechanism . . . . .	3
1.3	The Wittig Mechanism . . . . .	3
1.4	The Criegee Mechanism . . . . .	3
1.5	The general mechanism of Baeyer-Villiger oxygenation of a ketone using a peracid.	4
1.6	The stereoelectronic effects on the Baeyer-Villiger reaction. . . . .	5
1.7	The reaction conducted by Turner to confirm retention of stereochemistry. . . . .	6
1.8	The reaction conducted by Mislow and Brenner to confirm retention of stereochemistry in the absence of a diastereomer. . . . .	7
1.9	The most enantioselective of the first described metal-catalysed chiral Baeyer-Villiger oxidations. . . . .	13
1.10	An example of the highest e.e. reactions thus far attained for transition metal-catalysed Baeyer-Villiger reactions. . . . .	14
1.11	An example of the phosphoric acid-catalysed Baeyer-Villiger reactions. . . . .	15
1.12	An example of the flavin-based catalyst-catalysed Baeyer-Villiger reactions. . . . .	16
1.13	An example of epimerisation of a cyclohexanone derivative. . . . .	17
1.14	A Possible Ketone Rearrangement . . . . .	17
1.15	A Selenium Dioxide Ring Contraction . . . . .	18
1.16	The Baeyer-Villiger reaction observed for <i>Proactinomyces erythropolis</i> . . . . .	19
1.17	The Generation of Peroxyflavin in a BVMO. . . . .	20



1.18	The Baeyer-Villiger Monooxygenase Mechanism . . . . .	20
1.19	The binding of FAD and NADPH by CHMO. . . . .	23
1.20	Regioselective Transformations of CHMO . . . . .	24
1.21	Enantioselective Transformations of CHMO . . . . .	25
1.22	CHMO Transformation of bicyclo[3.2.0]hept-2-en-6-one . . . . .	25
1.23	The structure of PAMO . . . . .	27
1.24	PAMO X-ray structure, with the mutation site shown in red, the potentially affected loops in black and the FAD and NADPH cofactors in cylinder form. <sup>81</sup> PDB no. 1W4X . . . . .	30
2.1	The GC calibration curve for bicyclo[3.2.0]hept-2-en-6-one. . . . .	44
2.2	The GC calibration curve for 2-oxa-bicyclo[3.3.0]oct-6-en-3-one. . . . .	44
3.1	SDS-PAGE showing MO14 expression in two strains of <i>E. coli</i> . . . . .	62
3.2	SDS-PAGE showing a nickel ion affinity purification of MO14. . . . .	64
3.3	A predicted structure for MO14 . . . . .	65
3.4	An agarose gel of the digest of the newly cloned MO14 in pET-22b(+). . . . .	66
3.5	SDS-PAGE showing MO14C expression tests. . . . .	67
3.6	SDS-PAGE gel showing nickel affinity purification of C-terminally tagged MO14. . . . .	68
3.7	An example of a possible structure for Q-Sepharose. . . . .	69
3.8	SDS-PAGE showing the ion exchange purification. . . . .	70
3.9	Structure of the sepharose blue functionality. . . . .	71
3.10	SDS-PAGE showing the Sepharose Blue purification. . . . .	72
3.11	SDS-PAGE gel showing the ammonium sulfate precipitation. . . . .	73
3.12	SDS-PAGE gel showing the hydrophobic interaction chromatography. . . . .	75
3.13	SDS-PAGE gels of the MO14 control degradation experiment. . . . .	76
3.14	SDS-PAGE gels of the MO14 degradation experiment with AEBSF. . . . .	77

3.15 SDS-PAGE gels of the MO14 degradation experiment with a protease inhibitor cocktail. . . . .	77
3.16 Agarose gel showing the MO14-BRT17 fusion. . . . .	79
3.17 An SDS-PAGE gel showing the purification of MO14 by calcium-precipitation. . .	80
3.18 SDS-PAGE gel showing COMO14 expression. . . . .	82
3.19 SDS-PAGE showing expression of codon-optimised MO14 constructs in <i>E. coli</i> BL21 cells. . . . .	84
3.20 SDS-PAGE showing expression of codon-optimised MO14 constructs in Rosetta™2 (DE3) pLysS cells. . . . .	85
3.21 SDS-PAGE gel showing glutathione affinity purification of GST-COMO14. . . . .	86
4.1 Agarose Gels Showing the Results of Restriction Digest of Plasmid DNA by NdeI and NcoI . . . . .	89
4.2 Bicyclo[3.2.0]hept-2-en-6-one, <b>1</b> and 2-oxabicyclo[3.3.0]oct-6-en-3-one, <b>2</b> . . . .	90
4.3 Gas Chromatograph Traces of Model Substrate Conversions to Lactone by Baeyer-Villiger Monooxygenases from <i>Rhodococcus jostii</i> . . . . .	91
4.4 Structures of 1-indanone, <b>3</b> , $\alpha$ -tetralone, <b>4</b> and their corresponding expected lactone products, <b>5</b> and <b>6</b> , respectively. . . . .	92
4.5 Gas Chromatograph Traces of 1-indanone transformation by MO3 and MO4. . . . .	93
4.6 Gas Chromatograph Traces of $\alpha$ -tetralone transformation by MO10 and CHMO <sub>Acineto</sub> . . . . .	94
4.7 Cell Density Biotransformation . . . . .	95
4.8 Substrate concentration biotransformation . . . . .	97
4.9 Glucose Biotransformations . . . . .	99
4.10 Cyclodextrin Biotransformation . . . . .	100
4.11 The desired asymmetric sulfoxidation in the synthesis of esomeprazole. . . . .	102
5.1 MO14 conversion of bicyclo[3.2.0]hept-2-en-6-one. . . . .	115

5.2	SDS-PAGE showing expression of native ro03437 gene in <i>E. coli</i> Rosetta™2 (DE3) pLysS strain at different temperatures. . . . .	119
5.3	The fermentation-based conversion of bicyclo[3.2.0]hept-2-en-6-one over time by <i>E. coli</i> Rosetta™2 (DE3) pLysS cells expressing wild-type MO14 at 16 °C and 30 °C. . . . .	120
5.4	The fermentation-based conversion of bicyclo[3.2.0]hept-2-en-6-one over time by <i>E. coli</i> Rosetta™2 (DE3) pLysS cells expressing wild-type MO14 at 16 °C. . . . .	121
5.5	The ketone enantiomer levels during the fermentation experiment investigating the effect of temperature. . . . .	122
5.6	The lactone enantiomer levels during the fermentation experiment investigating the effect of temperature. . . . .	123
5.7	The fermentation-based conversion of bicyclo[3.2.0]hept-2-en-6-one over time by <i>E. coli</i> Rosetta™2 (DE3) pLysS cells expressing wild-type MO14 with variation of substrate concentration. . . . .	124
5.8	SDS-PAGE showing expression of native and codon-optimised ro03437 gene in <i>E. coli</i> Rosetta (TM) 2 (DE3) pLysS strain. . . . .	126
5.9	The fermentation-based conversion of bicyclo[3.2.0]hept-2-en-6-one over time by <i>E. coli</i> Rosetta™2 (DE3) pLysS cells expressing wild-type MO14 and <i>E. coli</i> BL21 cells expressing codon-optimised MO14. . . . .	127
5.10	e.e. of ketone substrate during codon-optimised fermentation experiment. . . . .	128
5.11	The fermentation-based conversion of bicyclo[3.2.0]hept-2-en-6-one over time by <i>E. coli</i> Rosetta™2 (DE3) pLysS cells expressing wild-type MO14 with delay of substrate addition. . . . .	129
6.1	The biotransformations of bicyclo[3.2.0]hept-2-en-6-one catalysed by MO14 and MO15. . . . .	133
6.2	The predicted structure for MO14 based on homology with PAMO. . . . .	134

6.3	The predicted structure for MO15 based on homology with PAMO. . . . .	135
6.4	Potential mutation targets. . . . .	137
6.5	The predicted structure for MO14 based on homology with CHMO <sub>Rhod</sub> . . . . .	138
6.6	An example of site-directed mutagenesis. . . . .	139
6.7	SDS-PAGE analysis of mutant expression. . . . .	140
6.8	MO14-P441V Mutant Transformation GC Trace . . . . .	142
6.9	MO15-V447P Mutant Transformation GC Trace . . . . .	143
6.10	MO14-I60V Mutant Transformation GC Trace . . . . .	144
6.11	MO15-V67I Mutant Transformation GC Trace . . . . .	145
6.12	MO14 Double Mutant Transformation GC Trace . . . . .	146
6.13	MO15 Double Mutant Transformation GC Trace . . . . .	147

# List of Tables

2.1	Achiral GC Conditions. . . . .	43
2.2	Chiral GC Conditions . . . . .	45
2.3	MO14 Insert PCR for C-terminal Cloning. . . . .	51
2.4	MO14 Insert PCR for Cloning into pMAL-BRT <sub>17</sub> . . . . .	54
2.5	COMO14 Insert PCR for Cloning into YSBLIC-3C. . . . .	56
2.6	Mutagenesis Primers. . . . .	58
2.7	Mutagenesis PCR Conditions. . . . .	59
4.1	Low Functionality Sulfide Biotransformations . . . . .	104
4.2	Halo-Substituted Sulfide Biotransformations . . . . .	107
4.3	Bulky-Substituted Sulfide Biotransformations . . . . .	110
4.4	Heterocyclic Sulfide Biotransformation . . . . .	113
6.1	Alignment of PAMO, MO14 and MO15 sequences. . . . .	137
6.2	Biotransformations of MO14 and MO15 mutants. . . . .	141

## **Acknowledgements**

I would like to thank my academic supervisor, Gideon Grogan, for his help and guidance during the course of this project and the BBSRC for the joint funding of the project. I would also like to thank my industrial supervisor, Mike Lloyd, for his assistance and support during this project, as well as Chirotech Technology Ltd., a subsidiary of Dr. Reddy's Laboratories, Ltd., for the joint funding of the project.

I would like to acknowledge the many people who have contributed to this project: Jared Cartwright and Mick Miller of the Technology Facility for assistance with the fermentation experiments; Karl Heaton for help with LC-MS; Ian Fairlamb, Jonathan Ward and Tom Ronson for assistance with organic synthesis and characterisation; the Grogan research group, particularly Charlotte Leese, for general assistance in the course of the project; and everybody at York Structural Biology Laboratory for making my time here so enjoyable.

I would also like to thank my friends and family, in particular my wife Rachel, for their love and support during this project. This thesis is also dedicated to the memory of my grandmother, Gillian May Shelton (1932-2013).

Finally, thanks to my Creator, through whom all things are possible.

## Author's Declaration

Some of the work presented in this thesis has previously been published in the following paper:

"E. coli cells expressing the BaeyerVilliger monooxygenase MO14 (ro03437) from *Rhodococcus jostii* RHA1 catalyse the gram-scale resolution of a bicyclic ketone in a fermentor", B. D. Summers *et. al.*, *Org. Biomol. Chem.*, **2015**, 13, 1897-1903

Except where stated, all work presented in this thesis represents the original contribution of the author. Any contribution from others is acknowledged as appropriate within the text.

The generation of COMO14 constructs and the mutations of MO14 and MO15 were conducted by Mick Miller of the Technology Facility. The degradation experiments on MO14 were conducted by Muhiadin Omar.

# Chapter 1

## Introduction

### 1.1 The Chemical Baeyer-Villiger Reaction

#### 1.1.1 Discovery

In 1899, while performing work on the ring cleavage of cyclic ketones, Adolf von Baeyer and Victor Villiger discovered that the application of potassium monopersulfate ( $\text{KHSO}_5$ ) to menthone or carvomenthone produced the relevant lactones in 40-50 % yields.<sup>1</sup> A year earlier, Heinrich Caro had discovered that adding potassium persulfate to concentrated sulfuric acid would yield a compound that could produce nitrosobenzene from phenylamine.<sup>2</sup> This new compound was produced by Baeyer and Villiger and reactions of this compound with ketones led to the discovery of the Baeyer-Villiger reaction. The search for similar compounds to potassium monopersulfate also led them to organic peracids, which had not previously been reported<sup>3</sup> and now represent the most common oxidising agent for the chemical Baeyer-Villiger reaction.



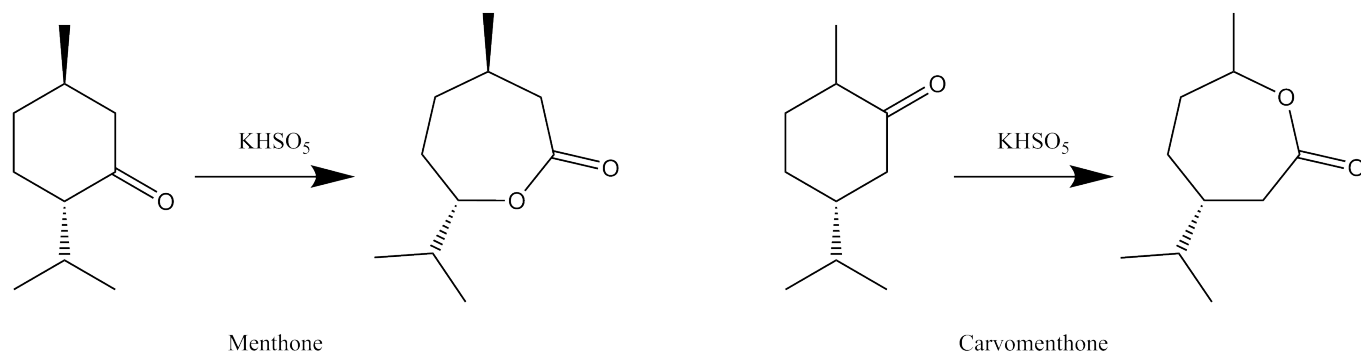


Figure 1.1: The first Baeyer-Villiger oxygenations

### 1.1.2 Mechanism

Von Baeyer and Villiger recognised the similarity of this new reaction to the Beckmann rearrangement and therefore suggested that a dioxirane is involved in the mechanism of the reaction, as was then postulated for the Beckmann rearrangement.<sup>4</sup> The dioxirane would then rearrange itself into the equivalent Baeyer-Villiger product. Lacking the ability to further characterise the reaction, this was the accepted mechanism for nearly forty years. In early 1940, Georg Wittig claimed to have isolated an intermediate in the Baeyer-Villiger oxygenation of fluorenone that appeared to suggest the formation of a carbonyl oxide.<sup>5</sup> He therefore proposed that the peracid generates a carbonyl oxide, followed by rearrangement into the Baeyer-Villiger product. Just nine years after Wittig had proposed his mechanism, Rudolph Criegee showed that this isolated intermediate was in fact merely a mixture of fluorenone and 9,9-bis(hydro-peroxy)fluorene.<sup>6</sup> He therefore produced his own concept of the mechanism, involving a tetrahedral transition state, now known as a 'Criegee intermediate'.<sup>7</sup>

#### The Doering and Dorfman Experiment

The mystery over the actual mechanism of the Baeyer-Villiger oxygenation was finally solved in 1953, following an oxygen labelling experiment performed by Doering and Dorfman.<sup>8</sup> By including  $\text{O}^{18}$  in benzophenone and reacting it with perbenzoic acid (PBA), they enabled the determina-

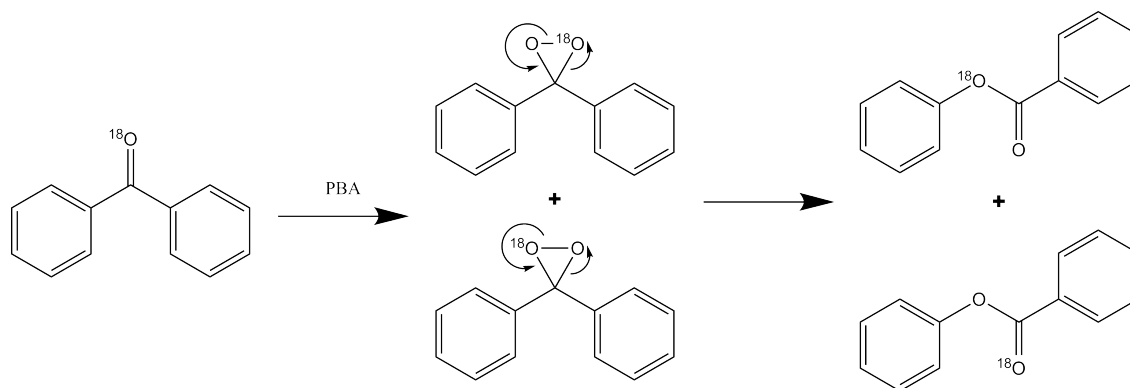


Figure 1.2: The von Baeyer Mechanism

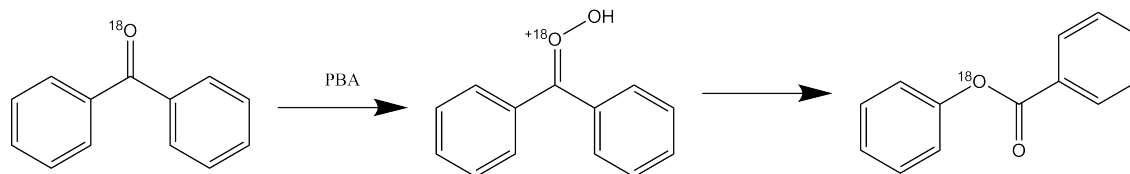


Figure 1.3: The Wittig Mechanism

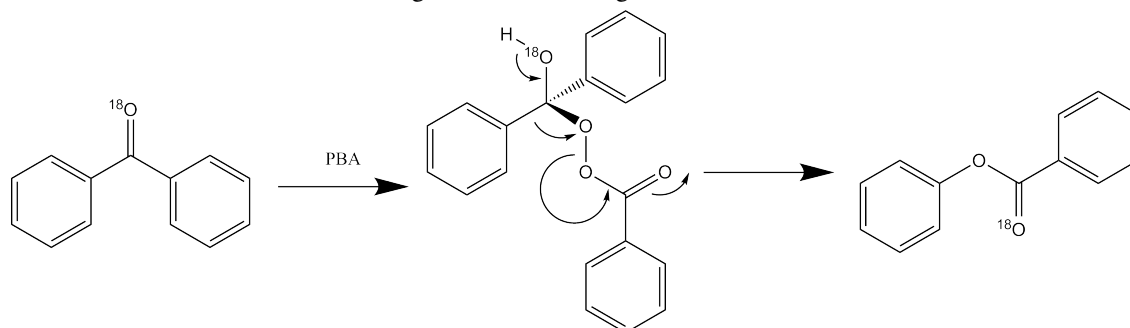


Figure 1.4: The Criegee Mechanism

tion of mechanism by the product generated. As can be seen in Figures 1.2-1.4, the von Baeyer mechanism results in a mixture of either the carbonyl or the alpha oxygen being the higher mass isotope, while the Wittig and Criegee mechanisms involve only the alpha or the carbonyl oxygens being the higher mass isotope respectively. The products were analysed in two ways: firstly, they were subjected to mass spectrometry and secondly, the products were pyrolyzed and the atom % excess of oxygen compared to a known standard. The results are only consistent with the mechanism suggested by Criegee.

### 1.1.3 Mechanistic Details

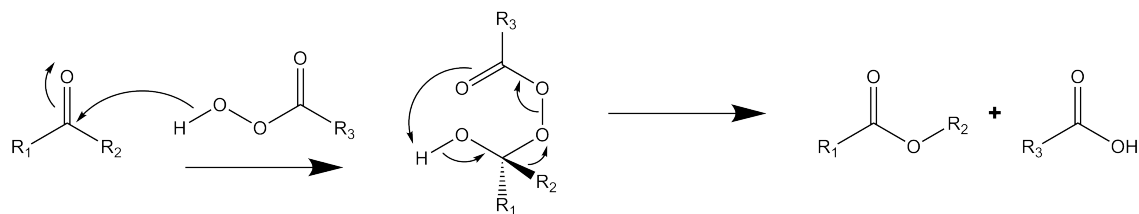


Figure 1.5: The general mechanism of Baeyer-Villiger oxygenation of a ketone using a peracid.

#### Migratory Preference

As well as determining the mechanism by which the Baeyer-Villiger reaction proceeds, Doering was also involved in finding out the preference of the reaction for migrating groups. In work before the new mechanism was discovered, a clear preference can be seen for branched substituents to migrate over methyl groups. He therefore postulated that a positively charged carbon atom would migrate more quickly, as a branched substituent has more ability to stabilise a positive charge and hence is more likely to form.<sup>9</sup> He then tested this theory by means of benzophenone, a symmetrical molecule, with substituents on one of the phenyl rings. From this experiment, he concluded that rings with electron-donating substituents, e.g. MeO or NH<sub>2</sub>, in the *para* position migrate faster than a phenyl ring, whereas rings with electron-withdrawing substituents, e.g. NO<sub>2</sub> or Cl, migrate slower than the phenyl ring. This would seem to confirm the suggestion that stabilising the positive charge increases the rate of reaction and would in turn indicate that, in general, electron-donating substituents increase the rate of this reaction.

#### Antiperiplanarity

As a result of the Criegee mechanism, the migrating group must be antiperiplanar to the oxygen-oxygen bond,<sup>10</sup> but also to the hydroxyl group lone pair. Evidence for the latter of these effects was relatively forthcoming,<sup>11</sup> but it took until quite recently for solid evidence of the former effect to be realised.<sup>12</sup> This evidence also shows that this electronic effect is more important to the reaction

than the preference of the reaction for particular migrating groups. The primary of these two effects is the antiperiplanarity of the oxygen-oxygen bond and migrating group and the secondary of these is the antiperiplanarity of the migrating group and the hydroxyl lone pair.

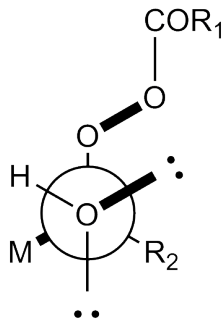


Figure 1.6: The stereoelectronic effects on the Baeyer-Villiger reaction. M represents the migrating group in the reaction.

The secondary stereoelectronic effect was demonstrated by means of the Baeyer-Villiger oxidation of a rigid bicyclic system, wherein the proton of the hydroxyl group and the bicyclic substrate undergo a steric clash, resulting in the 'locking' of the C-O bond, which subsequently demonstrated the necessity of an antiperiplanar alignment of the hydroxyl lone pair and the migrating group by the generated products, *i.e.* the migrating group was, for a range of substrates tested, the group in the designated alignment.<sup>11</sup>

The primary stereoelectronic effect was identified by the use of  $\alpha$ -fluoroketones, in order to generate dipole-dipole interactions between the fluorine atom and the peroxyester bond. *t*-butylcyclohexanone derivatives, fluorinated at the  $\alpha$  position in both axial and equatorial positions, were subjected to Baeyer-Villiger oxidation. The axially fluorinated substrate generated mostly the expected product as predicted by migratory preference, *i.e.* the non-substituted  $\alpha$  carbon migrated, as it is more electron-rich and therefore more able to stabilise a positive charge. For this substrate, the preferred migratory group is also antiperiplanar to the O-O bond. For the equatorially substituted substrate, however, the opposite is observed. The more electron-poor  $\alpha$  carbon is the one that preferentially migrates, in defiance of the general migratory aptitude rule, as it is now the carbon

located antiperiplanar to the O-O bond. This preference originates from a dipole-dipole interaction between the fluorine and the O-O bond causing the conformational arrangement in which these two groups are aligned, wherein the expected migratory group is aligned correctly, to be disfavoured. This was confirmed by the use of differing solvent polarity, as polar solvents stabilise dipole moments, and an increase in solvent polarity was associated with a decrease in the selectivity observed for the equatorially substituted reaction and no change for the axially substituted reaction.

### Conservation of Stereochemistry

In the mid-1900s, the lack of analytical techniques posed a significant barrier to determining whether reactions proceeded with conservation of stereochemistry. At the time, the simplest method was to employ a stereogenic centre neighbouring the reaction centre and compare diastereoisomerism before and after the reaction. In order to further characterise the Baeyer-Villiger reaction, Turner conducted the reaction on *cis*-1-acetyl-2-methylcyclohexane using perbenzoic acid. He found that he obtained exclusively *cis*-configured 2-methyl-cyclohexyl acetate, giving the first evidence that the Baeyer-Villiger reaction occurs with retention of stereochemistry.<sup>13</sup> Soon after this reaction was conducted, along with a similar experiment on 20-keto steroid oxygenation,<sup>14</sup> Mislow and Brenner confirmed the stereoselectivity in non-diastereomeric substrates by performing the reaction on 3-phenyl-2-butanone and producing the ester with 98 % conservation of stereochemistry.<sup>15</sup>

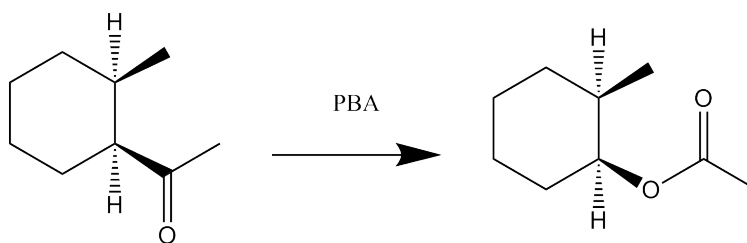


Figure 1.7: The reaction conducted by Turner to confirm retention of stereochemistry.

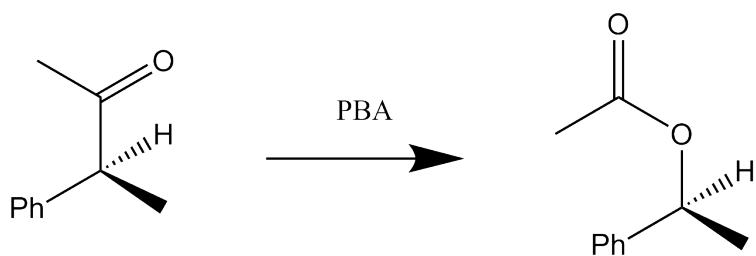


Figure 1.8: The reaction conducted by Turner to confirm retention of stereochemistry in the absence of a diastereomer.

### ***Endo/Exo* Conservation**

A further piece of useful information on the mechanism of this reaction is the question of *endo/exo* conservation, which was studied by Berson and Suzuki. They took (*R*)-1-bicyclo[2.2.1]hept-2-yl-ethanone and conducted a Baeyer-Villiger oxidation, producing the equivalent ester with conservation of both optical stereochemistry and the *exo* structure. This reaction was particularly notable, as it suggested that the migrating group does not leave the structure and then reattach but rather a concerted step occurs.<sup>16</sup> A more recent discovery was the confirmation that such retention of stereochemistry also occurs in unsubstituted oxygenation targets. For example, deuterium-labelled cyclohexanone was converted into caprolactone with conservation of stereochemistry.<sup>17</sup> There are, however, some limitations to this conclusion. Firstly the aromatic substituents can affect the initial step of the reaction, slowing down or speeding up the attack on the carbonyl due to steric effects, and secondly because the peroxy acid often has an effect on the migration rate.<sup>18</sup>

### **1.1.4 Kinetics**

As previously discussed, the kinetics of the Baeyer-Villiger reaction depend heavily on many factors including acidity of solution and substituent side groups. Hence, the determination of the rate-determining step of the reaction has been a difficult procedure. Early on in the Criegee mechanism's history, it was believed that the formation of its intermediate was the limiting step, as this explained best the three key observations that had been made of its kinetics. These observations were the increase in the rate of reaction in a more polar solvent, the weak acid's catalytic effect

and the change in the order of the reaction as the substitution was altered.<sup>19</sup>

A few years after this conclusion was reached, further work was done that suggested that the rearrangement, rather than the formation, of the Criegee intermediate was the limiting step.<sup>20</sup> This research was reproduced and the results confirmed,<sup>21</sup> but no decisive experiments could be conducted, with the interpretation of isotopic labelling inconclusive. No simple kinetics could be described, as it appears that either the intermediate formation or the subsequent rearrangement can be the rate-determining step, depending on the substituent effects earlier mentioned. The most current observations appear to indicate that an electron-donating substituent that stabilises the positive charge formation has a relatively quick rearrangement, but the formation of the Criegee intermediate is slower and thus the limiting step. By comparison, an electron withdrawing substituent slows the rearrangement, making that into the rate limiting step.<sup>22,23</sup>

It is important in drawing conclusion from kinetic data of any reaction to take into account effects of solvent and other present compounds, but particularly essential in the case of the Baeyer-Villiger reaction. For example, bicarbonate ions present in the solution can cause the deprotonation of the Criegee intermediate, which simplifies the rearrangement and increases the reaction rate.<sup>24,25</sup> Unfortunately, this cannot be exploited easily, as these basic ions also catalyse the decomposition of peracids,<sup>26</sup> which would reduce the available reactant and theoretically lower the rate of reaction beyond a certain point.

A similar catalytic effect is also observed for weak acids, which poses a particular issue in this reaction as trace amounts of acid are fairly ubiquitous in peracid solutions and often would not be removed before use in early works. This was first observed in the works of Friess and Soloway<sup>27,19</sup> and agreed well with previous observations that slight changes in reagent preparation affect the reactivity.<sup>28</sup> This effect is particularly pronounced when the peracid used is trifluoroperethanoic acid,<sup>20</sup> as the equivalent acid, trifluoroethanoic acid, raises the reaction rate so as to make the

reaction autocatalytic. Further evidence in favour of this catalysis is the reduction of the rate in the presence of a base as well as trifluoroacetic acid<sup>29</sup> and in a drastically increased rate of reaction observed in the presence of concentrated sulfuric acid.<sup>9</sup>

The strength of the acid also needs to be considered, as some difference between strong and weak acids can be observed. Strong acids have the potential to protonate the ketone or alternatively the Criegee intermediate, which would increase the rate of reaction significantly. This appears to be essential to the explanation of trifluoroacetic acid's high reactivity. This could be explained by the higher stability of strong acids as leaving groups,<sup>30</sup> however this seems unlikely due to the previously mentioned rate reduction when a base is present, suggesting a straightforward acid catalysis rather than leaving group effects. More difficult to explain is the effect of weak acids, as they cannot protonate ketones or the Criegee intermediate. This issue is clouded by apparently contradictory reports in the literature between acid catalysis<sup>27,19</sup> and increases in the rate in buffered solutions.<sup>25</sup>

Steric effects are also essential to bear in mind in this reaction; aryl groups in the alpha position slow the reaction by a measurable amount. This was shown by comparing three substrates: acetophenone, cyclohexyl methyl ketone and cyclohexyl phenyl ketone. Comparison of the first two mentioned allowed the assessment of whether cyclohexyl groups or phenyl groups migrate faster, with cyclohexyl being the result. This then allowed comparison of the two cyclohexyl-containing compounds, which showed that phenyl substituents at the alpha position to the carbonyl significantly reduce the rate of reaction.<sup>31</sup> This result appears to reinforce the theory that the rate-determining step varies depending on the reaction conditions.

### **1.1.5 Catalyst Design**

The Baeyer-Villiger reaction lends itself well to being catalysed, as there are many potential targets for catalysts to improve the rate of reaction. These include, but are not limited to, electrophilic



activation of either the substrate or intermediate and nucleophilic activation of the intermediate.

#### **Electrophilic Activation of Substrate**

As previously mentioned, acids catalyse the Baeyer-Villiger reaction. This catalysis may be due to electrophilic activation of the substrate, which can also be achieved by transition metal catalysts. One such catalyst involves a platinum-CF<sub>3</sub> arrangement, which coordinates the carbonyl to a platinum that then draws electron density from the ketone, making it more electrophilic and inducing the attack by the peroxide.<sup>32</sup> Similar catalysts based on platinum-phosphine complexes have also been found to work,<sup>33</sup> along with tin complexes, although the latter must usually be performed in anhydrous conditions, as they are commonly not water-stable.<sup>34,35</sup>

#### **Electrophilic Activation of Intermediate**

Alternatively, the carbonyl present in the intermediate can be electrophilically activated, again by coordination with an acid proton. This catalyses the rearrangement step, as the coordination causes the carbonyl oxygen draw more electron density away from the carbon, increasing the tendency for electrons to move towards the now more electron-poor carbon. The rearrangement of the intermediate most often being the rate-determining step means that this form of catalysis often has dramatic effects on the rate of reaction. Lewis acids particularly show good results when catalysing the reaction, as they can also catalyse the migration step by coordinating with the OH group.<sup>36</sup> Brønsted acids can complicate the reaction with hydrogen peroxide, as they are able cause the formation of potentially explosive polymeric peroxides.<sup>37</sup>

#### **Nucleophilic Activation of Intermediate**

As previously mentioned, addition of bicarbonate to the reaction medium approximately doubles the rate of reaction. This is believed to proceed by the generation of a charged Criegee intermediate that rearranges more quickly than the standard procedure.<sup>25</sup> Alternatively, it could be caused by the removal of residual acid (generated in the peracid synthesis) from the solution via salt formation.<sup>23</sup>

This possibility is reinforced by the lack of base catalysis when hydrogen peroxide is the attacking group.<sup>38</sup>

### Catalysts and Oxygen Source

Hydrogen peroxide as an oxygen source in the Baeyer-Villiger reaction has been identified for some time<sup>39</sup> and this reactant possess several advantages over the use of *m*CPBA. For example, the active oxygen content is higher, *i.e.* there is more oxygen per molecular mass unit, than in peracids, which provides economic benefits, and the waste product generated from its use is water, which is often easier to remove than the carboxylic acid waste products. This water waste product does have negative effects of its own, in the increased rate of hydrolysis of generated esters and potential issues with the reaction itself. Additionally, H<sub>2</sub>O<sub>2</sub> is prone to radical decomposition and requires activation for use in this role.

The positive aspects of hydrogen peroxide have nevertheless motivated the investigation of appropriate catalysts with which to activate this participant<sup>40</sup> and a range of these have been developed. The earliest examples of these attempts use either acid or base catalysis and mostly involve the reactions of strained cyclic ketones, such as the model substrate for BVMOs, bicyclo[3.2.0]hept-2-en-6-one. Although positive results were achieved,<sup>39,41</sup> these strained ketones are relatively receptive to such reactions and the success thereof may not be indicative of a useful method. More recent efforts using hydrogen peroxide have focussed on the development of a transition metal-based catalyst, however these have generally resulted in relatively poor turnover rates and questionable selectivity<sup>40</sup> or continue to have safety issues.<sup>42</sup>

Molecular oxygen, as in the biological Baeyer-Villiger oxidation, has also been investigated for use chemically, for example when combined with 'sacrificial' aldehydes to generate peracids *in situ* using a nickel complex as a catalyst. Initially, this system was used to oxidise olefins to epoxides,<sup>43</sup> but has since been expanded to include the Baeyer-Villiger oxidation.<sup>40</sup> Fe<sub>2</sub>O<sub>3</sub> has also

been proposed as a Baeyer-Villiger oxidant catalyst using molecular oxygen<sup>44</sup> and shows excellent retention of configuration, however this procedure still results in the formation of a peracid and therefore the waste carboxylic acid must be dealt with.

Since the most important benefit of using a biological agent to perform this reaction is the great asymmetry that can be achieved, a comparison to the available classical agents is worthwhile. In this case, only very recently have catalysts been developed that are capable of achieving similar *e.e.* to BVMOs, however at present the substrate scope is limited to cyclobutanones and still involves generation of a peracid.<sup>45</sup>

### **Chiral Conversions**

The ability to perform these oxygen insertion reactions is of great benefit in organic synthesis, and the retention of stereochemistry observed is a great benefit, however perhaps even more useful would be the generation of chirally pure species from prochiral substrates. In general, stereochemistry can be quite difficult to achieve, requiring complex catalysts, however some success in Baeyer-Villiger reactions has been attained using carefully designed catalysts.

Transition metal catalysts represent one method by which asymmetric Baeyer-Villiger oxidations may be achieved, with the first example of such a reaction being discussed in 1994.<sup>46</sup> This initial example utilises, in the most enantioselective example described, a complex catalyst centred around a copper core and achieves a 47 % yield with *e.e.* of 69 %. This system also uses molecular oxygen and an aldehyde moiety to generate the product.

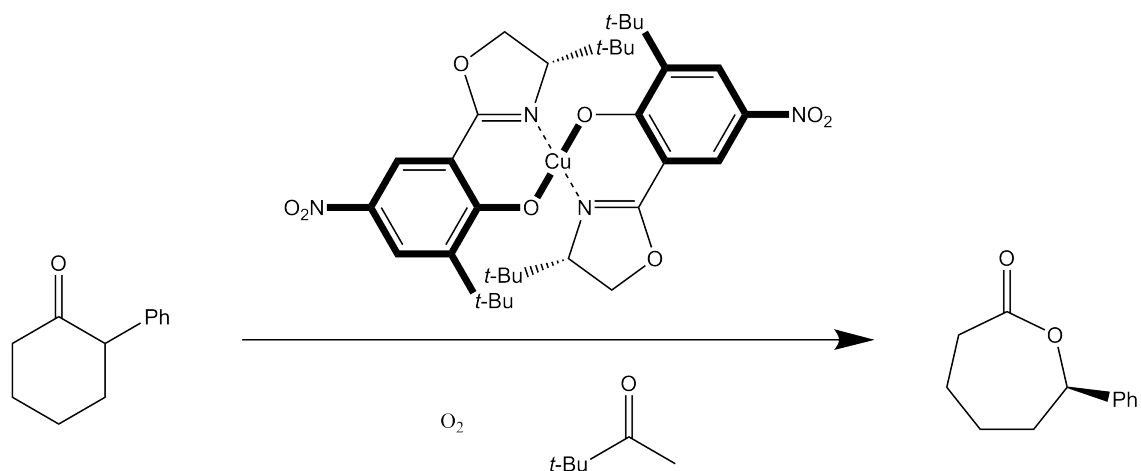


Figure 1.9: The most enantioselective of the first described metal-catalysed chiral Baeyer-Villiger oxidations.

Since this initial description, a variety of transition metal-based complexes have been designed to generate chiral products from prochiral substrates, including those based on titanium,<sup>47</sup> platinum,<sup>48,49</sup> zirconium,<sup>50</sup> scandium,<sup>51</sup> cobalt,<sup>52</sup> palladium<sup>53</sup> and tin.<sup>54</sup> Perhaps the most selective example of transition metal-catalysed Baeyer-Villiger transformation is described by Bolm *et. al.* using a chiral complex of Cu(II), which was able to catalyse the oxidation of a range of fused ring systems to cyclobutanone by molecular oxygen with 90+ % e.e, albeit with unspecified enantiomers. This complex appears unable to attain the same level of enantiospecificity for any reactants other than cyclobutanones, hence does not represent a versatile catalyst.<sup>55</sup>

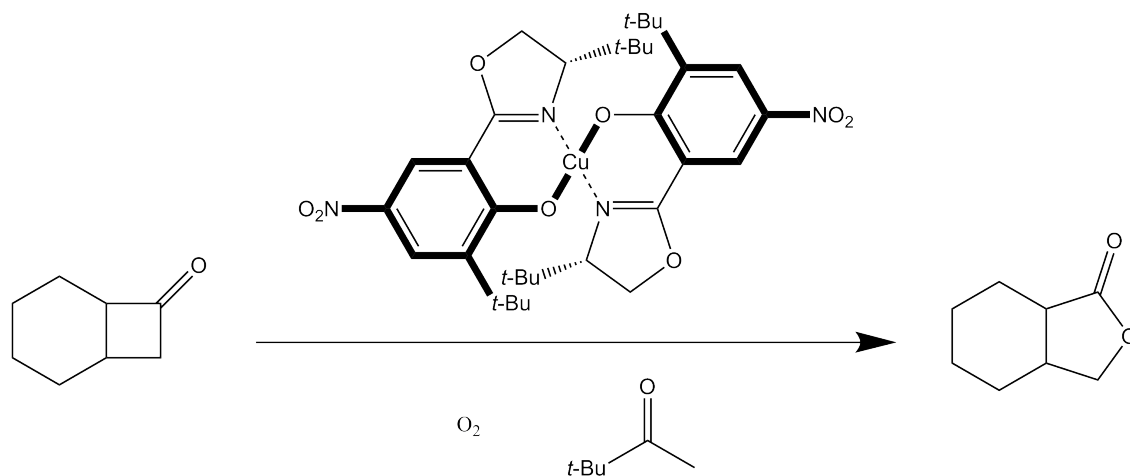


Figure 1.10: An example of the highest e.e. reactions thus far attained for transition metal-catalysed Baeyer-Villiger reactions. This reaction proceeds with 92 % e.e.

The platinum-based catalysts generally involved the use of phosphine ligands, however some investigation of species similar to the ligands, chiral phosphoric acids, has also been conducted in relation to chiral Baeyer-Villiger reactions. Brønsted acids have previously been shown to catalyse the Baeyer-Villiger reaction,<sup>36</sup> with stronger acids demonstrating a greater catalytic ability and a selection of 18 phosphoric acids have been investigated, reaching a maximum of 93 % e.e. for conversions of cyclobutanone derivatives.<sup>56</sup>

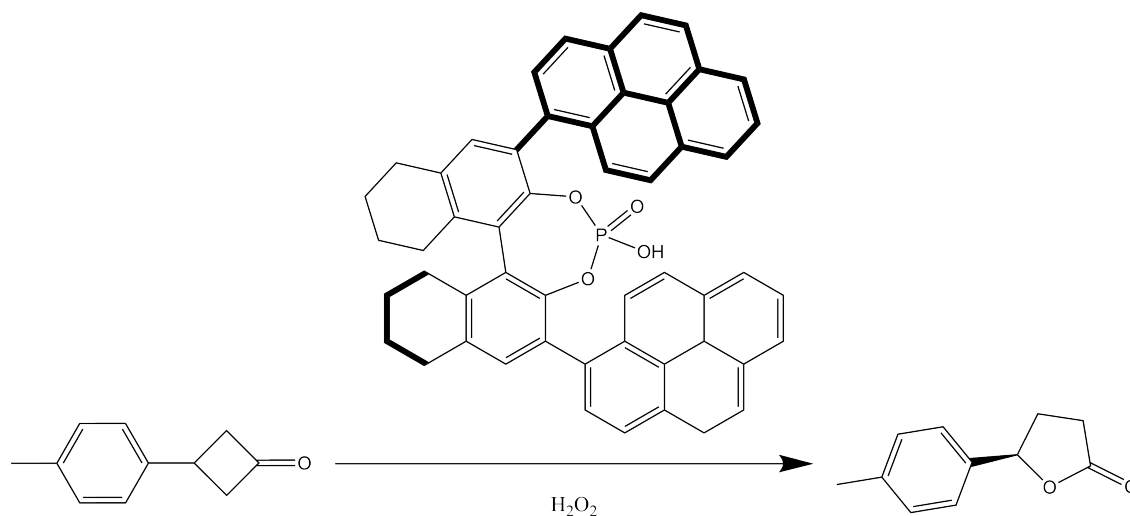


Figure 1.11: An example of the phosphoric acid-catalysed Baeyer-Villiger reactions. This reaction proceeds with 93 % e.e.

Finally, there have been some efforts to emulate the activity of Baeyer-Villiger monooxygenase enzymes, which are capable of performing the Baeyer-Villiger reaction with enantioselectivity significantly higher and for a greater range of substrates than is demonstrated by chemical catalysts. This activity is based on a flavin cofactor and work has been conducted using a wide variety of flavin-derived catalysts to perform a chiral Baeyer-Villiger reaction, the most enantioselective of which attains an e.e. of 74 %. Although this selectivity is lower than other chemical catalysts, it demonstrates the use of an organic chiral catalyst for this reaction and that flavin-based design may offer a successful catalyst scaffold.

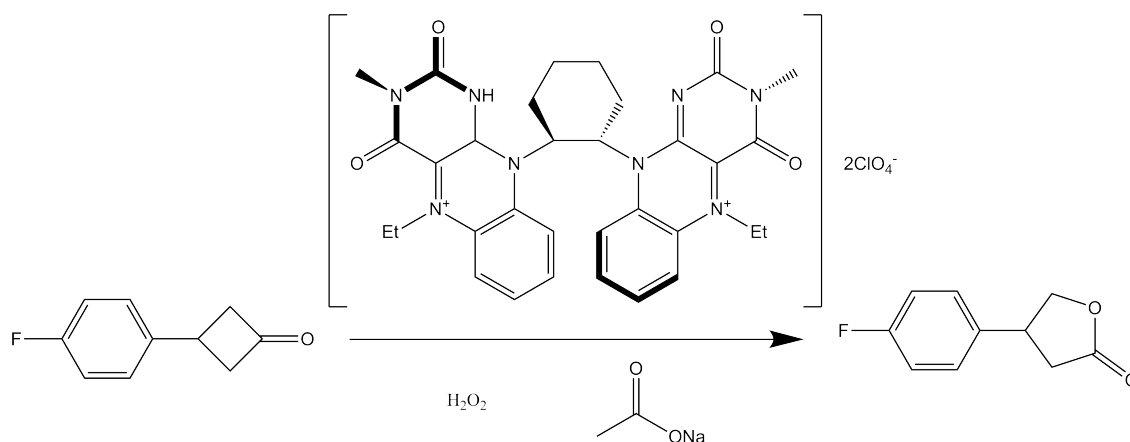


Figure 1.12: An example of the flavin-based catalyst-catalysed Baeyer-Villiger reactions. This reaction proceeds with 74 % e.e.

A wide range of catalysts have been investigated for their ability to perform a chiral Baeyer-Villiger reaction, including transition metal, organic and inorganic-based catalysts. The activity of these catalysts is generally not applicable to a wide range of reactants, being mostly limited to cyclobutanones, and is not usually capable of e.e. values greater than 90 %.

### 1.1.6 Side Reactions

As with any organic reaction, there are several potential side reactions that can affect the Baeyer-Villiger oxygenation. In this section, several of the most commonly occurring side reactions will be discussed in depth, however there are also several less troublesome potential pathways.<sup>57,58,59</sup>

#### Epimerisation

Most importantly from a synthetic point of view is the possible epimerisation of starting ketone, which can lead to a different end product but would still involve a Baeyer-Villiger reaction taking place. Epimerisation is the inversion of stereochemistry at a stereocentre and, amongst ketones and lactones, is a fairly common issue when conditions induce proton exchange. This is because ketones and lactones often possess highly acidic alpha hydrogens, owing largely to the mesomeric stabilisation effect offered by the carbonyl, which can exchange with any present in the solvent

and cause epimerisation.<sup>60</sup>

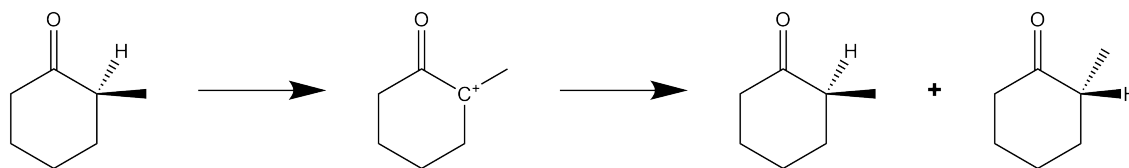


Figure 1.13: An example of epimerisation of a cyclohexanone derivative.

### Ketone Rearrangement

Less common than epimerisation and more easily detected is the rearrangement of ketones before the Baeyer-Villiger oxygenation takes place. There are several ways in which this process can occur, however in the example given, a protonation of a cyclic ketone occurs then a ring contraction that leaves a carbocation next to the now smaller ring.<sup>61</sup> This is followed by a ring expansion, as shown in Figure 1.14.

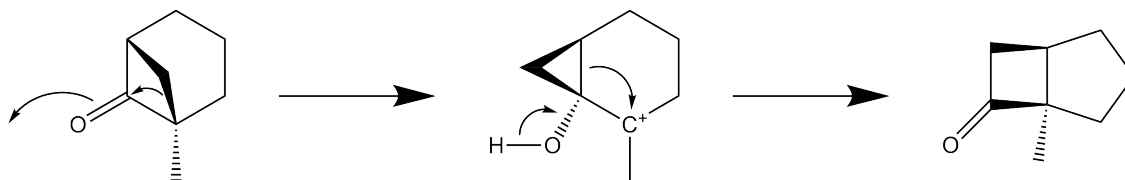


Figure 1.14: A Possible Ketone Rearrangement

### Selenium Dioxide Ring Contraction

Before this side reaction was discovered, selenium dioxide ( $\text{SeO}_2$ ) was often used as a catalyst for the Baeyer-Villiger reaction. What was not known, however, was that combining this catalyst with a hydrogen peroxide reagent can cause a ring contraction, leaving a carboxylic acid next to a cyclic ring system. This reaction competes with the Baeyer-Villiger reaction, leading to lower yields and purities.<sup>62</sup>



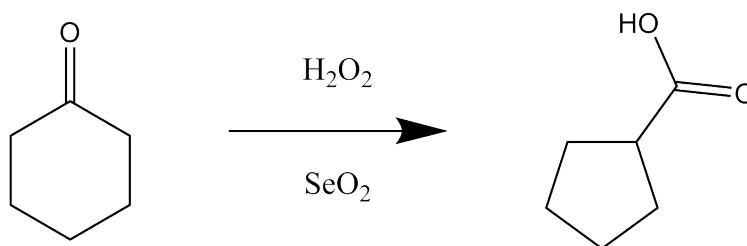


Figure 1.15: A Selenium Dioxide Ring Contraction

### 1.1.7 Summary

Overall, the Baeyer-Villiger reaction represents a key transformation in synthetic chemistry; the ability to selectively add an oxygen atom adjacent to a carbonyl is a versatile tool in the design of new pathways. The predictability of selectivity observed in these reactions, resulting from a thorough investigation of the relevant characteristics, allows for particularly convenient reaction design. There is some difficulty in the overall selectivities and yields obtained from these reactions, as there tend not to be exceptional, *i.e.* >99 %, conversions or selectivities, hence a study of the biological Baeyer-Villiger reaction may provide some reactions both higher in yield and selectivity.

## 1.2 The Biological Baeyer-Villiger Reaction

### 1.2.1 Discovery

Baeyer-Villiger oxygenations are also carried out within biological systems, mostly in bacteria. The earliest recording of such a reaction was made in 1948, when cholestanone was oxygenated in the presence of *Proactinomyces erythropolis* and small amounts of the Baeyer-Villiger oxygenation product were observed.<sup>63</sup> A Baeyer-Villiger process was also observed for the breakdown of eburicoic acid in the presence of *Glomerella fusarioides*, which led to the proposal of a Baeyer-Villiger mechanism for the reaction.<sup>64</sup> Following the discovery of these initial BVMOs, several more examples of bacteria achieving Baeyer-Villiger oxygenations were observed in steroid conversions<sup>65,66</sup> and these conversions appeared to suggest a double Baeyer-Villiger oxygenation pro-

cedure. This was reinforced by the isolation of the intermediate between oxidations<sup>67</sup> and via inhibition studies.<sup>68</sup> Baeyer-Villiger oxidations are also found outside of steroid modifications, in ketone degradations<sup>69,70</sup> and several natural product syntheses.<sup>71,72,73</sup>

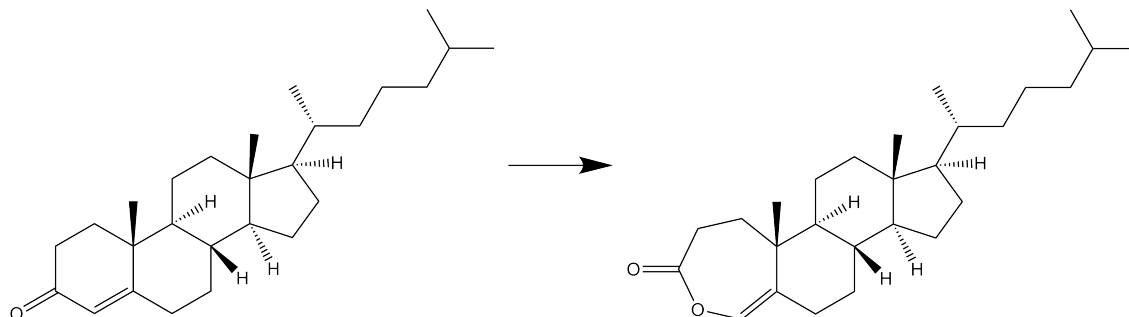


Figure 1.16: The Baeyer-Villiger reaction observed for *Proactinomyces erythropilis*.

Baeyer-Villiger monooxygenases (BVMOs) are oxidoreductases and thus catalyse redox reactions, acting on their substrate in conjunction with a cofactor, generally a flavin moiety. NAD(P)H is also required to act as an electron donor in the reaction and entails the use of a cofactor regeneration system, as the enzyme itself is not capable of restoring the electron to the NAD(P)H. BVMOs perform the Baeyer-Villiger reaction using molecular oxygen as a reactant, activated by means of the non-covalently bound flavin moiety, which is usually FAD. BVMOs are part of the same evolutionary family of enzymes as flavin-containing monooxygenases (FMOs) and N-hydroxylating monooxygenases (NMOs).<sup>74</sup> This was determined by comparing the BVMO sequence motifs with those of FMOs<sup>75</sup> and NMOs.<sup>76</sup> Several parallels also exist in the structure and catalytic activities of these classes of enzyme, as well as the sequence similarity.<sup>77</sup>

BVMOs are identifiable from these other two classes of monooxygenase by means of a protein sequence motif, FXGXXXHXXXW(P/D), which has been identified in nearly all BVMO homologues.<sup>74</sup> This sequence is found on the surface of the protein and is therefore believed to be related to a conformational change that occurs during substrate binding.

## 1.2.2 Mechanism

The understanding of the mechanism of general Baeyer-Villiger monooxygenases is largely derived from studies of cyclohexanone monooxygenase from *Acinetobacter calcoaceticus* (CHMO<sub>Acineto</sub>), and shows the presence of FAD and the dependence of the reaction on both NADPH and molecular oxygen.<sup>78</sup> A simplification of the derived mechanism is shown in Figures 1.17 and 1.18 and described below.

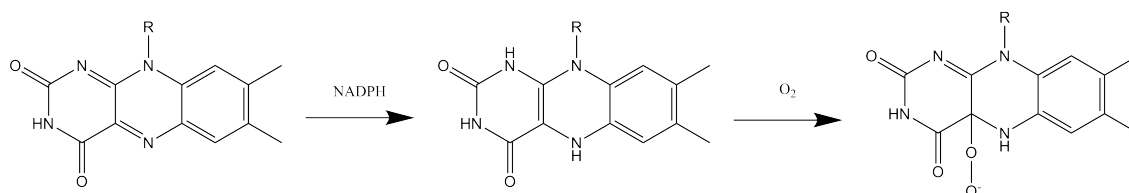


Figure 1.17: The Generation of Peroxyflavin in a BVMO.

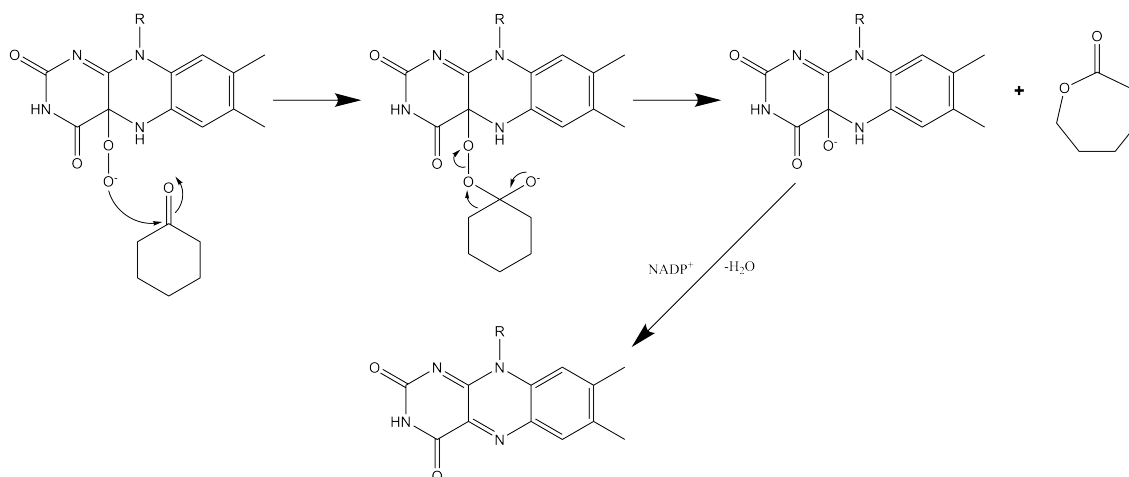


Figure 1.18: The Baeyer-Villiger Monooxygenase Mechanism

The process begins with the reduction of enzyme-bound FAD by NADPH, which then undergoes oxidation by molecular oxygen to give a negatively charged flavin 4a-peroxide. This intermediate is the species that actually performs the Baeyer-Villiger oxygenation reaction, and has been shown to be present in equilibrium with the equivalent hydroperoxide.<sup>79</sup> This peroxide then performs the role of nucleophile in the Baeyer-Villiger reaction, attacking the carbonyl group of the ketone and

yielding the Criegee intermediate. The intermediate rearranges and releases the product lactone; subsequent elimination of water regenerates the FAD moiety.

This enzymatic reaction is subject to identical stereoelectronic conditions as its non-biological equivalent, *i.e.* the migrating C-C bond must be antiperiplanar to the peroxy bond and also to a hydroxyl lone pair. Isotopic labelling has been used<sup>80</sup> to confirm that the configuration of the migrating centre is retained, in the same way as in the chemical reaction.<sup>15</sup> This allows CHMO<sub>Acineto</sub> and other BVMOs to catalyse reactions in a regio- and enantioselective fashion, by only permitting one C-C bond to be held in this orientation. Alterations to the amino acid residues in the area around the tightly-bound FAD molecule, the 'active site', allow tight control over the specific reaction catalysed.

### 1.2.3 Baeyer-Villiger Monooxygenase Structure

There are currently crystal structures of relatively few BVMOs available, two examples of which are phenylacetone monooxygenase (PAMO) from *Thermobifida fusca*<sup>81</sup> and cyclohexanone monooxygenase from *Rhodococcus* sp. strain HI-31 (CHMO<sub>Rhod</sub>).<sup>82</sup> These two structures show several key features of BVMOs, one of which is the domain structure. There are two large domains, one of which binds FAD and the other NADPH, plus one smaller subdomain. This subdomain is  $\alpha$ -helical in nature and is located within the NADP-binding domain. This subdomain appears to be an insertion of 120 amino acids and is located within the NADPH binding site, after a  $\beta\alpha\beta$  sequence. It may also play a role in the FAD-binding site, owing to its location, and may be said to perform a modulating role between the domains. This topology cannot be found in other protein structures and is therefore likely an indicator of potential BVMO activity, as it does appear to provide amino acid residues to the substrate binding site.

FAD binds at the bottom of the interface of the two main domains and makes both H-bonds with backbone N-atoms and many van der Waals interactions with a number of adjacent aromatic

residues, whose presence is conserved. NADPH, by comparison, attaches to the surface of the NADPH-binding domain and forms hydrogen bonds with a glycine-rich sequence. This is also stabilised by further forces, including electrostatic interactions between the phosphate group and neighbouring amino acid residues.

In recent years, the structure of CHMO<sub>Rhod</sub> during binding of FAD and NADPH has been further elucidated, revealing domain movements and a sliding co-factor.<sup>82</sup> Specifically, there is a rotation of the NADPH binding domain that results in a significant shift in the position of the protein backbone and a smaller movement observed in the helical domain. These movements are enabled due to the flexible nature of the loops connecting the domains. The NADP<sup>+</sup> binds by means of hydrogen bonding to the GXXGXXG motif, which is one of the characteristic motifs observed in BVMOs. Additionally, the cofactor forms electrostatic interactions with the T210 and R209 residues, further stabilising the cofactor, as well as a stacking interaction with R209. The signature motif of type I BVMOs, FXGXXXHXXXWP, is positioned at the beginning of the NADPH domain and has previously been difficult to assign a role to, however the comparison of these structures to those of PAMO and related flavin monooxygenases suggests that the aromatic ends of the sequence anchor it in the NADPH-binding domain, which then permits the central histidine residue to form a hydrogen bond to a linker segment, causing steric effects to position the NADPH. This explanation appears to only be valid for CHMO<sub>Rhod</sub>, however, as the positioning of this sequence in PAMO shows no relation to substrate binding,<sup>81</sup> indicating that the role of this sequence may be more complicated.

#### **1.2.4 Example Baeyer-Villiger Monooxygenases**

To gain a thorough understanding of Baeyer-Villiger monooxygenase structure, activity and transformational capabilities, a more in-depth look at the two BVMOs for which X-ray structures have been produced is useful.

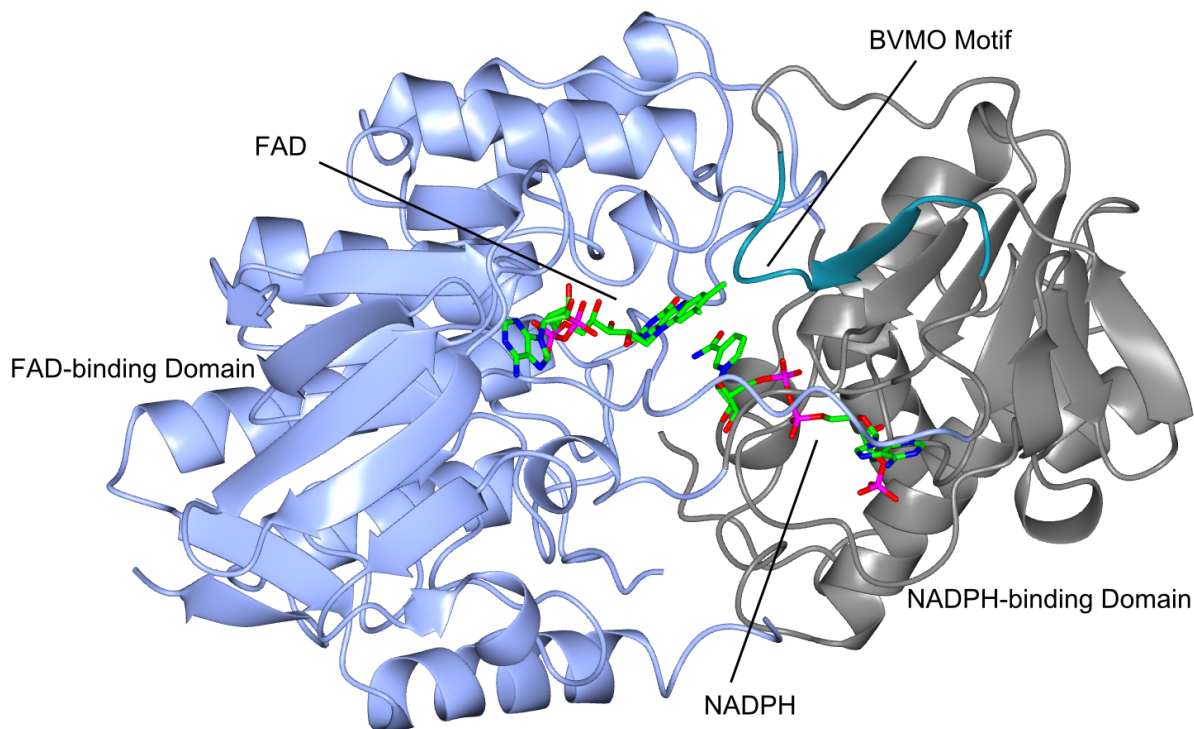


Figure 1.19: The binding of FAD and NADPH by CHMO. PDB Ref. 3GWD.

### Cyclohexanone Monooxygenase

First published in 1975,<sup>83</sup> CHMO<sub>Acineto</sub> is a monomeric enzyme with a mass of 59 kDa made up of 543 amino acids.<sup>78</sup> In addition to its activity against cyclohexanone, CHMO<sub>Acineto</sub> has been observed to perform transformations on a wide range of alternative substrates including cyclohexanone derivatives,<sup>79</sup> simple cyclic ketones<sup>79</sup> and sulfides.<sup>84</sup> CHMO<sub>Acineto</sub> is not generally capable of transforming aromatic or short chain acyclic ketones.

The continued interest in the activity of CHMO<sub>Acineto</sub> is largely due to the exceptional regio- and enantio-selectivity exhibited during biotransformations of cyclic ketones, which have been conducted in both whole-cell and isolated enzyme experiments.<sup>85,86,87,88</sup> The nature of the regioselectivity is that, in the case of 2-substituted cyclopentanones and cyclohexanones, CHMO<sub>Acineto</sub>

converts the species exclusively to the 3-substituted products, as seen in Figure 1.20.<sup>85,89,90</sup> The exceptional enantioselectivity is demonstrated in the conversion of racemic 2- aliphatically substituted cyclopentanones and cyclohexanones, shown in Figure 1.21. In these cases, at chain lengths beyond methyl groups, the product is generated with  $>95\%$  e.e.<sup>85,89,90</sup>

The regio- and enantio-selectivity of CHMO<sub>Acineto</sub> can also be observed jointly in a single transformation, that of bicyclo[3.2.0]hept-2-en-6-one, which has become the diagnostic test of BVMO activity.<sup>91,92,93</sup> Traditional chemical conversions of this substrate tend to favour production of racemic 2-oxalactone,<sup>36</sup> with small amounts of racemic 3-oxalactone produced in the case of some catalysts.<sup>36</sup> In the case of CHMO<sub>Acineto</sub>, however, each regioisomer is produced exclusively in a single enantiomer, in near equimolar quantities, shown in Figure 1.22.<sup>94,95</sup>

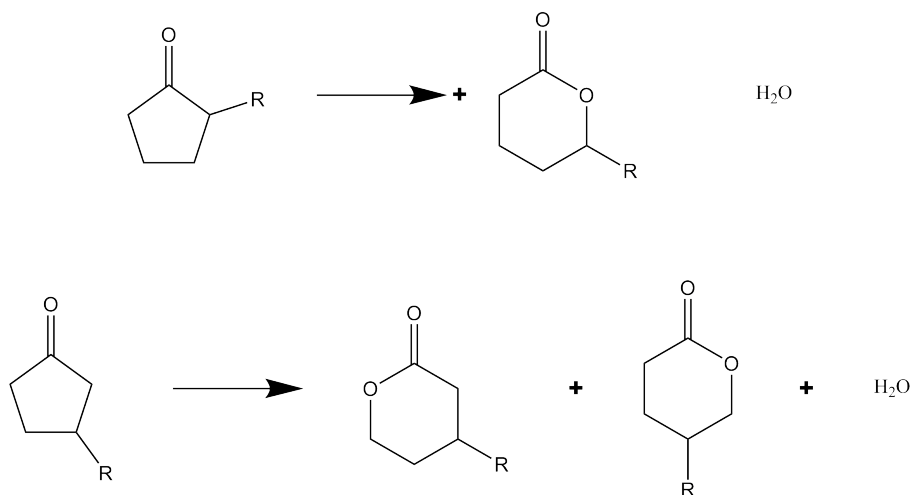


Figure 1.20: Regioselective Transformations of CHMO

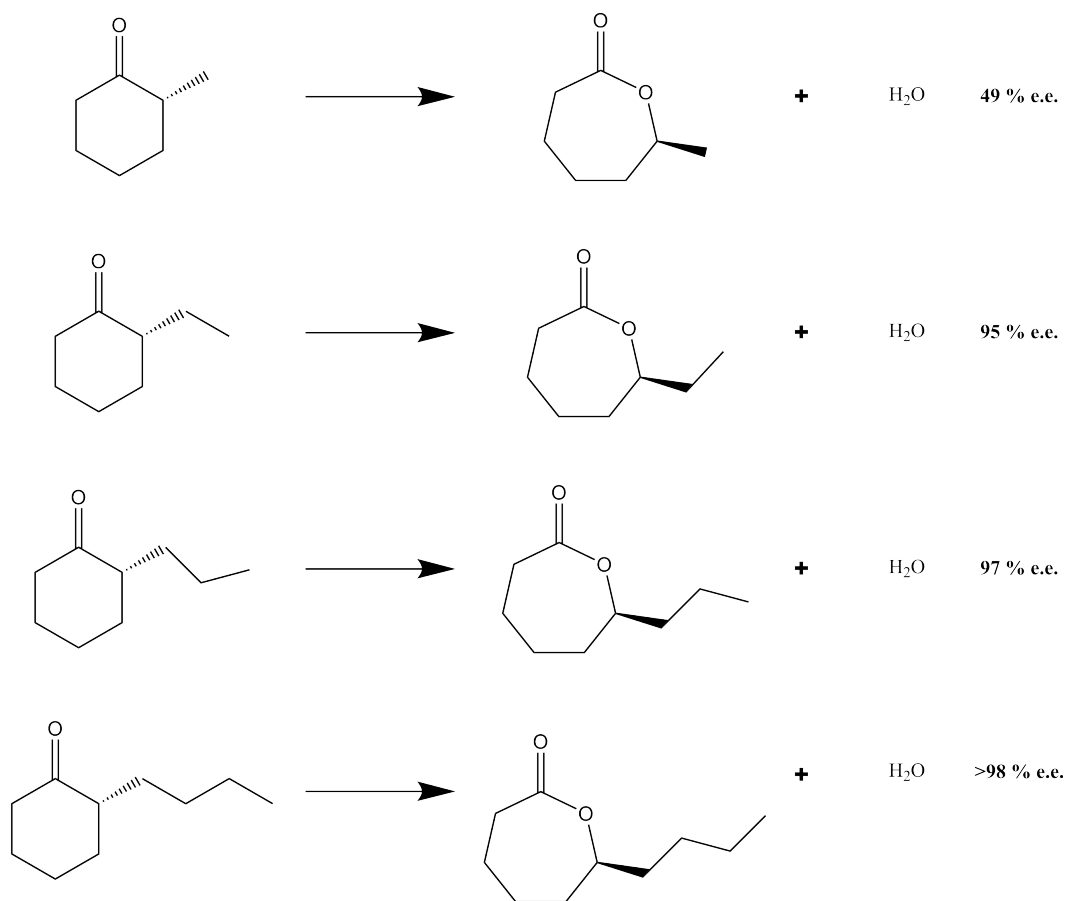


Figure 1.21: Enantioselective Transformations of CHMO

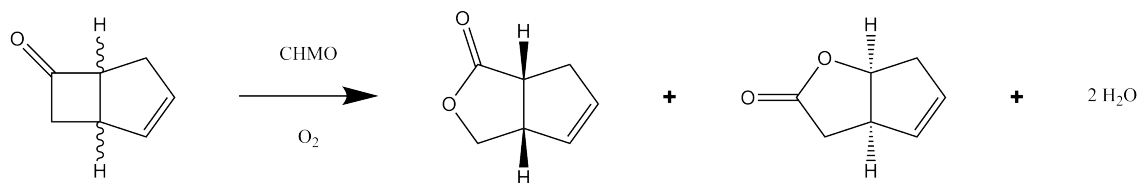


Figure 1.22: CHMO Transformation of bicyclo[3.2.0]hept-2-en-6-one

### Phenylacetone Monooxygenase

$CHMO_{Acineto}$  is of interest industrially owing to its broad range of substrates and high regio- and enantioselectivity against the majority of substrates. Industrial uses of enzymes tend to favour thermo-stability as this allows for higher rates of conversion. To this end, PAMO represents an



ideal target for industrial application. Discovered in 2005, it is so named due to its specificity towards phenylacetone, and the discovery was inspired by a genome annotation of the *T. fusca* genetic sequence.<sup>96</sup> On the discovery of this BVMO, initial trials were conducted with a range of potential BVMO substrates and showed good activity towards most aromatic ketone and long chain acyclic ketones. Comparison to CHMO<sub>Acineto</sub> shows significantly less activity toward cyclic aliphatic ketones, *e.g.* PAMO shows no activity towards the ideal substrate for CHMO<sub>Acineto</sub>, cyclohexanone.<sup>96,78</sup> PAMO also shows the ability to convert substrates in the presence of organic solvents,<sup>97</sup> which is again a very useful ability in organic synthesis.

The crystal structure of PAMO was solved in 2004<sup>81</sup> and was one of the key structures in identifying key structural features of BVMOs, allowing further BVMOs to be identified both structurally and by gene sequence. The structure, solved with the cofactor FAD bound, reveals the two expected domains: the FAD-binding and the NADPH-binding domains. Additionally, it shows that PAMO is natively a monomer and had a mass of 65 kDa, as well as the fact that the FAD is not bound covalently. This last detail was confirmed by denaturation with 3 M urea. An active site was postulated on the basis of the positioning of the FAD moiety between the two domains of the structure and also identifies the residue R337 as being of importance to the enzyme's function, due to the proximity of this residue to the catalytically active isoalloxazine ring of the FAD.

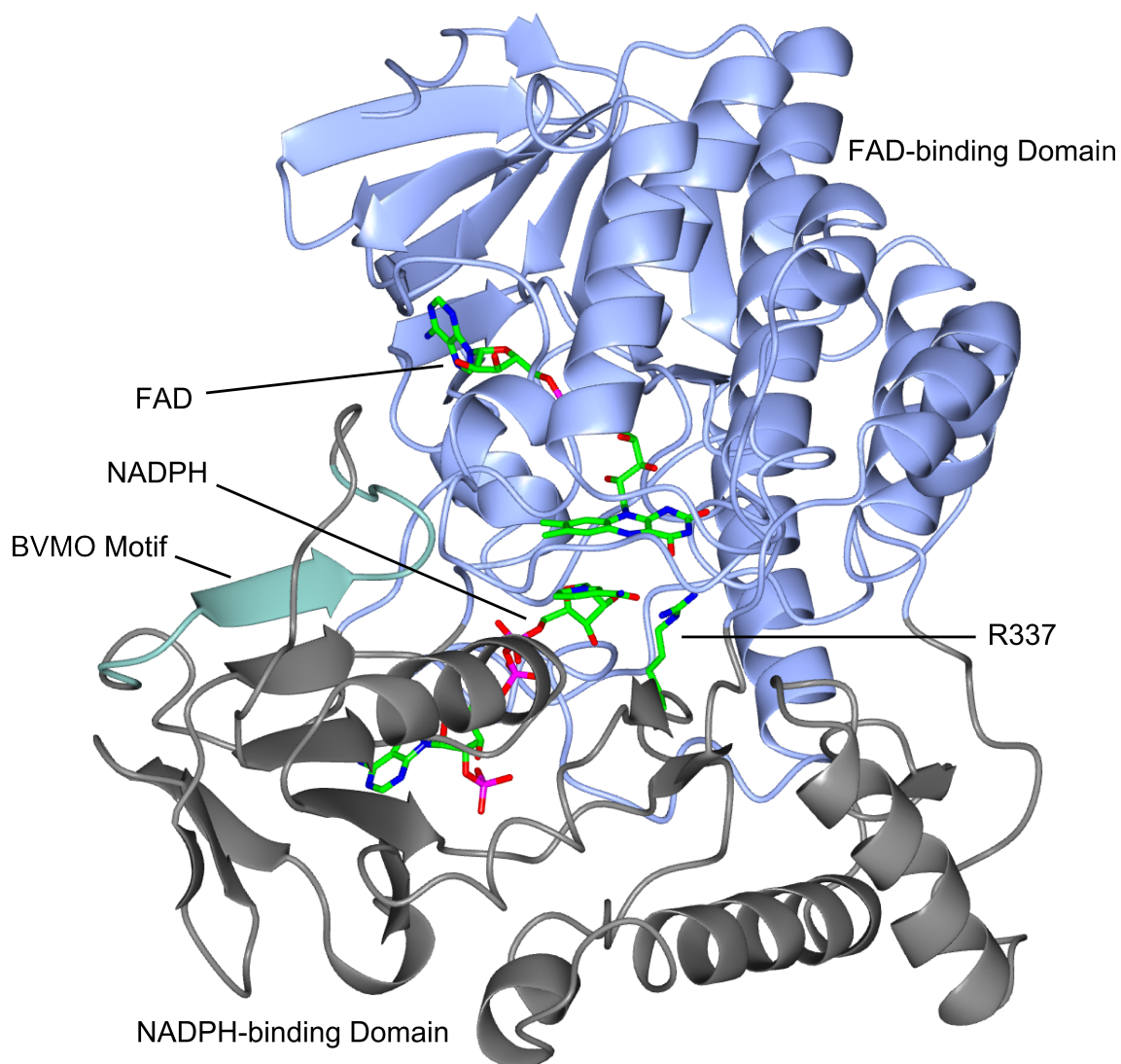


Figure 1.23: The structure of PAMO. PDB ref. 2YLR.

There are a number of potential explanations for the relevance of R337 to the activity of PAMO. One suggestion is that the negative charge developed during the reaction may be stabilised by the guanidinium group on the residue. Alternatively, this residue may occupy two positions and move between them - one to stabilise the reaction and one to permit FAD reduction by NADPH. This idea of two positions would seem to agree with the observation of significant movement of the NADP-binding domain in  $CHMO_{Rhod}$ , as this movement may be to remove R337 from the space

required for FAD reduction. This arginine residue is highly conserved amongst other BVMOs and this reinforces the suggestion that this residue is important to the BVMO activity. Interestingly, the standard BVMO motif is not located within the PAMO active site, although it had previously been thought to be a key factor in BVMO activity.<sup>81</sup>

### **1.2.5 Genetic Modification of Baeyer-Villiger Monooxygenases**

In recent years, there has been a significant push towards directed evolution of BVMOs to produce the desired activity. Generally, this procedure involves selecting a BVMO with desired properties and some amount of activity towards the relevant substrate, then random or directed mutagenesis experiments conducted. If necessary, the most active mutants are then taken and the process repeated until an acceptable level of activity toward the substrate or enantioselectivity of the biotransformation is achieved.

#### **Genetic Modification of PAMO to Induce Allostery**

A good example of mutating BVMOs is the experiment conducted by Wu *et. al.*,<sup>98</sup> in which the BVMO PAMO was modified to induce allostery to the enzyme. Allosteric effects involve the alteration of the properties of the active site of the enzyme by means of the docking of a molecule at a different site on the enzyme to the substrate-binding active site. There are many conditions that can result in the change of allosteric effects; including pH, ionic strength, temperature etc.; however the thermostability of PAMO and the solved X-ray structure of this enzyme make it an ideal target for mutagenesis-induced allostery. The thermostability makes PAMO an interesting target for industrial purposes, as higher temperatures will generally result in more efficient biotransformations, and the solved X-ray structure allows for informed selections of residues for targeted saturation mutagenesis, a more productive method of experiment design.

As mentioned before, PAMO accepts a very limited selection of substrates and an investigation of potential allosteric effects that could be induced by mutagenesis would be of interest. In choosing

a site for mutagenesis, the decision was made to focus on sites at the interface of domains; specifically the NADP-binding and FAD-binding domains, which should cause significant changes to the relative positions of these two domains. Based on the X-ray structure available,<sup>81</sup> the site chosen for randomisation is Gln93/Pro94, which represents a 'hot-spot' in the N-terminal region of an  $\alpha$  helix that could cause movement of the loop segment Trp177-Glu180. Simulations of the phenylacetone binding to PAMO suggest that the mutated residue would be approximately 18 Å from the substrate binding site; sufficiently far for changes to be attributed to allosteric effects rather than direct effects.

The mutations were conducted using NDT codon degeneracy, wherein the codons are mutated to an N (A, G, C or T), D (A, G or T) T sequence, and those selected were from the initial Gln93/Pro94 to any of the possible resultant twelve amino acids (Phe, Leu, Ile, Val, Tyr, His, Asn, Asp, Cys, Arg, Ser, and Gly). Of the approximately 400 transformants that were produced and analysed by GC for both activity and enantioselectivity against the substrate 2-ethylcyclohexanone, two were formed that could catalyse the conversion of the substrate within a 24 h period - Gln93Val/Pro94Phe and Gln93Asn/Pro94Asp. The second of these two proved to be the more active and was therefore selected for all further studies.

When tested for activity and enantioselectivity against a range of cyclohexanone derivatives, this mutant showed acceptance of a broad range of substituents on the cyclohexanone ring and more impressively a very high rate of enantioselectivity, achieving conversions from 11-45 % but e.e. values of greater than 85 % for all but the 4-methylphenyl derivative of cyclohexanone. It is also notable that the activity of PAMO towards the original substrate is not significantly impaired, with  $k_{cat}/K_m$  dropping from 32,000  $M^{-1}s^{-1}$  to 27,000  $M^{-1}s^{-1}$ .

This change represents a drop in activity, but clearly the ability of the enzyme to transform this substrate has not been wholly lost. Additionally, the thermostability of PAMO is reduced only slightly, dropping the temperature required to decrease activity by 50 % after incubation for 60

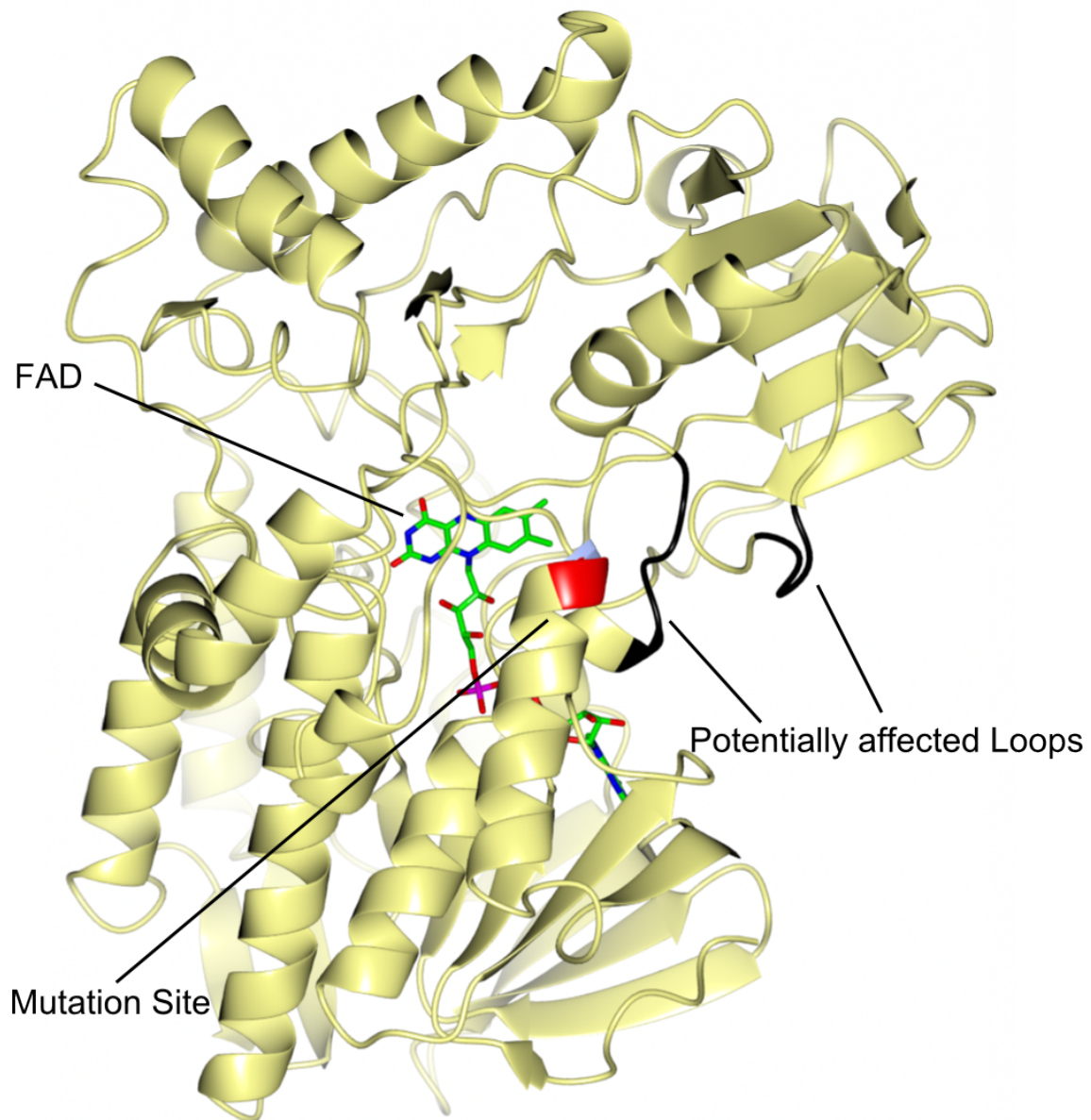


Figure 1.24: PAMO X-ray structure, with the mutation site shown in red, the potentially affected loops in black and the FAD and NADPH cofactors in cylinder form.<sup>81</sup> PDB no. 1W4X

minutes by only 2.0 °C.

This example shows that, although BVMOs are not generally thought of as allosterically controlled enzymes, it is possible to generate allosteric effects by means of mutagenesis. This conclusion is, perhaps, not surprising as BVMOs contain many of the characteristics that are observed in such enzymes, *i.e.* semirigid domains connected by flexible regions. Also, as the movement of cofactor-binding domains is essential for catalysis to occur in BVMOs,<sup>82</sup> the alteration of these domains by mutagenesis affecting the binding site of the substrate is similar to traditional allosteric effects. In conducting this experiment, the ability to generate different activities in BVMOs by means of mutagenesis is demonstrated.

#### **Genetic Mutation of CHMO<sub>Acineto</sub> to Improve Oxidative Stability and Thermostability**

CHMO<sub>Acineto</sub> represents a significant opportunity for industrial application of a BVMO, as the regio- and enantio-selectivity of this enzyme are generally exceptional, and it also shows activity against a wide range of substrates. In comparison to the previously studied PAMO, CHMO shows much higher yields in general than those observed for PAMO and would therefore be a preferable biocatalyst for synthetic purposes. For example, CHMO is able to transform the model substrate, bicyclo[3.2.0]hept-2-en-6-one with yields in excess of 75 %<sup>88</sup>, whereas wild-type PAMO reaches 50 %.<sup>99</sup> BVMOs are generally too unstable to manipulate outside of whole-cell conditions, however the expertise required to handle whole cells is not necessarily available in a synthetic or industrial environment, hence the need to improve the stability. Such an improvement would also benefit whole-cell reactions, as the catalytic lifetime would be increased and Opperman and Reetz therefore conducted a mutagenesis experiment designed to improve the stability and therefore the utility of CHMO<sub>Acineto</sub> in large-scale synthetic processes.<sup>100</sup>

During the biotransformation process, it is possible for the peroxyflavin moiety to degrade and form hydrogen peroxide if the substrate is not available.<sup>101</sup> Hydrogen peroxide is a potent cause

of oxidation and major sites for protein oxidation are available sulfur atoms in methionine and cysteine, the oxidation of which can lead to inactivation of the enzyme and mutation thereof can increase stability.<sup>102,103</sup> In addition to the negative effects of binding to these residues in the active site, the activity can be compromised by effects over a distance<sup>104</sup> and mutation of these residues may also improve thermostability, as both the production of oxidant and the rate of the oxidation reaction will be more rapid at higher temperatures.

As there are no Cys or Met residues that are conserved in both PAMO and CHMO<sub>Acineto</sub>, standard site-directed mutagenesis was conducted on all sulfur-containing residues in CHMO<sub>Acineto</sub> converting the residues to small hydrophobic side-chains. 96 clones were generated and several mutations that resulted in a significant increase in oxidative stability, confirmed by incubation with H<sub>2</sub>O<sub>2</sub>, or thermostability, confirmed by incubation at 37 °C for 1 h. One residue in particular, Cys330, granted a large increase in both oxidative and thermostability when mutated and, when mutated to leucine, also shows comparable activity to the wild-type CHMO<sub>Acineto</sub>.

Identified single-site mutations were then combined into multiple mutants, generating a number of mutants, two of which were selected for further investigation: MUT16, which had the mutations Met-5-Ile, Met-291-Ile, Cys-330-Ser, Cys-376-Leu, Met-412-Ile, Met-481-Ala and Cys-520-Val; and MUT15, which contained the same mutations as MUT16 and additionally Met-400-Ile. These two mutants were selected due to their high thermostability, as they both retained close to 100 % activity relative to wild type after incubation at 38 °C for 1 h, and additionally due to their high oxidative stability; both showing >40 % activity after incubation with 100 mM H<sub>2</sub>O<sub>2</sub>. MUT15 retains almost full activity until the incubation temperature was increased to >45 °C, at which point activity dropped rapidly, whereas MUT16 showed gradual decrease in activity as incubation temperature increased above 38 °C. For comparison, the activity of the wild type begins to degrade above 30 °C and is completely lost by 38 °C. With respect to oxidative stability, MUT16 is particularly improved, maintaining about 40 % activity after incubation with a 6 x 10<sup>4</sup> molar excess of

H<sub>2</sub>O<sub>2</sub>, whereas the wild type CHMO loses all activity after incubation with 5 mM H<sub>2</sub>O<sub>2</sub>.

Considering the effect that these mutations have on substrate scope and specificity, as well as selectivity, is also important. The two combinatorial mutants were therefore compared to the wild type enzyme with respect to a range of 2- and 4- substituted cyclohexanone derivatives, as well as the model BVMO substrate, bicyclo[3.2.0]hept-2-en-6-one. Neither mutant had any observed effect on either the activity compared to wild type, nor the selectivity, ratio of 'normal' to 'abnormal' lactones, or stereoselectivities, indicating that these mutants represent very convenient modifications to the wild type CHMO<sub>Acineto</sub>.

Regrettably, it seems that although there is some overlap in the mutations that improve thermostability and oxidative stability, there is some amount of separation between achieving these two goals. This effect is magnified when mutations are combined, as can be observed by the addition of the Met-400-Ile mutation to MUT15, which results in a significant loss in oxidative stability for a relatively less significant increase in thermostability. The observation that some mutations confer increases to both characteristics has previously been observed<sup>105,106</sup> however, the improvement of two characteristics simultaneously is challenging and it is possible that less than optimal routes must be selected for similar endeavours.<sup>107</sup>

These two examples of the manipulation of BVMOs to provide either an increase in substrate scope, in the case of PAMO, or an improvement to the physical characteristics of the enzyme, as for CHMO<sub>Acineto</sub>, demonstrate the flexibility this class of enzyme to be used for a wide range of applications. In addition to these two examples, a broad selection of other BVMOs exists across an expansive selection of potential substrates. These biocatalysts represent a much improved reaction profile in terms of necessary reactants, efficiency, stereoselectivity and ecological soundness.



### 1.2.6 Industrial Application of BVMOs

BVMOs represent an ideal target for industrial applications owing to the high selectivity that can be obtained, in addition to practical benefits such as the reduced need for expensive catalysts and ecological benefits from the use of less harsh reaction conditions.

#### Isolated Enzyme Systems

The use of isolated BVMOs has been studied mostly for CHMO<sub>Acineto</sub>, which represents the Type I BVMOs and therefore requires a regeneration system for the NADPH cofactor. The necessity of a cofactor and the subsequent regeneration system represents one of the key obstacles to a useful industrial process. As the cofactor is expensive and used in stoichiometric quantities, non-regenerative approaches are unviable on financial grounds. Several different systems have been examined, including a mutated formate dehydrogenase enzyme;<sup>108</sup> an alcohol dehydrogenase, which itself forms a substrate for CHMO<sub>Acineto</sub>;<sup>109</sup> and the most common example, the glucose-6-phosphate/glucose-6-phosphate dehydrogenase system.<sup>110</sup> These systems work alongside the Baeyer-Villiger monooxygenase, conducting a redox reaction using NADP<sup>+</sup> to dehydrogenate their substrate, which reforms the needed NADPH.

Although excellent results can be obtained by the use of these methods, the use of a cofactor regeneration system is rarely ideal, as the systems themselves can often prove expensive and similar results can be obtained by the use of whole cell techniques. Nevertheless, an example of the capabilities of this type of system is valuable. An efficient, one-pot conversion of cyclohexanol to caprolactone was effected by the use of alcohol dehydrogenase to transform the cyclohexanol to cyclohexanone, followed by a Baeyer-Villiger reaction by CHMO<sub>Acineto</sub> with overall 94-97 % conversion with reactant concentration of 60 mM.<sup>111</sup> This transformation compares favourably to the chemical process, in that it does not require the generation of a peracid *in situ* and maintains a selectivity greater than the 85-90 % in the chemical process.

## Whole-Cell Systems

The use of a whole-cell catalyst allows the reaction to be conducted without the need for expensive cofactors and regeneration systems, as the host organism itself is exploited for the native regeneration and cofactor supply. The majority of investigation into BVMO applications on a whole-cell basis at large scale has been conducted with CHMO<sub>Acineto</sub>, as it was this enzyme that revealed the potential for whole-cell biotransformations,<sup>112</sup> and these experiments face a number of obstacles. The most well-studied of substrates is bicyclo[3.2.0]hept-2-en-6-one, as the model BVMO substrate, and this discussion will focus on biotransformations of this substrate. Two of the main issues that must be resolved for this process to be applicable industrially are the inhibition of BVMOs by substrate and product and also issues of product recovery.

The substrate and product inhibition are well-described in work conducted on kinetic study of CHMO<sub>Acineto</sub>, wherein the optimum substrate concentration was revealed to be just 0.2-0.4 g L<sup>-1</sup>, or approximately 2 mM.<sup>113</sup> This compares very poorly to the isolated enzyme systems, and motivated the use of an *in situ* substrate feeding and removal process. Additionally, the use of such a system should result in the relief of product inhibition, which reduced the specific activity of the enzyme to zero at concentrations of 4.5-5.0 g L<sup>-1</sup>.

Such a system has been described and involves the use of an adsorbent resin, onto which the substrate, bicyclo[3.2.0]hept-2-en-6-one, is loaded and then applied to the whole cell solution. This resulted in the conversion of the substrate to a yield of 75-80 %.<sup>88</sup> The use of a substrate feeding system has since led to the 200 L scale biotransformation of the same substrate by CHMO<sub>Acineto</sub>.<sup>114</sup> In this case, cells are fermented to generate a large quantity of protein, harvested and subsequently used for biotransformation. The substrate is fed in at a rate low enough to maintain the activity of biocatalyst and product inhibition was maintained negligible by ensuring that overall substrate applied was kept below potentially harmful levels. Although this has been successful on a relatively

large scale, it is important to note two issues that may become more significant on an industrial, *i.e.* 1,000 L+, scale and these are oxygen availability and substrate mixing.

### **1.3 Conclusions**

Ultimately, the use of classical Baeyer-Villiger oxidations on the industrial scale is hampered by the ecological, safety and selectivity issues involved in this course of development. When a simple and well-studied biological method for conducting the reaction exists, it is difficult to justify the investigation of non-enzymatic pathways in preference to the biological alternative, which uses safe and ecologically sound oxidants. It is possible, however, that for particular substrates, the time barrier to development of a BVMO by genetic engineering may be significant enough that it becomes preferable to investigate classical routes, although these cases will become rarer as more BVMOs, and therefore more potential substrates, are characterised.

### **1.4 Project Aims**

The aims of this PhD project are to investigate the potential for industrial application of Baeyer-Villiger monooxygenase enzymes derived from the species *Rhodococcus jostii* sp. RHA1. Particular attention will be paid to the enzyme named MO14, encoded by the gene *ro03437*, as it has previously been shown to possess exceptional regio- and enantioselectivity against the model BVMO substrate, bicyclo[3.2.0]hept-2-en-6-one. The study of this enzyme will involve:

Work towards purification with the intention of a subsequent X-ray crystal structure, detailed in Chapter 3: Purification.

An investigation of the biotransformational capabilities of these enzymes, detailed in Chapter 4: Biotransformations.

A small-scale fermentation study of the biotransformation of the model reaction for MO14, detailed in Chapter 5, Fermentations.

A mutation-based study of the origin of regioselectivity in MO14 will also be conducted, detailed in Chapter 6: Mutations.

## Chapter 2

# Materials and Methods

The Baeyer-Villiger monooxygenase *ro03437* named MO14, along with 22 other Baeyer-Villiger monooxygenases, from *Rhodococcus jostii* sp. RHA1, were investigated for their potential use in industrial synthesis of pharmaceutically useful compounds.

This chapter describes the production of the enzymes; the biotransformation tests, both whole-cell and fermentation, used to determine activity, regio- and enantioselectivity; the mutation procedures and all other experiments used to conduct the research that follows.

### 2.1 General Methods

This section describes procedures used across multiple areas of this project, *e.g.* agarose gel electrophoresis, SDS-PAGE, transformation of competent *E. coli* and gas chromatography.

#### 2.1.1 Agarose gel electrophoresis

DNA samples were analysed by agarose gel electrophoresis. Electrophoresis-grade agarose and SybrSafe DNA gel stain were purchased from Invitrogen. A 1 kb ladder, used as a standard marker in these gels, was purchased from New England Biolabs as well as the DNA loading buffer.

A typical 0.75 % agarose gel consisted of 0.75 g of agarose, 100 mL of TAE buffer and 2  $\mu\text{L}$  10,000x SybrSafe DNA gel stain. Samples for analysis were prepared using 6x DNA gel loading buffer, exact amount varying depending on the volume of sample to be analysed, *e.g.* 2  $\mu\text{L}$  added to 10  $\mu\text{L}$  of sample, 10  $\mu\text{L}$  added to 50  $\mu\text{L}$  of sample. Marker was prepared with 6  $\mu\text{L}$  distilled water, 1.5  $\mu\text{L}$  DNA loading buffer, and 1.5  $\mu\text{L}$  1 kb ladder, resulting in a solution containing 0.75  $\mu\text{g}$  of DNA. Electrophoresis was conducted at 100 V for 1 hour in TAE buffer and the DNA detected using a SYNGENE-UV imager.

TAE buffer: 40 mM Tris/acetate, 2 mM EDTA, pH 7.9

DNA Loading Buffer:

### **2.1.2 SDS-Polyacrylamide Gel Electrophoresis:**

12 % polyacrylamide gel was prepared by mixing purified water, resolving buffer and acrylamide then adding ammonium persulfate and tetramethylethylenediamine (TEMED) to catalyse polymerisation. This was poured into a gel stand and allowed to set, with a layer of butanol on top to ensure a flat surface to the gel. Once set, another gel of lower acrylamide concentration was prepared and allowed to set on top of the resolving gel. A gel comb was inserted into the stacking gel before it set to form wells into which the protein could be loaded. This 'stacking' gel ensures that all of the proteins reach the resolving gel at the same time and are thus resolved equally. The samples are mixed with loading buffer and heated to 94 °C to denature the protein, which ensures roughly equal charges will be present for all of the samples. The gel is submerged in running buffer and the samples, along with a protein marker, loaded into wells in the stacking gel. The gel is then run at 200V for 50 minutes.

After the gel has run, the stacking gel is removed and the resolving gel stained. This is done by submerging it in coomassie blue stain and microwaving for one minute then rocking for thirty minutes. The coomassie blue is then removed and the gel washed in distilled water. Destain is then

added, microwaved for one minute and rocked for thirty minutes.

12 % Resolving Gel (2 gels):

3.2 mL Sterile deionised water

2.5 mL Resolving buffer

4.5 mL Acrylamide

50  $\mu$ L 10 % w/v Ammonium Persulfate

8  $\mu$ L Tetramethylethylenediamine

Stacking Gel (2 gels):

3.2 mL Sterile deionised water

1.3 mL Stacking buffer

0.5 mL Acrylamide

25  $\mu$ L 10 % w/v Ammonium persulfate

8  $\mu$ L Tetramethylethylenediamine

8  $\mu$ L Bromophenol blue - to aid visualisation of wells.

Loading Buffer (10 mL):

4.8 mL Sterile deionised water

1.2 mL 0.5 M Tris (pH 6.8)

1.0 mL Glycerol

2.0 mL 10 % w/v SDS

0.5 mL 0.1 % w/v/ Bromophenol blue

0.5 mL  $\beta$ -mercaptoethanol

Running Buffer:

125 mL of a 10 L stock containing 576 g Glycine and 120 g Tris

5 mL 10 % w/v Sodium dodecyl sulfate

310 mL Deionised water

Coomassie Blue Stain (2 L):

4 g Coomassie brilliant blue

500 mL Propan-2-ol

200 mL Glacial acetic acid

1300 mL Deionised water

Destain (5 L):

250 mL Propan-2-ol

350 mL Glacial acetic acid

4400 mL Deionised water

### **2.1.3 Transformation of chemically competent *E. coli***

Kanamycin sulphate was purchased from Invitrogen, chloramphenicol from Sigma, LB medium ingredients from Fisher Scientific and LB-agar from LAB M Ltd. Chemically competent *E. coli* Rosetta<sup>TM</sup>2 (DE3) pLysS, *E. coli* XL-10 Gold and *E. coli* BL21 were purchased from Merck, Agilent and Novagen respectively. Ingredients for LB medium were purchased from Fisher Scientific and agar from LAB M Ltd.

50  $\mu\text{L}$  of chemically competent *E. coli* were thawed on ice, then 1  $\mu\text{L}$  of plasmid was added under sterile conditions. The mixture was incubated on ice for 30 minutes, then subjected to a heat shock at 42 °C for 45 seconds. The cells were then returned to the ice for 2 minutes, then added to 1 mL LB under sterile conditions, before incubation at 37 °C for 1 hour. *E. coli* BL21 cells were then plated onto LB agar containing 100  $\mu\text{g mL}^{-1}$  ampicillin and 30  $\mu\text{g mL}^{-1}$  kanamycin. *E. coli* Rosetta<sup>TM</sup>2 (DE3) pLysS and *E. coli* XL-10 Gold cells were plated onto LB agar containing 30



$\mu\text{g mL}^{-1}$  kanamycin and  $34 \mu\text{g mL}^{-1}$  chloramphenicol.

LB Medium (1 L): 10 g tryptone, 5 g yeast extract, 10 g NaCl, deionised H<sub>2</sub>O. LB agar (1 L): 10 g tryptone, 5 g yeast extract, 10 g NaCl, 15 g agar, deionised H<sub>2</sub>O.

#### **2.1.4 DNA Restriction Digest:**

500 ng of plasmid DNA, concentrated to  $70 \text{ ng}/\mu\text{L}$ , was added to  $10 \mu\text{L}$  deionised water containing  $1 \mu\text{L}$  of a 10x stock of NEBuffer4,  $1 \mu\text{L}$  of a 10x stock of NcoI and  $1 \mu\text{L}$  of a 10x stock of NdeI. These were mixed in a  $500 \mu\text{L}$  Eppendorf tube and gently mixed. This solution was then incubated at  $37^\circ\text{C}$  for three hours and analysed by 1 % agarose gel electrophoresis.

NEBuffer4:

50 mM Potassium acetate

20 mM Tris-acetate

10 mM Magnesium acetate

1 mM Dithiothreitol

pH 7.9

#### **2.1.5 Starter Cultures**

5 mL of LB medium containing the relevant antibiotic was inoculated with a colony of bacteria under sterile conditions, then incubated at  $37^\circ\text{C}$  for 18 hours.

#### **2.1.6 Protein Expression**

A 5 mL starter culture of, for example, *E. coli* Rosetta<sup>TM</sup>2 (DE3) pLysS was added to 500 mL LB medium containing  $30 \mu\text{g mL}^{-1}$  kanamycin and  $34 \mu\text{g mL}^{-1}$  chloramphenicol under sterile conditions. This was then incubated at  $37^\circ\text{C}$  until the OD<sub>600</sub> reached approximately 0.8, confirmed

by spectrophotometer. At this point, production of protein was initiated by addition of IPTG to a final concentration of 1 mM under sterile conditions, followed by incubation at 16 °C for 18 hours. At this point, cells were pelleted by centrifugation at 4,225 x g in a Sorvall GS3 rotor in a Sorvall RC5B Plus centrifuge, resuspended in Buffer R and sonicated to lyse the cells. The lysed cells were sonicated at 24,676 x g for 20 minutes to remove cell debris, yielding clear cell lysate.

Buffer R:

10 mM Sodium dihydrogen phosphate

40 mM Disodium hydrogen phosphate

15 % v/v Glycerol

Sterile deionised water

### 2.1.7 Achiral GC Analysis:

Analysis was carried out on an Agilent Technologies 6890N gas chromatograph with an HP-5 column (30 m x 0.32 mm x 0.25  $\mu$ m). The carrier gas used was helium, at 83 kPa, with injector temperature of 250 °C and detector temperature of 320 °C. The conditions for each substrate analysis are shown below.

Table 2.1: Achiral GC Conditions.

Substrate	Temperature (°C)	Retention Time of Substrate (Minutes)	Retention Time of Product (Minutes)
Bicyclo[3.2.0]hept-2-en-6-one	130	1.8	3.1
Methyl Phenyl Sulfide	180	2.0	3.3
Methyl p-tolyl Sulfide	150	2.4	4.6
2-Chloro Thioanisole	180	2.2	3.0
3-Chloro Thioanisole	180	2.2	3.0
4-Chloro Thioanisole	180	2.2	3.0
4-Nitro Thioanisole	180	2.6	3.6
Benzyl Methyl Sulfide	150	2.3	5.1
Ethyl Phenyl Sulfide	180	1.9	3.0
2-Methoxy Thioanisole	180	2.3	3.7
4-Fluoro Thioanisole	150	1.9	3.1
2-Methylthio-Pyridine	180	1.8	2.3
4-Methoxy Thioanisole	180	2.3	3.9

In order to determine concentrations of bicyclo[3.2.0]hept-2-en-6-one directly from the GC data, a series of dilutions of both the substrate and lactone product in ethyl acetate were generated and used to produce conversion curves that would allow simple conversion of GC Response (pA) to concentration (mM). These curves are shown in Figures 2.1 and 2.2.

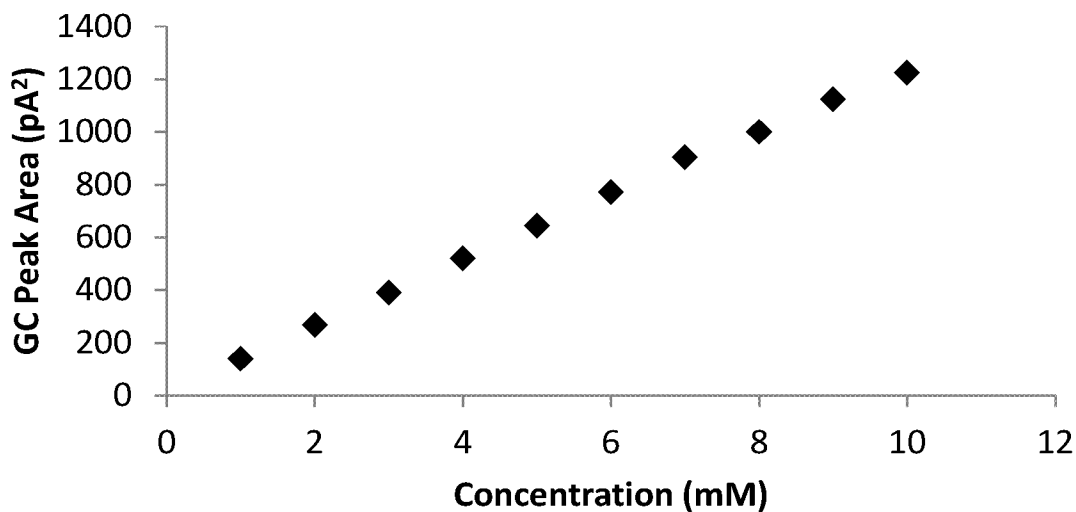


Figure 2.1: The GC calibration curve for bicyclo[3.2.0]hept-2-en-6-one.

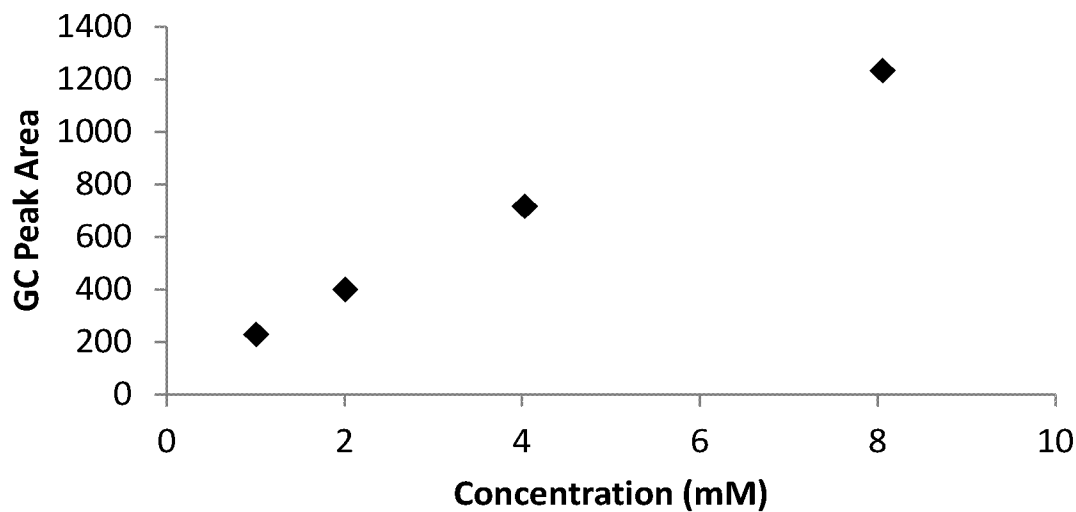


Figure 2.2: The GC calibration curve for 2-oxa-bicyclo[3.3.0]oct-6-en-3-one.

The sulfide conversions were calculated directly from GC peak area as a ratio of substrate peak to product peak.

### 2.1.8 Chiral GC Analysis:

Analysis was carried out on an Agilent Technologies 6890N gas chromatograph with a BGB-175 column (30 m x 0.32 mm x 0.25  $\mu$ m). The carrier gas used was helium, at 83kPa, with injector temperature of 250 °C and detector temperature of 320 °C. The conditions for each substrate analysis are shown below. No conversions to concentration were conducted, as all calculations were to be comparing one isomer peak to another, hence they are directly comparable.

Table 2.2: Chiral GC Conditions. \*: No assignment of *R/S*- enantiomers yet achieved

Substrate	Temperature (°C)	Retention Time of <i>R</i> -Enantiomer Product (Minutes)	Retention Time of <i>S</i> -Enantiomer Product (Minutes)
Bicyclo[3.2.0]hept-2-en-6-one	180	41.8	42.1
Methyl Phenyl Sulfide	180	12.8	14.2
Methyl p-tolyl Sulfide	180	14.7	15.0
2-Chloro Thioanisole	180	17.8	19.5
3-Chloro Thioanisole	180	20.5*	24.9*
4-Chloro Thioanisole	180	21.1	22.5
4-Nitro Thioanisole	180	-	-
Benzyl Methyl Sulfide	140	146.0	142.0
Ethyl Phenyl Sulfide	180	13.3	14.3
2-Methoxy Thioanisole	180	24.9*	32.6*
4-Fluoro Thioanisole	180	11.7*	12.8*
2-Methylthio-Pyridine	180	12.5*	13.0*
4-Methoxy Thioanisole	180	29.4*	31.4*

## 2.2 Biotransformations

### 2.2.1 Plasmid Miniprep

All 23 Baeyer-Villiger monooxygenases from *N. farcinica* as well as CHMO<sub>Acineto</sub> had previously been cloned by Szolkowy<sup>115</sup> and were miniprepped to ensure consistency of material throughout the project. Each of the genes encoding these proteins were available in the YSBLIC-3C vector and were transformed into *E. coli* Rosetta<sup>TM</sup>2 (DE3) pLysS, in the case of the BVMOs from *N.*

*farcinica*, or *E. coli* BL21 for CHMO. Starter cultures were then generated from these transformants and used to produce high quantities of the plasmids by means of a Qiagen Plasmid Miniprep Kit.

### **2.2.2 Cell Stock Production:**

Clones of the target genes in the pET-YSBLIC-3C vector were sourced from previous work by Szolkowy and expressed using the bacterial strain *E. coli* Rosetta 2 (DE3) pLysS. Bacteria were grown on LB agar plates containing 60  $\mu$ M kanamycin and 105  $\mu$ M chloramphenicol overnight at 37 °C, then stored at 4 °C for a maximum of two weeks. Cell stocks were created from the 500 mL growths in LB broth, again containing 60  $\mu$ M kanamycin and 105  $\mu$ M chloramphenicol, with a 2 % inoculum from an overnight culture of the relevant strain. Cells were grown at 37 °C to an OD of 0.6, then induced with 1 mM isopropyl- $\beta$ -D-thiogalactopyranoside and grown overnight at 20 °C. The 500 mL cultures were pelleted, then resuspended in Buffer R at an OD of  $\sim$ 20 and frozen at -80 °C in 1mL aliquots.

### **2.2.3 Whole Cell Biotransformations:**

50 mg of substrate was dissolved in 5 mL of ethanol, then 10  $\mu$ L of the solution added to one 1 mL cell stock aliquot, yielding a final concentration of 1 % (v/v) ethanol. These were then incubated at 30 °C with shaking and samples taken after 2 h and 24 h. The product was extracted using a 1:1 ratio ethyl acetate to produce a 0.5 mL sample, which was analysed by GC.

### **2.2.4 MO14 Sulfide Biotransformations:**

Cells containing MO14 were prepared following the Cell Stock Production method above but, rather than being frozen, the 500 mL culture pellets were subjected to sonication at 20 microns for 30 seconds, then left on ice for 30 seconds. This was repeated twice, then the cell lysate was centrifuged at 24,676 x g for 20 minutes. The pellet from this was discarded and the supernatant

filtered through a 0.8  $\mu\text{m}$  syringe filter to generate approximately 50 mL of clarified cell lysate per 1 L of cell culture media. 1 mL of this clarified cell lysate was then added to an NADPH regeneration system and 1 mg sulfide in 50  $\mu\text{L}$  ethanol. This was placed in a 30 °C incubator for 24 hours, before the product was extracted using a 1:1 ratio ethyl acetate to produce a 0.5 mL sample, which was analysed by GC.

NADPH Regeneration System:

1 mg NADPH

0.52 mg Glucose-6-phosphate

0.14 mg Glucose-6-phosphate dehydrogenase

## **2.3 Purification**

### **2.3.1 Nickel Ion Affinity Chromatography:**

HiTrap Chelating HP 5 mL column purchased from GE Healthcare Life Sciences, NaCl purchased from Fisher Scientific and EDTA and imidazole purchased from Sigma. Cells were prepared according to the cell stock production procedure, but resuspended in buffer A, rather than buffer R. They were then placed on ice and sonicated for 3 x 30 seconds, with 30 second pauses between sonications. The lysed cells were then centrifuged at 12k rpm for 20 minutes and the pellet discarded. The supernatant was filtered through a 0.45  $\mu\text{m}$  syringe filter, followed by a 0.22  $\mu\text{m}$  filter and kept on ice. A HiTrap 5 mL Chelating HP column was prepared for nickel ion affinity chromatography according to the following steps, using a peristaltic pump:

1. Wash with 20 mL deionised water.
2. Wash with 20 mL of a solution containing 0.1 M EDTA and 0.5 M NaCl
3. Wash with 20 mL 0.5 M NaCl.
4. Wash with 20 mL deionised water.

5. Charge column with 20 mL 0.1 M NiSO<sub>4</sub> · 6 H<sub>2</sub>O.
6. Wash with 20 mL deionised water.
7. Wash with 20 mL Buffer A.
8. Load filtered protein, reserving an SDS-PAGE gel sample.
9. Wash with 20 mL Buffer A.

The column was then attached to an FPLC machine and a gradient run from buffer B into buffer C, after a buffer B wash step. The imidazole, at sufficient concentration, displaced the protein from the nickel ions due to having a higher affinity for them. Hence, 4 mL fractions were collected and assessed for protein content by SDS-PAGE.

Buffer A:

300 mM NaCl

50 mM Tris/HCl

pH 7.5

Buffer B:

300 mM NaCl

50 mM Tris/HCl

30 mM Imidazole

pH 7.5

Buffer C:

300 mM NaCl

50 mM Tris/HCl

500 mM Imidazole

pH 7.5

### **2.3.2 Ion Exchange Chromatography:**

Cell lysate was prepared according to the nickel ion affinity purification procedure, but resuspended in buffer containing only 50 mM Tris/HCl (pH 7.5). A HiLoad 26/10 column was loaded with FF Q Sepharose, purchased from GE Healthcare Life Sciences, and equilibrated into 50 mM Tris at pH 7.5 using an FPLC machine. The filtered protein was loaded onto the column via a loop attached to the FPLC and the column was then run from buffer containing 0 M NaCl to 1 M NaCl. 4 mL fractions were collected and assessed for protein content by SDS-PAGE.

### **2.3.3 Sepharose Blue Chromatography:**

Cell lysate was prepared according to the nickel ion affinity purification procedure, but resuspended in buffer containing only 50 mM Tris/HCl (pH 7.5). A HiTrap 5 mL Blue HP column, purchased from GE Healthcare Life Sciences, was prepared for use by washing with 20 mL 0.1 M NaOH, followed by 20 mL deionised water. The filtered protein was loaded onto the column via a peristaltic pump, then transferred to an FPLC machine. The column was then run from buffer containing 0 M NaCl to 1 M NaCl, and 4 mL fractions were collected and assessed for protein content by SDS-PAGE.

### **2.3.4 Ammonium Sulfate Precipitation:**

After cell lysate was produced by the method outlined in the Ion Exchange Chromatography procedure, the supernatant was transferred to a 250 mL conical flask and a magnetic stirrer bar added. The flask was placed on a stirrer and ammonium sulfate slowly added until the saturation was 30 %. This was left stirring, covered, for an hour to allow protein to precipitate, before being centrifuged at 12k rpm for 20 minutes and the supernatant returned to the conical flask. The pellet was kept at 4 °C. This procedure was repeated for 50 % and 80 % ammonium sulfate saturation, and the



pellets resuspended in a minimum of buffer. The resuspended pellets, along with any remaining unpelleted protein, were analysed by SDS-PAGE.

### **2.3.5 Hydrophobic Interaction Chromatography:**

The pellets from the ammonium sulfate precipitation containing the most protein were taken and filtered through a 0.45  $\mu\text{m}$  syringe filter, followed by a 0.22  $\mu\text{m}$  filter and kept on ice. A HiLoad 26/10 column was loaded with Phenyl Sepharose, purchased from GE Healthcare Life Sciences, and equilibrated into 50 mM Tris at pH 7.5 using an Äkta machine. The filtered protein was loaded onto the column via a 2 mL loop attached to the Äkta and the column was then run on a gradient from buffer containing 1.7 M ammonium sulfate to buffer containing 0 M ammonium sulfate. 4 mL fractions were collected and assessed for protein content by SDS-PAGE.

### **2.3.6 C-terminal Cloning:**

The MO14 gene was to be recloned into a C-terminally tagged vector in order to investigate the effect this would have on nickel affinity purification.

#### **Plasmid Digest**

The pET-22b(+) plasmid was digested with NdeI and EcoRI at 37 °C for 3 hours, then analysed by agarose gel. Reaction:

3  $\mu\text{L}$  10x NEBuffer 4

1  $\mu\text{L}$  NdeI

1  $\mu\text{L}$  EcoRI

2 mg plasmid

H<sub>2</sub>O to 30  $\mu\text{L}$

The results of this digest were then analysed by agarose gel and the digested vector extracted using a Qiagen Gel Extraction Kit.

## Gene Insert Generation

NdeI, EcoRI, NEBuffers, T4 Ligase and Buffer purchased from New England Biosciences, KOD DNA Polymerase and Buffer purchased from Merck Millipore. The MO14 gene to be inserted was subjected to PCR in order to produce sufficient insert for cloning. Primers were designed to ensure successful overlap with the pET-22b(+) plasmid and were as follows, with the restriction sites in bold font:

Forward: GCA AGT GTC **ATA TGT** CAA AGA CCA TTT CTG CCG ACG TCG ACG T

Reverse: TCT GAT AAG **AAT TCG** GAC ACG GTG GAG GCC GCG CGG GC

The PCR reaction was performed as follows:

5  $\mu$ L 10x KOD DNA Polymerase Buffer

5  $\mu$ L 2 mM dNTPs

3  $\mu$ L 25 mM MgSO<sub>4</sub>

2.5  $\mu$ L DMSO

1  $\mu$ L YSBLIC-3C plasmid containing MO14 gene

1  $\mu$ L Forward primer (20 pmol  $\mu$ L<sup>-1</sup>)

1  $\mu$ L Reverse primer (20 pmol  $\mu$ L<sup>-1</sup>)

H<sub>2</sub>O to 50  $\mu$ L

PCR Program:

Table 2.3: MO14 Insert PCR for C-terminal Cloning.

Step	Time	Temperature	Repeats
Initial Denature	2 min	94 °C	
Denature	30 sec	94 °C	35
Anneal	30 sec	60 °C	
Extend	30 sec	72 °C	
Final Extend	3 min	72 °C	

The PCR results were analysed by agarose gel and the insert bands extracted with a Qiagen Gel Extraction Kit. The insert was then digested with NdeI and EcoRI at 37 °C for 1 hour as follows:

3  $\mu$ L 10x NEBuffer 4

1  $\mu$ L NdeI

1  $\mu$ L EcoRI

1 mg insert

H<sub>2</sub>O to 30  $\mu$ L

The results of this digest were then analysed by agarose gel and the digested insert extracted using a Qiagen Gel Extraction Kit.

#### **Ligation**

The digested pET-22b(+) vector and digested MO14 gene insert were ligated at 15 °C overnight as follows:

1  $\mu$ L 10x T4 DNA Ligase Buffer

1  $\mu$ L 10 mM ATP

1  $\mu$ L T4 DNA Ligase

3:1 molar ratio insert:plasmid

H<sub>2</sub>O to 10  $\mu$ L

The ligated plasmids were transformed into *E. coli* XL-10 Gold, plated onto LB agar and grown at 37 °C overnight. The colonies were then used to miniprep the cloned plasmid.

### **2.3.7 MO14 Degradation Experiment**

Cell lysate containing MO14 was produced as previously detailed, with the exceptions that the resuspension buffer for the pelleted cells contained either 1 mM AEBSF or a protease inhibitor

cocktail tablet, both purchased from Sigma. The cell lysate samples were then incubated at 4 °C overnight and samples taken hourly for analysis by SDS-PAGE.

### **2.3.8 Calcium Precipitation Purification**

MO14 was cloned into the pMAL-BRT<sub>17</sub> vector prior to a purification attempt using the newly-generated protein.

#### **pMAL-BRT<sub>17</sub> Vector Digest**

The pMAL-BRT<sub>17</sub> vector was acquired from the lab of Scott Banta and the stab miniprep to generate sufficient material for use. The plasmid was then digested using HindIII as follows:

5  $\mu$ L H<sub>2</sub>O

2  $\mu$ L 10x Buffer R

12.5  $\mu$ L pMAL-BRT<sub>17</sub> (80 ng  $\mu$ L<sup>-1</sup>)

0.5  $\mu$ L HindIII

The results of this digest were then analysed by agarose gel and the digested vector extracted using a Qiagen Gel Extraction Kit.

#### **MO14 Insert Production**

The MO14 gene to be inserted was subjected to PCR in order to produce sufficient insert for cloning. Primers were designed to ensure successful overlap with the pET-22b(+) plasmid and were as follows:

Forward: AAT ACT CCT CAA GCT TAT GTC AAA GAC CAT TTC TGC

Reverse: GGC CAG TGC CAA GCT TTC AGG ACA CGG TGG AGG C

The PCR reaction was performed as follows:

5  $\mu\text{L}$  10x KOD DNA Polymerase Buffer  
 5  $\mu\text{L}$  2 mM dNTPs  
 3  $\mu\text{L}$  25 mM  $\text{MgSO}_4$   
 1  $\mu\text{L}$  DMSO  
 1  $\mu\text{L}$  YSBLIC-3C plasmid containing MO14 gene  
 1  $\mu\text{L}$  Forward primer (20 pmol  $\mu\text{L}^{-1}$ )  
 1  $\mu\text{L}$  Reverse primer (20 pmol  $\mu\text{L}^{-1}$ )  
 H<sub>2</sub>O to 50  $\mu\text{L}$

PCR Program:

Table 2.4: MO14 Insert PCR for Cloning into pMAL-BRT<sub>17</sub>.

Step	Time	Temperature	Repeats
Initial Denature	2 min	94 °C	
Denature	30 sec	94 °C	35
Anneal	30 sec	60 °C	
Extend	30 sec	72 °C	
Final Extend	3 min	72 °C	

The PCR results were analysed by agarose gel and the insert bands extracted with a Qiagen Gel Extraction Kit. The insert was then digested with HindIII at 37 °C for 1 hour as follows:

3  $\mu\text{L}$  10x Buffer R  
 1  $\mu\text{L}$  HindIII  
 1 mg insert  
 H<sub>2</sub>O to 30  $\mu\text{L}$

The results of this digest were then analysed by agarose gel and the digested insert extracted using a commercial Qiagen Gel Extraction Kit.

### **InFusion Ligation**

The insert and plasmid were ligated using the InFusion system by incubation at 50 °C for 15 min as follows:

1  $\mu\text{L}$  MO14 gene insert (80 ng  $\mu\text{L}^{-1}$ )

2  $\mu\text{L}$  pMAL-BRT<sub>17</sub> (40 ng  $\mu\text{L}^{-1}$ )

2  $\mu\text{L}$  5x Infusion premix

5  $\mu\text{L}$  H<sub>2</sub>O

The ligated plasmids were transformed into *E. coli* XL-10 Gold, plated onto LB agar and grown at 37 °C overnight. The colonies were then used to miniprep the cloned plasmid.

### **2.3.9 Codon-Optimised Gene Cloning**

The YSBLIC-3C plasmid was digested with BseRI at 37 °C for 1.5 hours, then analysed by agarose gel. Reaction:

3  $\mu\text{L}$  10x NEBuffer 4

1  $\mu\text{L}$  BseRI

1 mg plasmid

H<sub>2</sub>O to 30  $\mu\text{L}$

The results of this digest were then analysed by agarose gel and the digested vector extracted using a Qiagen Gel Extraction Kit.

### **Gene Insert Generation**

BseRI purchased from New England Biosciences. The codon-optimised MO14 gene to be inserted was subjected to PCR in order to produce sufficient insert for cloning. Primers were designed to ensure successful overlap with the YSBLIC-3C plasmid and were as follows:

Forward: GCA AGT GTC ATA TGT CAA AGA CCA TTT CTG CCG ACG TCG ACG T

Reverse: TCT GAT AAG AAT TCG GAC ACG GTG GAG GCC GCG CGG GC

The PCR reaction was performed as follows:

5  $\mu\text{L}$  10x KOD DNA Polymerase Buffer

5  $\mu\text{L}$  2 mM dNTPs

3  $\mu\text{L}$  25 mM  $\text{MgSO}_4$

2.5  $\mu\text{L}$  DMSO

1  $\mu\text{L}$  YSBLIC-3C plasmid containing MO14 gene

1  $\mu\text{L}$  Forward primer (20 pmol  $\mu\text{L}^{-1}$ )

1  $\mu\text{L}$  Reverse primer (20 pmol  $\mu\text{L}^{-1}$ )

$\text{H}_2\text{O}$  to 50  $\mu\text{L}$

PCR Program:

Table 2.5: COMO14 Insert PCR for Cloning into YSBLIC-3C.

Step	Time	Temperature	Repeats
Initial Denature	2 min	94 °C	
Denature	30 sec	94 °C	35
Anneal	30 sec	60 °C	
Extend	30 sec	72 °C	
Final Extend	3 min	72 °C	

The PCR results were analysed by agarose gel and the insert bands extracted with a Qiagen Gel Extraction Kit. The insert was then digested with BseRI at 37 °C for 1 hour as follows:

3  $\mu\text{L}$  10x NEBuffer 4

1  $\mu\text{L}$  BseRI

1 mg insert

$\text{H}_2\text{O}$  to 30  $\mu\text{L}$

The results of this digest were then analysed by agarose gel and the digested insert extracted using a Qiagen Gel Extraction Kit.

### **Ligation**

The digested pET-22b(+) vector and digested MO14 gene insert were ligated at 15 °C overnight as follows:

1  $\mu$ L 10x T4 DNA Ligase Buffer

1  $\mu$ L 10 mM ATP

1  $\mu$ L T4 DNA Ligase

3:1 molar ratio insert:plasmid

H<sub>2</sub>O to 10  $\mu$ L

The ligated plasmids were transformed into *E. coli* XL-10 Gold, plated onto LB agar and grown at 37 °C overnight. The colonies were then used to miniprep the cloned plasmid.

### **2.3.10 Glutathione-S-transferase Purification**

Cell lysate was prepared according to the nickel ion affinity purification procedure, but resuspended in buffer containing only 50 mM Tris/HCl (pH 7.5). A 1 mL GSTrap HP column, purchased from GE Healthcare Life Sciences, was prepared for use by washing with 20 mL 0.1 M NaOH, followed by 20 mL deionised water. The filtered protein was loaded onto the column via a peristaltic pump, then transferred to an FPLC machine. The column was then run from buffer containing no glutathione to 10 mM reduced glutathione, and 4 mL fractions were collected and assessed for protein content by SDS-PAGE.



## 2.4 Fermentations

Fermentations were carried out using a 7 L capacity Fisher BC10 fermenter with conditions controlled by an Applikon Bio Controller ADI 1010. 2 L of Terrific Broth (TB) containing 30 mg L<sup>-1</sup> kanamycin and 2 mL Antifoam C were added to the fermenter, then 50 mL of a starter culture of cells expressing the relevant gene encoding MO14 were added to the fermenter and the mixture stirred at 37 °C to maintain oxygen levels at 30 % of optimum. Once the solution reached an OD<sub>600</sub> of 0.6, gene expression was induced by addition of IPTG to a concentration of 1 mM and the temperature controlled according to the experiment. In most experiments, the required amount of the substrate, bicyclo[3.2.0]hept-2-en-6-one, was then added to the desired concentration. 500 µL samples were removed at hourly intervals and each extracted into 500 µL ethyl acetate, to yield samples for analysis by gas chromatography.

## 2.5 Mutations

Mutation experiments were conducted on codon-optimised MO14, as this allowed easier design of mutagenesis primers, due to high levels of GC content in the gene. MO15 mutation were conducted with wild-type MO15.

Table 2.6: Mutagenesis Primers.

Mutation	Primer Sequence
MO14 P441V	Forward: GTA TAA TAT GGT GCT GGC AAT TG Reverse: CAA TTG CCA GCA CCA TAT TAT AC
MO14 I60V	Forward: GCA CGT TGT GAT GTG GAA AGC GTT CAT TAT AGC Reverse: GCT ATA ATG AAC GCT TTC CAC ATC ACA ACG TGC
MO15 V447P	Forward: GTG CTG GCG AAC ATG CCG CTC GGC GCC GAA CAG Reverse: CTG TTC GGC GCC GAG CGG CAT GTT CGC CAG CAC
MO15 V67I	Forward: CGG CGC CCG GTG CGA CAT AGA AAG CGT CGA CTA TTC Reverse: GAA TAG TCG ACG CTT TCT ATG TCG CAC CGG GCG CCG

### 2.5.1 Site-Directed Mutagenesis

In a 500  $\mu\text{L}$  PCR tube were added:

1  $\mu\text{L}$  Template DNA, *i.e.* codon-optimised MO14 or wild-type MO15 in the YSBLIC-3C vector (50-100 ng  $\mu\text{L}^{-1}$ )

0.5  $\mu\text{L}$  Forward primer (20 pmol  $\mu\text{L}^{-1}$ )

0.5  $\mu\text{L}$  Reverse primer (20 pmol  $\mu\text{L}^{-1}$ )

5  $\mu\text{L}$  5x Pfu Turbo DNA Polymerase Buffer

5  $\mu\text{L}$  2 mM dNTPs

1  $\mu\text{L}$  DMSO

1  $\mu\text{L}$  Pfu Turbo DNA Polymerase

H<sub>2</sub>O to 25  $\mu\text{L}$

PCR Program:

Table 2.7: Mutagenesis PCR Conditions.

Step	Time	Temperature	Repeats
Initial Denature	5 min	95 °C	
Denature	30 sec	95 °C	35
Anneal	30 sec	50 °C	
Extend	30 sec	72 °C	
Final Denature	72 sec	95 °C	
Final Extend	5 min	72 °C	

The results of this PCR were then analysed by agarose gel and the products extracted using a Qiagen Gel Extraction Kit. The plasmids were transformed into *E. coli* XL-10 Gold, plated onto LB agar and grown at 37 °C overnight. The colonies were then used to miniprep the plasmid containing the mutant gene.

## Chapter 3

# Purification of MO14

### 3.1 Protein Production

In addition to investigating the ability of MO14 to convert *cis*-bicyclo[3.2.0] hept-2-en-6-one to its corresponding lactone in whole-cell systems, purification and crystallisation of the protein facilitate the determination of a structure for the protein. Crystallisation would allow the further clarification of the active site of the enzyme and would help to explain the observations relating to substrate features from the sulfide biotransformation experiments. Additionally, the generation of this structure would aid in the description of the mechanism of MO14, as was conducted for CHMO<sub>Rhod</sub>, revealing large domain movements and the movement of a cofactor during the reaction to conduct flavin reduction followed by stabilisation of the reaction intermediate.<sup>82</sup>

There are a wide range of purification methods available, many of which involves chromatographic methods to separate the protein from contaminants; in these systems, the cell lysate solution is passed through a column of a polymer matrix that has been impregnated with the necessary separation tools. More recently, techniques have been developed using magnetic beads to allow the protein to be removed from the solution without requiring the slow elution from column-based techniques by disruption of binding.<sup>116</sup>

The first step in achieving the production of pure MO14 was to design an expression system that would generate large amounts of protein in the soluble phase. This solubility is essential, as the majority of the purification methods to be attempted require either the passing of a protein through a chromatographic column or separation by precipitation from a solution. This generation of soluble protein can pose a significant problem, particularly when expressing heterologous proteins *i.e.* those deriving from a source organism differing from the expression organism. This difference can result in misfolding, which tends to result in the formation of inclusion bodies, which are insoluble collections of protein. These inclusion bodies pose a significant challenge to purification.<sup>117</sup>

Previous work in this area has indicated the potential utility of two commercial *Escherichia coli* strains for the purpose of protein expression: *E. coli* Rosetta<sup>TM</sup>2 (DE3) and *E. coli* Rosetta<sup>TM</sup>2 (DE3) pLysS.<sup>118</sup> Both of these strains are Rosetta<sup>TM</sup>2 strains and are therefore optimised for expression of eukaryotic protein, as they contain higher levels of tRNAs that commonly occur in recombinant proteins and generally exist in low quantities in wild type *E. coli*. The increased presence of these molecules will improve the yield generated by increasing the availability of the required tRNAs, meaning that the gene is translated more efficiently by the host organism. Both strains are also lysogens of  $\lambda$ DE3, which means they possess a copy of the T7 RNA polymerase gene, which allows the control of gene expression by induction with IPTG. These two strains of *E. coli* are very similar, with the key difference being the presence of a T7 lysozyme expression system in the pLysS variant. This protein acts on the T7 RNA polymerase and reduces the basal transcription of the gene, which aids in the production of potentially toxic genes by preventing their generation until sufficient production of T7 RNA polymerase is induced by the addition of IPTG.

Both host strains were transformed with the gene encoding MO14 and a small scale culture of 5 mL was generated and induced with IPTG in order to assess the expression levels of the enzyme

in each strain. The cells were lysed and both the whole cell lysate and soluble fraction were analysed by SDS-PAGE. Control experiments with no transformation of the cells were also conducted and are shown with the expression results in Figure 3.1; MO14 is the band visible approximately level with the 66 kDa marker.

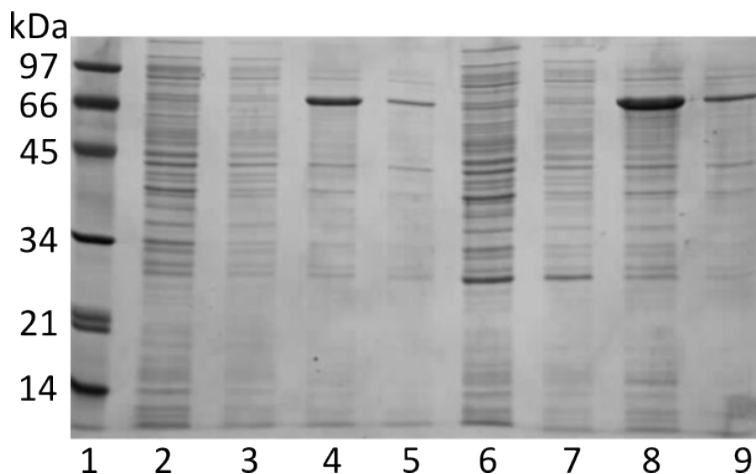


Figure 3.1: SDS-PAGE showing MO14 expression in two strains of *E. coli*. Lane 1: Low molecular weight marker (Biorad) with molecular weights given on the left in kiloDaltons. Lane 2: Vector-only control expression in *E. coli* Rosetta™2 (DE3), total lysate. Lane 3: Vector-only control expression in *E. coli* Rosetta™2 (DE3), soluble fraction. Lane 4: MO14 expression in *E. coli* Rosetta™2 (DE3), total lysate. Lane 5: MO14 expression in *E. coli* Rosetta™2 (DE3), soluble fraction. Lane 6: Vector-only control expression in *E. coli* Rosetta™2 (DE3) pLysS, total lysate. Lane 7: Vector-only control expression in *E. coli* Rosetta™2 (DE3) pLysS, soluble fraction. Lane 8: MO14 expression in *E. coli* Rosetta™2 (DE3) pLysS, total lysate. Lane 9: MO14 expression in *E. coli* Rosetta™2 (DE3) pLysS, soluble fraction.

Both strains show the capability to produce MO14 in both soluble and insoluble fractions, which would allow the use of either of these expression strains for the purpose of further protein production. It appears that the prevention of gene expression until addition of IPTG is carried out results in a small increase in the overall yield of MO14 generated, as the Rosetta™2 (DE3) pLysS strain shows slightly better expression both solubly and insolubly. This potentially indicates that MO14 has a negative effect on the viability of the *E. coli* cell, hence *E. coli* Rosetta™2 (DE3) pLysS was selected as the expression strain of choice for further experimentation. As the purification of MO14 would require significantly more protein than was generated in the expression tests for comparison of host strains, the expression was scaled up. General expression was conducted on

several litre scale, with smaller starter cultures being generated and used to inoculate the larger media to ensure rapid growth and protein production could be achieved.

## **3.2 Chromatographic Purification**

### **3.2.1 Nickel Ion Affinity**

The first method of protein purification tested was nickel ion affinity chromatography, a form of immobilised metal affinity chromatography (IMAC), which purifies proteins based on the affinity that they possess towards a nickel ion. The proteins bind to the nickel ion, which removes them from the solution, then this binding is disrupted by a species with a greater affinity for nickel than the protein. The most common cause of this affinity is the histidine residue, which chelates to the nickel ion and causes the binding. In some cases, it may be possible for this binding to occur simply with histidines present on the surface of the protein, however these are few in number, as histidine residues are hydrophobic and therefore tend to be located within the structure of the protein.<sup>119</sup>

Far more common is the use of a histidine 'tag', which can be cloned onto the terminus of the protein. This tag usually consists of six histidine residues, which bind strongly to the nickel ion and allow the simple separation of the protein. This tag is present in the YSBLIC-3C vector and is separated from the target gene by a 3C protease site, which allows the tag to be removed from the protein in the case of crystallisation difficulties. These can arise due to the unstructured character of the histidine tag causing problems with the generation of an X-ray snapshot of the protein crystal.

As the protein was cloned into the YSBLIC-3C vector with an N-terminal hexahistidine tag already present, protein production was carried out with no alterations, after which the soluble fraction of the cell lysate was applied to a nickel column, washed with low concentration imidazole to

disrupt non-specific binding of *E. coli* fragment proteins to the nickel and eluted with increasing concentrations of imidazole. The resulting elution fractions were analysed by SDS-PAGE, shown in Figure 3.2.

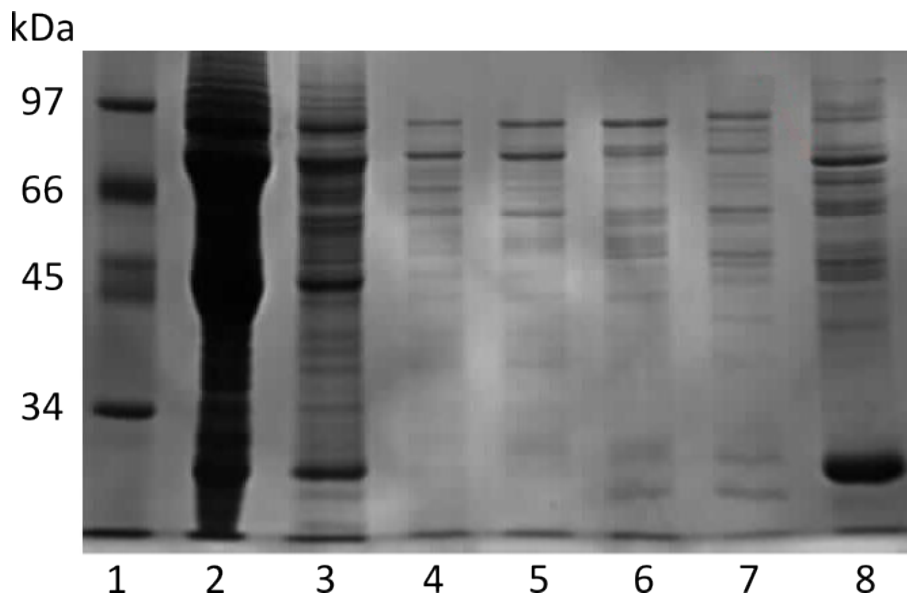


Figure 3.2: SDS-PAGE showing a nickel ion affinity purification of MO14. Lane 1: Low molecular weight marker (Biorad) with molecular weights given on the left in kiloDaltons. Lane 2: Total cell lysate sample. Lane 3: Soluble fraction of cell lysate after 0.8 $\mu$ m filtration. Lanes 4-8: Elutions from nickel column at increasing imidazole concentrations.

We can see that there is a large quantity of impurities that have co-eluted with MO14 from the nickel column. Especially significant is the impurity of approximately 20 kDa size, as the disruption of binding by the low concentration of imidazole should have resulted in a much lower presence of other protein bands, however non-specific binding of proteins to IMAC is known and a comparison with other affinity tags can often show a higher degree of purity than that attained by polyhistidine affinity.<sup>120</sup> The standard procedure from this point would be to proceed to size exclusion chromatography, however the high level of impurities present mean that this course of action would likely not improve the purity of the protein sufficiently for further applications. An alternative purification method is therefore required to separate MO14 from other proteins.

### 3.2.2 C-terminal Histidine Tag

In some cases, the difficulties in purifying proteins by means of nickel ion affinity can be caused by the burial of a histidine tag in the tertiary structure of the protein. This phenomenon occurs when the terminus of the protein to which the histidine tag is attached is located within the core of the protein structure and is therefore inaccessible to the nickel ions. At this point, a crystal structure of MO14 is unavailable, so the conformation of the N-terminus cannot be determined. Alignment of the MO14 sequence with the structure of PAMO, with which MO14 shares considerable sequence identity, allows the prediction of a protein structure based on these two factors.<sup>121</sup> Shown in Figure 3.3 is this prediction, with the N-terminus displayed in red and C-terminus displayed in blue.

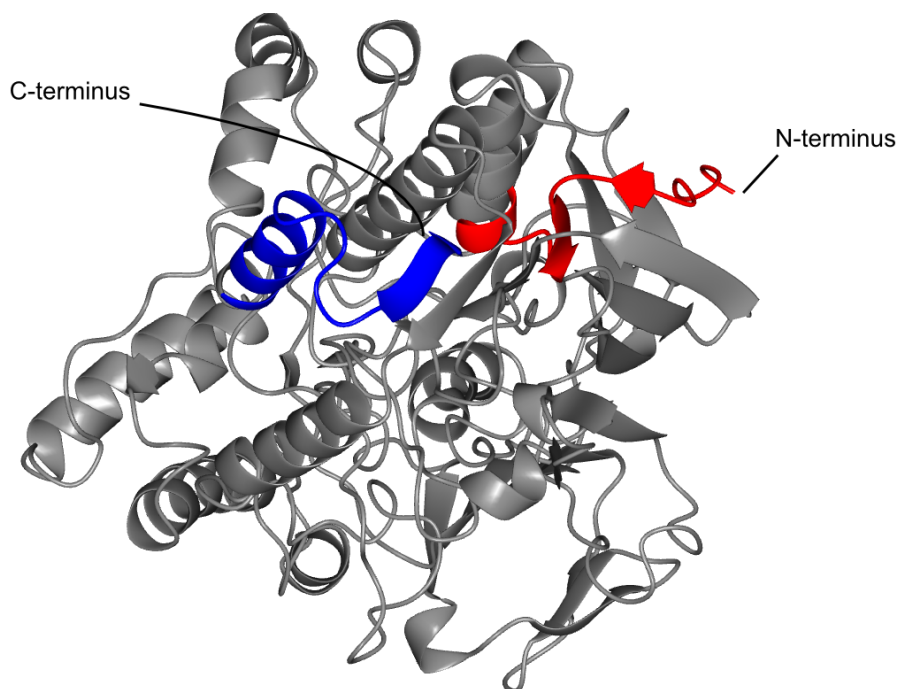


Figure 3.3: A predicted structure for MO14 with the 20 N-terminal residues highlighted in red and the 20 C-terminal residues in blue.

This prediction shows the N-terminus to be located in a near ideal location for access to the nickel ions. The prediction of protein structures is imprecise, however, and it is possible that the addition of a hexahistidine tag may result in slightly different folding of the protein to the wild type. For



these reasons, it was decided to investigate the possibility of switching the position of the tag to the C-terminus which, as Figure 3.3 shows, is also predicted to be unburied.

In order to produce this C-terminal tag, the gene encoding MO14 needed to be recloned into a plasmid encoding such a tag. The plasmid selected was pET-22b(+), which contains the same T7 promoter site and *lac* operon utility as the YSBLIC-3C plasmid. These features allow a simple swap of plasmid without the need to alter the techniques used to produce MO14. Standard cloning procedure was used to insert MO14 into the new vector and a digestion was performed with NdeI and EcoRI, which was analysed by agarose gel, shown in Figure 3.4.

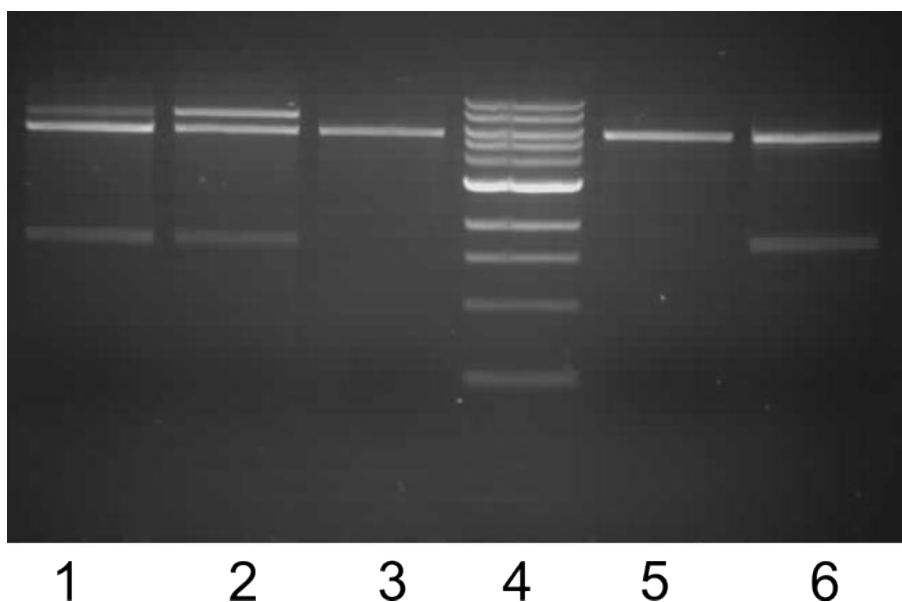


Figure 3.4: An agarose gel of the digest of the newly cloned MO14 in pET-22b(+). Lanes 1-3, 5 and 6: Digested samples of DNA from various colonies containing the new plasmid. Lane 4: Marker with bands at 10.0 kilobases (kb), 8.0 kb, 6.0 kb, 5.0 kb, 4.0 kb, 3.0 kb, 2.0 kb, 1.5 kb, 1.0 kb and 0.5 kb.

Samples 1 and 2 of the digest show incomplete digestion of the plasmid containing the MO14 gene, indicated by the presence of the expected MO14-encoding band at around 1.6 kb, the vector band at around 6.0 kb and the combined band around 7.6 kb. Samples 3 and 5 show a lack of the MO14-encoding band, indicating that the cloning has been unsuccessful. Finally, sample 6 shows the ideal result - complete digestion of the vector to produce both the MO14-encoding band and

the empty vector band. Sample 6 was then taken for further use in the purification of MO14.

This new plasmid was sequenced and confirmed to contain the MO14-encoding gene and was therefore used to transform *E. coli* Rosetta™2 (DE3) pLysS, before an expression test was conducted to assess the effect of the new position of the histidine tag on the expression levels of the protein. These were conducted as for the selection of expression strain, with a comparison to the N-terminally tagged MO14 expression, with the SDS-PAGE analysis shown in Figure 3.5.

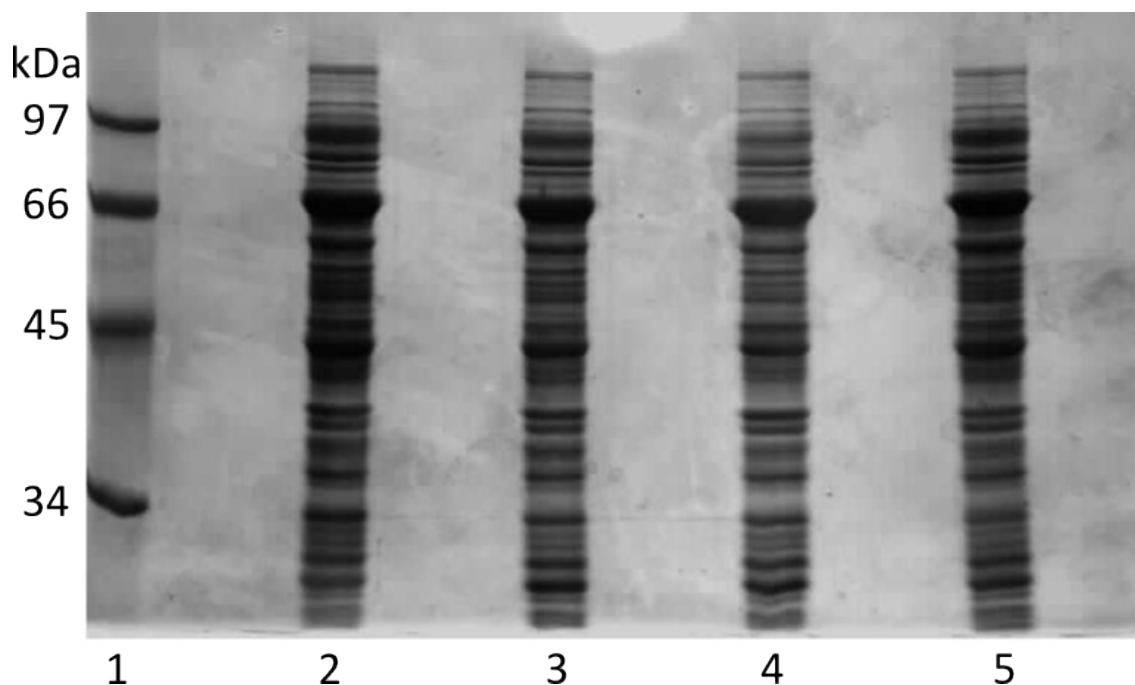


Figure 3.5: SDS-PAGE showing MO14C expression tests. Lane 1: Low molecular weight marker (Biorad) with molecular weights given on the left in kiloDaltons. Lanes 2-4: MO14C expression from three different transformation colonies. Lane 5: MO14 positive control expression.

The expression observed appears to result in very similar levels of protein produced to the N-terminally tagged protein, hence the production was scaled up and further attempts were made to purify MO14 by nickel ion affinity chromatography using this new C-terminally tagged protein. The SDS-PAGE analysis of the fractions obtained therefrom is shown in Figure 3.6.

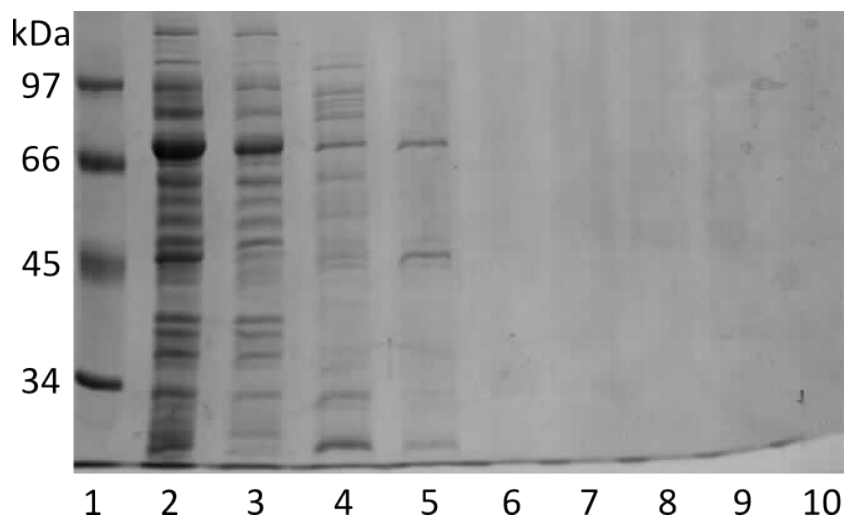


Figure 3.6: SDS-PAGE gel showing nickel affinity purification of C-terminally tagged MO14. Lane 1: Low molecular weight marker (Biorad) with molecular weights given on the left in kiloDaltons. Lane 2: Soluble fraction of MO14C expression. Lane 3: Non-binding fraction following application to nickel column. Lanes 4-10: Elution fractions from increasing concentration of imidazole.

This method has again resulted in disappointing results, this time revealing a lack of binding of the protein to the column as, in Lane 3, we can see that the majority of the protein applied to the column has passed through into the run-through fraction. The large quantity here would seem to suggest that the C-terminus is buried, as the result for the N-terminally tagged protein in Figure 3.2 showed a relatively large amount of protein eluting from the column, albeit with significant impurities. For this experiment, however, we see relatively less impurity present in the sample, but a poorer binding overall. These two experiments promote attempts to achieve the purification of MO14 by means other than the simple histidine tagging, due to the difficulties encountered in producing pure protein.

### 3.2.3 Ion Exchange Chromatography

The next method attempted was ion exchange chromatography. The protein binding in this procedure is based on ionic interactions; proteins possess a charge significant enough to form these interactions with a suitably charged sepharose molecule, called Q-Sepharose. This consists of a sepharose polymer with a functionalised group covalently attached, example shown in Figure 3.7.

The large quantity of atoms with the capability to form ionic interactions aids in the binding of the protein. After application of the protein to the column, the concentration of NaCl in the buffer solution is gradually increased until disruption of the binding occurs due to the ionic strength of the NaCl interfering with the protein-sepharose interaction, with separation of proteins occurring due to the differing strengths of protein binding.

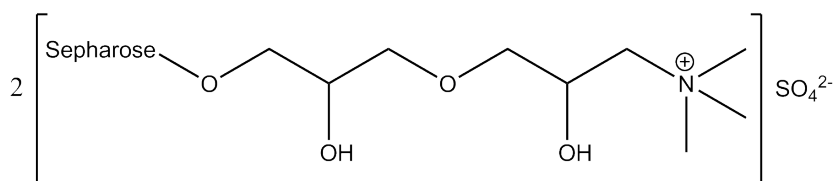


Figure 3.7: An example of a possible structure for Q-Sepharose.

This purification required the suspension of a different buffer, as the standard buffer contains 300 mM NaCl, which is omitted for this experiment, leaving the buffer as 50 mM Tris-HCl at pH 8.0. The solubility of MO14 may deteriorate as a result of this change, as the salt molecules assist with solubilisation, however the expression of MO14 occurs with a reasonable degree of solubility and no significant effect on the results was expected or observed. Cell lysate was applied to the column and eluted with buffer on a gradient up to 1 M NaCl and the results of an SDS-PAGE analysis of the fractions generated by this purification are shown in Figure 3.8.

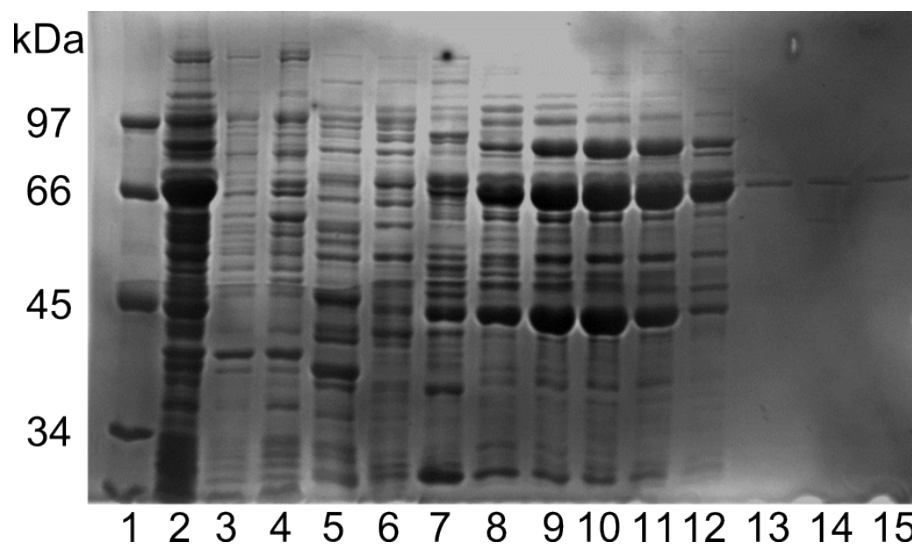


Figure 3.8: SDS-PAGE showing the ion exchange purification. Lane 1: Low molecular weight marker (Biorad) with molecular weights given on the left in kiloDaltons. Lane 2: Soluble fraction of MO14 expression. Lane 3: Non-binding fraction following application to ion exchange column. Lanes 4-15: Elution fractions at increasing NaCl concentration.

This method of purification, while it did remove a fair proportion of the impurities present in the cell lysate, unfortunately left a number of high-concentration proteins in the purified fractions, as seen below. This could be due to the similar strength of other protein bonds to the column, which could be solved by using a slower change in the ionic strength of the buffer, which would allow other proteins that bind at a similar strength to separate out more thoroughly in the fractions. Alternatively, a combined purification involving both a nickel purification and a subsequent ion exchange purification may result in more successful purification. Since the largest impurity bands can generally be seen in both purification methods, and there is the need for a large change in buffer between the two experiments, which may result in the degradation of MO14, a different purification strategy was attempted.

### 3.2.4 Sepharose Blue Purification

This method of purification relies on the ability of MO14 to bind to the ADP-containing molecules, NADPH and FAD. The Sepharose Blue, structure shown in Figure 3.9, has a high affinity for the

dinucleotide fold; a structure found in proteins that is key to the binding of cofactors containing ADP.<sup>122</sup> The protein containing this fold will therefore bind to a column based on the strength of the binding to NADPH or FAD. The protein is removed from the column by increasing salt concentration, which disrupts the binding in the same manner as in ion exchange chromatography, *i.e.* the ionic strength of NaCl causes the bond to break.

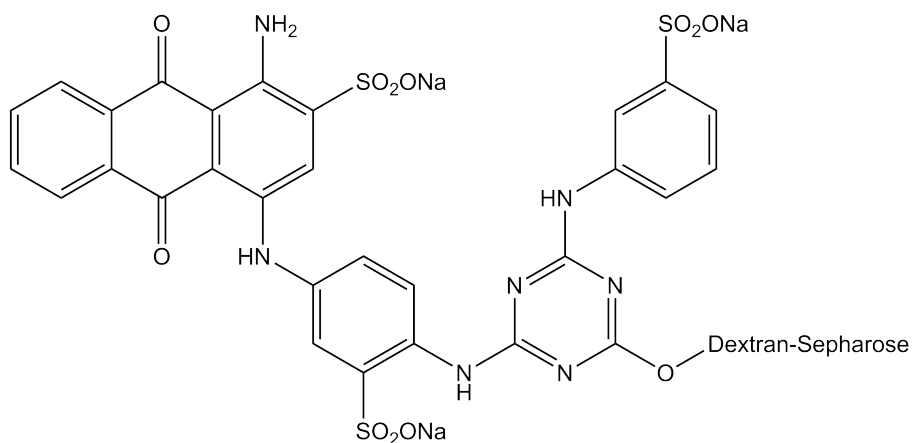


Figure 3.9: Structure of the sepharose blue functionality.

The protein was suspended in the same buffer as for the ion exchange chromatography and eluted with up to 1 M NaCl as before. Fractions were analysed by SDS-PAGE and are shown in Figure 3.10.

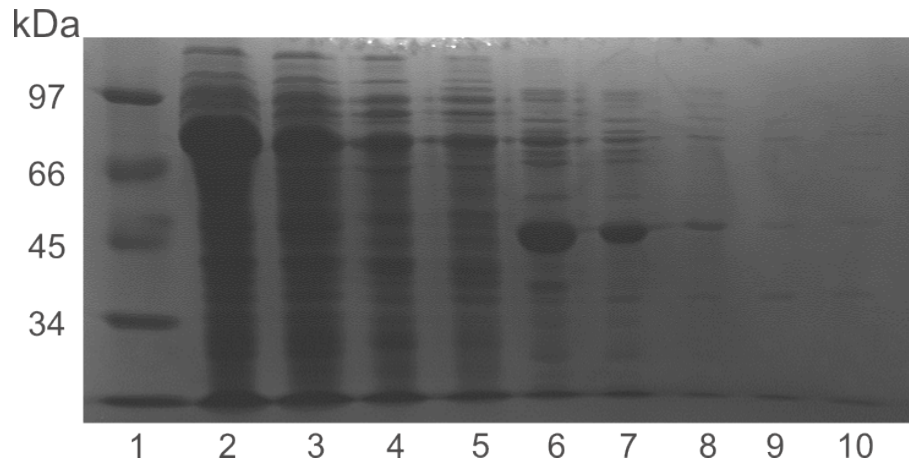


Figure 3.10: SDS-PAGE showing the Sepharose Blue purification. Lane 1: Molecular mass marker, masses shown in kDa on left; Lane 2: Total cell lysate; Lane 3: Soluble fraction from cell lysate; Lane 4: Non-binding runthrough from application to column; Lane 5: Initial wash of column with no NaCl; Lanes 6-10: Elution fractions with increasing NaCl concentration.

It is clear from the analysis that very little binding of MO14 to the column occurs, with the largest MO14 bands visible in the flow-through and initial elution from the column; *i.e.* before the presence of NaCl. This could be because the protein already contains NADPH and FAD from the host organism, leaving no active sites free for binding to the column, which could be resolved by expression of the protein in a species that utilised NADH and FMN as cofactors for native proteins or by thorough washing of the protein before application to the column. Alternatively, this issue could be caused by a buried binding site for the ADP-binding domain, which would render it inaccessible to the Sepharose Blue molecule, which cannot easily be solved.

### 3.2.5 Ammonium Sulfate Precipitation

At this point, it was felt that reducing the amount of impurity in the cell lysate prior to engaging chromatographic purification methods might improve the purification process. To this end, ammonium sulfate precipitation was used as a method. In this process, ammonium sulfate is added stepwise to a protein sample, causing the protein to aggregate and precipitate in a reversible manner. At each step, the precipitated sample is centrifuged and resuspended in buffer and the process

is repeated until the desired level of separation is achieved. By taking samples at set ammonium sulfate saturations, the fraction containing the lowest levels of impurity and the highest level of the desired protein can be resuspended and purified more easily than a total crude sample.

In this experiment, it was anticipated that relatively large fractions should initially be taken in order to find the precipitation point of MO14; following this, narrower ammonium sulfate concentrations could be utilised to ensure a good degree of purity as a starting point for following purification attempts. The ammonium sulfate concentrations decided upon were 30 %, 50 % and 80 % w/v concentrations and these were generated taking into account the large increase in volume that is observed on additions of these quantities of ammonium sulfate. The fractions were analysed by SDS-PAGE, and are shown in Figure 3.11.

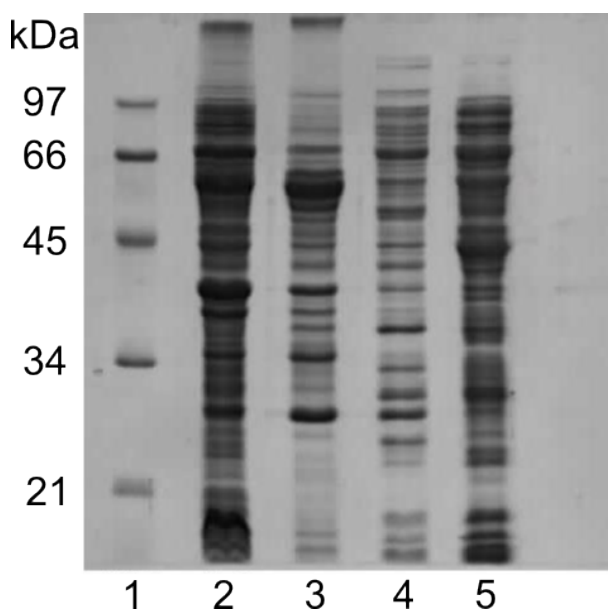


Figure 3.11: SDS-PAGE gel showing the ammonium sulfate precipitation. Lane 1: Low molecular weight marker (Biorad) with molecular weights given on the left in kiloDaltons. Lane 2: Soluble fraction of MO14 expression. Lane 3: 30 % ammonium sulfate fraction. Lane 4: 50 % ammonium sulfate fraction. Lane 5: 80 % ammonium sulfate fraction. Lane 6: >80 % ammonium sulfate fraction.

As can be seen, the majority of the MO14 protein, molecular weight 60.6 kDa, was found in the 50 % and 80 % ammonium sulfate cuts. Regrettably, the largest impurity was not removed by the



use of a broad ammonium sulfate cut, however the general removal of impurities is useful and this procedure therefore became the first step for all following purification attempts.

### **3.2.6 Hydrophobic Interaction**

After the ammonium sulfate precipitation, the next purification method tried was hydrophobic interaction chromatography. This involves a phenyl sepharose column and loading the protein onto the column in a high salt concentration. Phenyl sepharose has a much simpler functionalisation than the previously used sepharose derivatives, consisting of a single phenyl group. The high salt concentration encourages the hydrophobic areas of the protein to form hydrophobic interactions with the phenyl group on the sepharose, binding it to the column. Lowering the salt concentration of the buffer then changes the equilibrium of the solution, causing the protein to solubilise in the flowthrough.

This purification requires the use of the 'opposite' condition to ion exchange and sepharose blue purifications, in that the salt concentration is high to begin with to encourage hydrophobic interactions, and then is reduced to re-solubilise the protein in the buffer solution. In this case, cells expressing MO14 were resuspended in 50 mM Tris/HCl, 1 M NaCl prior to sonication, hence these were the conditions in which the cell lysate was applied to the column. The concentration of NaCl was decreased steadily and fraction taken and analysed by SDS-PAGE, shown in Figure 3.12.

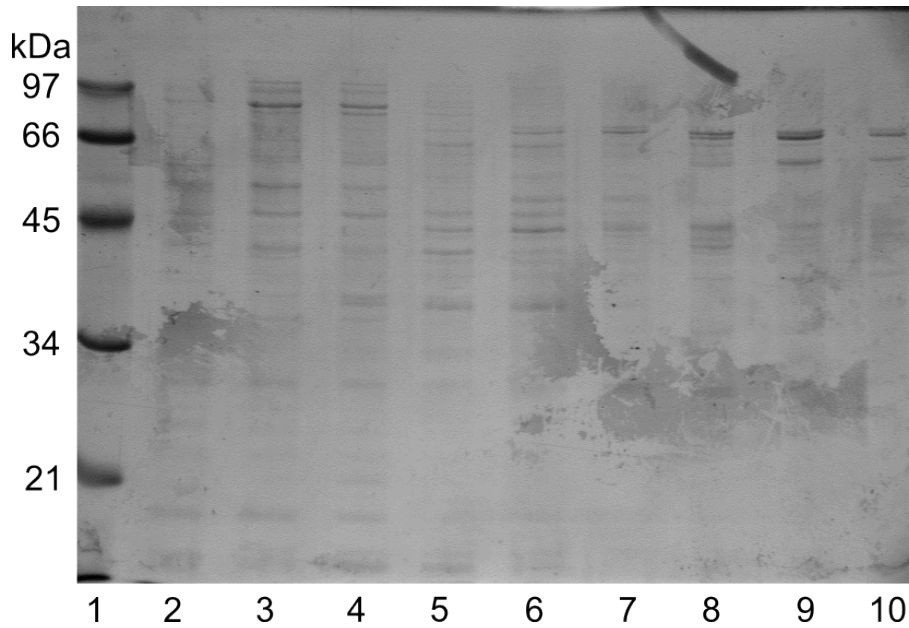


Figure 3.12: SDS-PAGE gel showing the hydrophobic interaction chromatography. Lane 1: Low molecular weight marker (Biorad) with molecular weights given on the left in kiloDaltons. Lanes 2-10: Elution fractions at decreasing NaCl concentration.

The purification observed here appears to be relatively successful; although a large quantity of MO14 appears to have been lost either by lack of binding and therefore passing into the runthrough or non-specific binding being disrupted at high NaCl levels, the final fractions obtained appear to have achieved a high level of purity. Improvement of this purification may be attempted by use of a higher initial concentration of NaCl to encourage more binding of the protein onto the column by ensuring more repulsion of hydrophobic areas of the protein into contact with the phenyl sepharose or by using cyclic loading of the cell lysate onto the column, where the sample will effectively be loaded several times to ensure more thorough binding.

An issue remains, however, which can be seen throughout the purification methods conducted thus far, albeit more clearly in the hydrophobic interaction purification: the protein appears to degrade when applied to a column. There are consistently a number of bands above and below the expected weight of MO14, which do not appear in expression gels, *e.g.* Figure 3.1. It was thought that the protein may be being degraded by proteases present in the *E. coli* expression system, hence

an experiment was conducted to ascertain if this was the origin of the phenomenon. MO14 was expressed as usual, but resuspended in buffers containing protease inhibitors; one containing 0.1 mM AEBSF, which acts as a protease inhibitor, one containing a tablet of a cocktail of protease inhibitors and one with no protease inhibitor added. These samples were then incubated at room temperature for 24 hours and the resulting samples taken for SDS-PAGE analyses, shown in Figures 3.13-3.15.

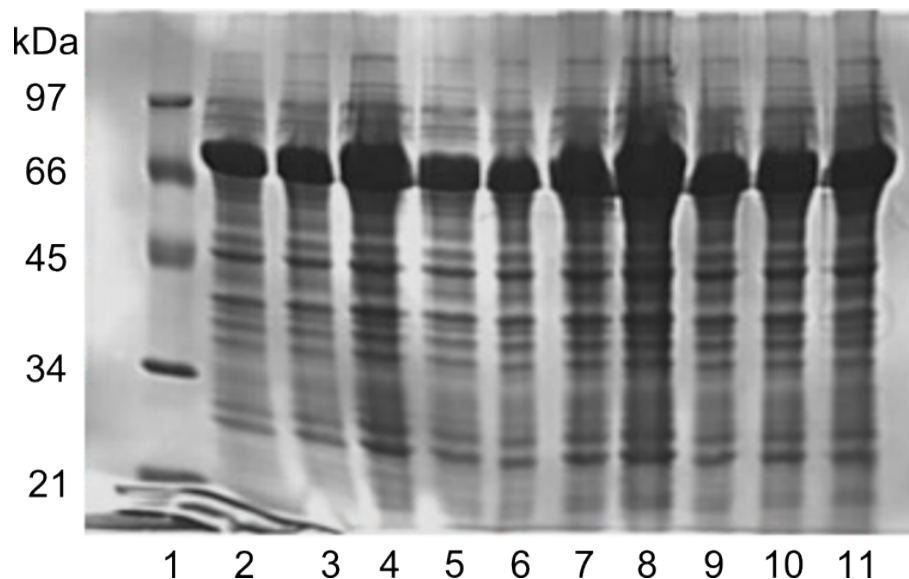


Figure 3.13: SDS-PAGE gels of the MO14 control degradation experiment. Lane 1: Low molecular weight marker (Biorad) with molecular weights given on the left in kiloDaltons. Lanes 2-10: MO14 degradation over time from initial sample to 8 h sample. Lane 11: MO14 degradation 24 h sample.

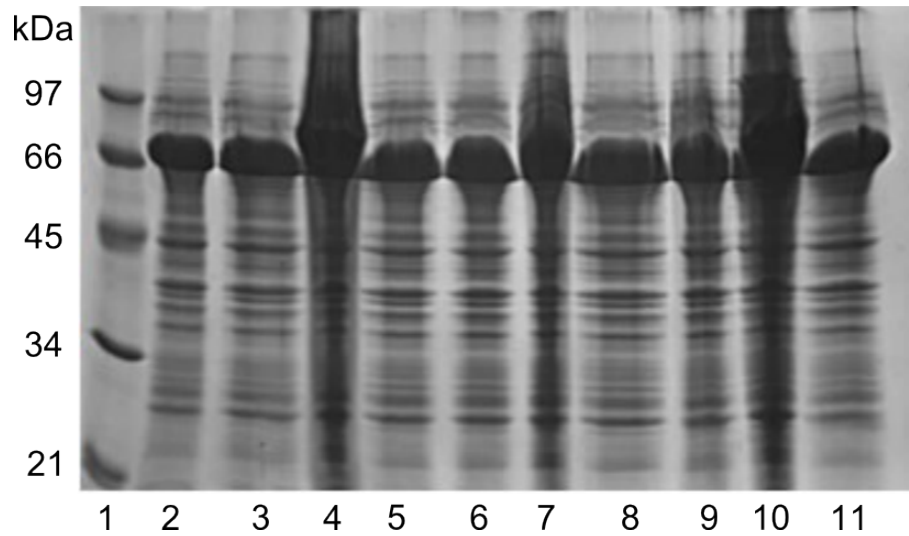


Figure 3.14: SDS-PAGE gels of the MO14 degradation experiment with AEBSEF. Lane 1: Low molecular weight marker (Biorad) with molecular weights given on the left in kiloDaltons. Lanes 2-10: MO14 degradation over time from initial sample to 8 h sample. Lane 11: MO14 degradation 24 h sample.

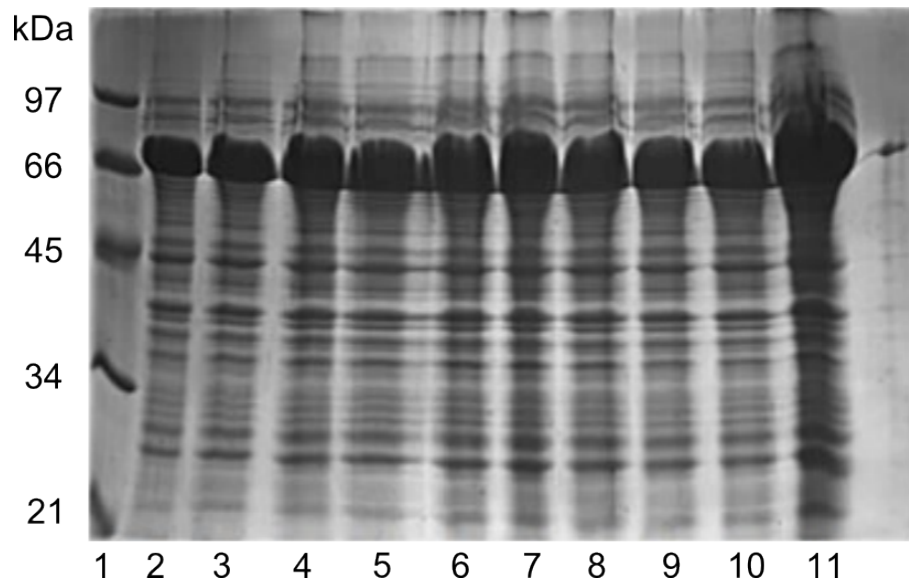


Figure 3.15: SDS-PAGE gels of the MO14 degradation experiment with a protease inhibitor cocktail. Lane 1: Low molecular weight marker (Biorad) with molecular weights given on the left in kiloDaltons. Lanes 2-10: MO14 degradation over time from initial sample to 8 h sample. Lane 11: MO14 degradation 24 h sample.

Neither of the two expressions with protease inhibitors show any sign of degradation of MO14 and the control experiment shows only a slight increase in the bands associated with the degradation

after 24 h. The time-scale of the experiments conducted thus far would not give sufficient time for proteases native to *E. coli* to perform the observed degradation, hence it is suspected that MO14 has a degree of instability when applied to a column. In order to avoid this concern, an investigation was undertaken to identify a method of purification that would avoid column use.

### **3.3 Column-Free Purification**

Recently, a procedure for a column-free purification method has been developed that uses a calcium-binding sequence repeat to facilitate purification. BRT17 is a 17-fold repeat of a calcium responsive sequence from the block V RTX domain in the adenylate cyclase toxin CyaA from *B. pertussis*.<sup>123</sup> By creating a fusion of this protein sequence with MO14, it may be possible to create a protein that will reversibly precipitate in the presence of calcium ions. This would permit a simple, column-free purification of MO14 in which calcium ions are added to a solution of cell lysate, the fused protein will then precipitate and can be pelleted, resuspended in a calcium-free buffer and then further purification conducted if necessary. In order to conduct this purification, MO14 was cloned into the pMAL-BRT17 plasmid used in the cited article using the inPhusion cloning system; an agarose gel of the produced vector is shown in Figure 3.16.

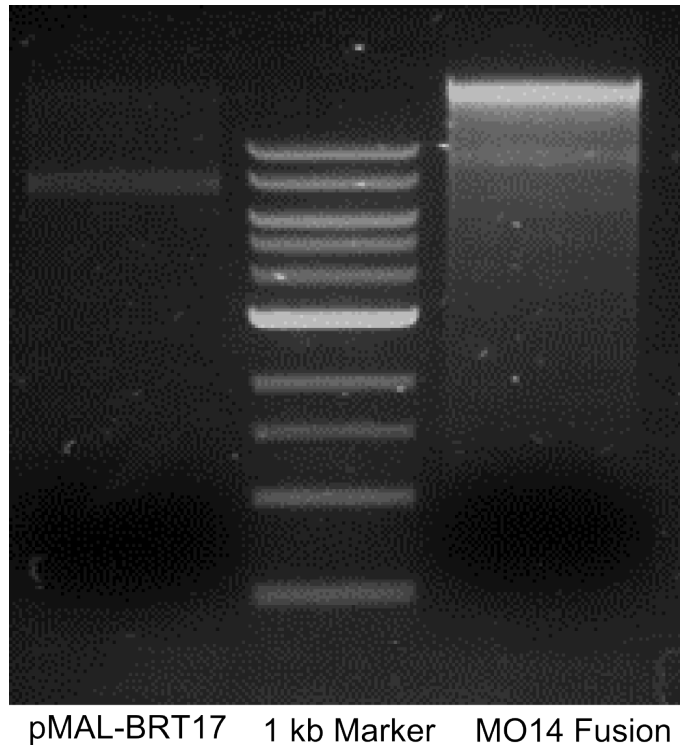


Figure 3.16: Agarose gel showing the MO14-BRT17 fusion. Marker bands are 10, 8, 6, 5, 4, 3, 2, 1.5, 1 and 0.5 kilobase pairs. The vector containing MO14 is the band visible at approximately 9.5 kb, roughly the size of MO14 (about 1.6 kb) larger than the initial vector.

The experiment itself was conducted by production of MO14 in cells, sonication and the soluble fraction was added to a solution of calcium chloride to a final concentration of 100 mM. This concentration should result in the insolubility of the protein, which then permits centrifugation to pellet the protein. 4 washes of the pellet were then conducted, with centrifugation to pellet the protein in between each wash, and a final resuspension in buffer with 100 mM  $\text{CaCl}_2$  replaced by 100 mM EGTA. EGTA is a strong chelator of calcium ions and should therefore remove all traces of the calcium from the protein solution, leaving a pure solution of MO14. Due to the importance of maintaining the buffer concentration and the untested effect of ammonium sulfate precipitation on this fused protein, the ammonium sulfate precipitation was not conducted on the sample prior to this purification method being attempted. Samples were taken throughout the process and analysed by SDS-PAGE, which is shown in Figure 3.17.

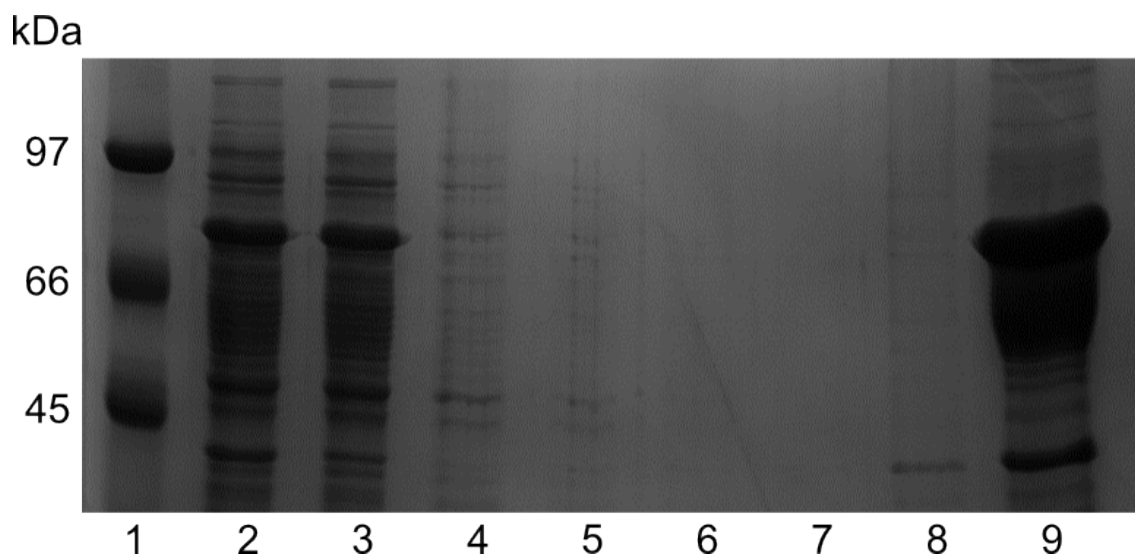


Figure 3.17: An SDS-PAGE gel showing the purification of MO14 by calcium-precipitation. Lane 1: Molecular Mass Marker, masses in kDa on the left. Lane 2: Total cell lysate; Lane 3: Soluble fraction; Lane 4: Supernatant after initial pelleting of MO14; Lanes 5-8: Supernatants from washing of pellet; Lane 9: Final sample after treatment with EGTA.

This technique has some issues as well, with both the presence of the impurity at around 45 kDa, although this may be simply the calcium-binding tag, and significant bands present that would seem to be indicative of protein degradation. This additional degradation, which appears more severe than previously observed, is likely due to the increased size of the protein and thus the increased number of protease-active sites available for attack. Further experimentation will involve investigation of the tolerance of this purification method to both the presence of protease inhibitors, such as the studied AEBSF, to attempt to prevent at least some degree of this degradation, and also a prior ammonium sulfate precipitation, to remove the large non-protease induced impurity. The convenience and simplicity of this procedure motivates additional focus, as the purification can be conducted very quickly and using relatively easily available materials.

### 3.4 Codon-Optimised Constructs

MO14 is an enzyme found naturally in *R. jostii* sp. RHA1, a bacteria that may have a different distribution of tRNAs to *E. coli*, as mentioned in the selection of the expression strain. Alongside

the chromatographic purification attempts on MO14 cloned into the YSBLIC-3C vector, an investigation was also undertaken to determine if modifying the genetic code of MO14 to provide more suitable encoding for *E. coli* would improve yield of protein. This process involves the synthesis of a gene that, rather than requiring additional tRNAs to be present in the host organism, redesigns the genetic code to emphasise the use of codons that are already present. This process leaves the amino acid sequence of the protein identical, and should therefore maintain folding and biotransformational activity, while ensuring that expression can be carried out more simply.

The sequence of MO14 was analysed by use of the GenScript online gene synthesis tool, and a new sequence designed to optimise production of the protein in the *E. coli* organism. Sequence designs generally do not involve more specialised design for individual strains of the host organism, but focus on making the best use of the genetic machinery generally present. The sequences of MO14 before and after optimisation can be found in the appendix. After the design was completed, the new gene was cloned into the YSBLIC-3C plasmid. The plasmid containing the codon-optimised MO14 (COMO14) was then transformed into *E. coli* Rosetta 2 (DE3) pLysS, cultures grown and induced using 1 mM IPTG, the cells lysed by sonication and the resulting solutions analysed for protein production by SDS-PAGE, shown in Figure 3.18.



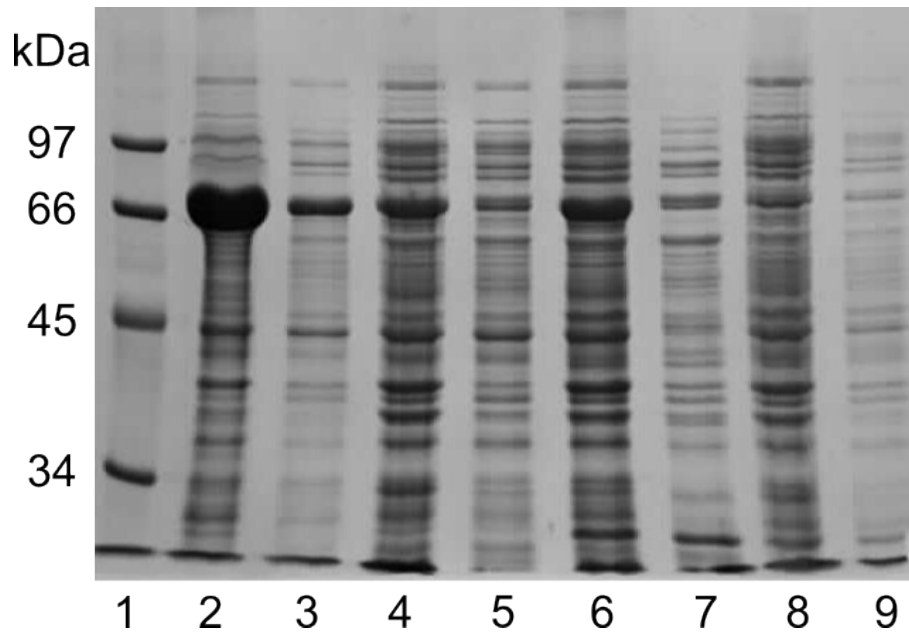


Figure 3.18: SDS-PAGE gel showing COMO14 expression. Lane 1: Low molecular weight marker (Biorad) with molecular weights given on the left in kiloDaltons. Lane 2: MO14 expression, total lysate. Lane 3: Wild-type MO14 expression, soluble fraction. Lanes 4, 6 and 8: COMO14 expressions from different picked transformation colonies, total lysate. Lanes 5, 7 and 9: COMO14 expressions from different picked transformation colonies, soluble fractions corresponding to lanes 4, 6 and 8 respectively.

It was anticipated that the level of soluble protein would be improved from the wild-type MO14, as the machinery present in the cell would permit faster production. What is observed is no increase in the production and, in some case, the level of MO14 is notably lower than for the wild-type expression. As incorrect cloning may have caused this difference, the simple hexahistidine-tagged codon-optimised MO14 was externally sourced, with several other constructs. These constructs were designed to aid in the purification of MO14, which had thus far proved troublesome.

- His-MBP-3C-MO14 : Maltose Binding Protein offers an alternative purification strategy. Tag size is approximately 40 kDa and the fused protein is expected to be about 100 kDa.
- His-GST-3C-MO14 : Glutathione-S-Transferase offers an alternative purification strategy. Tag size is approximately 26 kDa and the fused protein is expected to be about 85 kDa.
- His-IM9-3C-MO14 : IM9 protein improves solubility of fused proteins, which may improve

the relatively low soluble yield of MO14. Tag size is approximately 9.5 kDa and the fused protein is expected to be about 75 kDa.

- His-GFP-3C-MO14 : Green Fluorescent Protein aids visualisation and therefore simplifies purification. Tag size is approximately 27 kDa and the fused protein is expected to be about 85 kDa.
- His-3C-MO14 : Control of histidine-tagged MO14. The histidine tag is not expected to significantly change the mass of the fused protein, due to its small size.

Firstly, an expression test was performed using each of the constructs to see whether they expressed, and if any expression occurred into the soluble fraction. There is a possibility that the reason for the relatively poor expression of COMO14 is due to the use of the Rosetta<sup>TM</sup>2 (DE3) pLysS strain, as the altered tRNA quantities may result in an overall decrease in the ability of the cells to produce the codon-optimised version of the gene. The constructs were expressed in both *E. coli* BL21 cells and *E. coli* Rosetta 2 (DE3) pLysS cells, which would allow a comparison of the two methods of expression improvement; altering the gene to better suit the bacteria and altering the bacteria to better suit the gene. Expression tests were conducted and are shown in Figures 3.19 and 3.20.

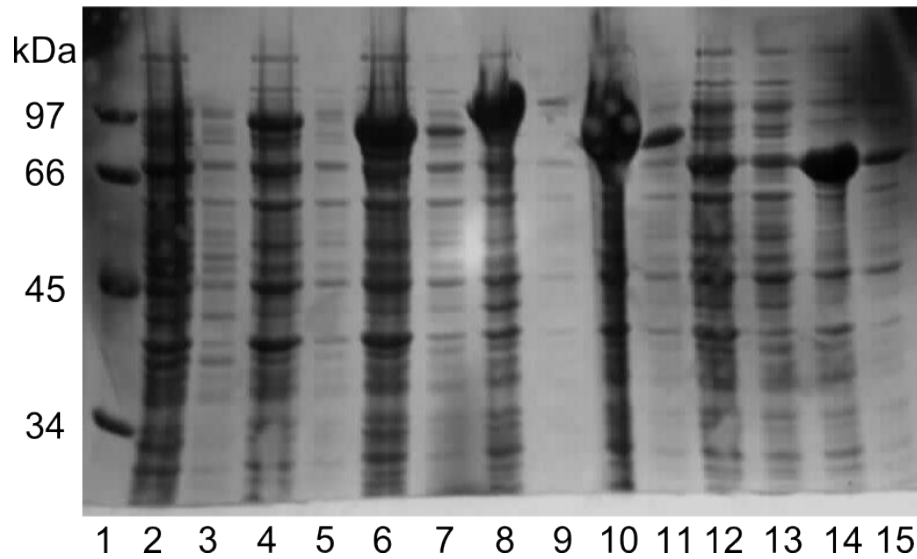


Figure 3.19: SDS-PAGE showing expression of codon-optimised MO14 constructs in *E. coli* BL21 cells. Lane 1: Low molecular weight marker (Biorad) with molecular weights given on the left in kiloDaltons. Lane 2: Vector-only control expression, total lysate. Lane 3: Vector-only control expression, soluble fraction. Lane 4: GFP-MO14 expression, total lysate. Lane 5: GFP-MO14 expression, soluble fraction. Lane 6: GST-MO14 expression, total lysate. Lane 7: GST-MO14 expression, soluble fraction. Lane 8: MBP-MO14 expression, total lysate. Lane 9: MBP-MO14 expression, soluble fraction. Lane 10: IM9-MO14 expression, total lysate. Lane 11: IM9-MO14 expression, soluble fraction. Lane 12: His-3C-MO14 expression, total lysate. Lane 13: His-3C-MO14 expression, soluble fraction. Lane 14: MO14 control expression, total lysate. Lane 15: MO14 control expression, soluble fraction.

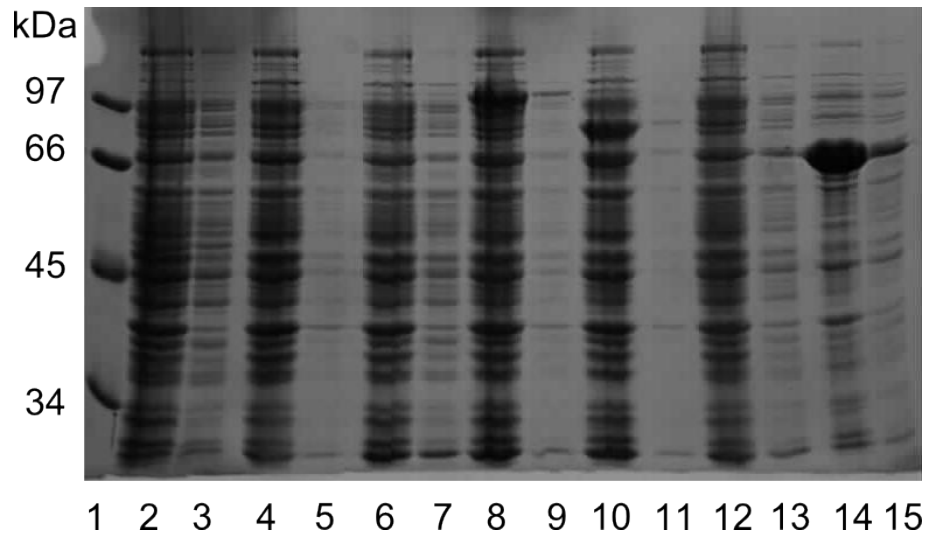


Figure 3.20: SDS-PAGE showing expression of codon-optimised MO14 constructs in Rosetta<sup>TM</sup>2 (DE3) pLysS cells. Lane 1: Low molecular weight marker (Biorad) with molecular weights given on the left in kiloDaltons. Lane 2: Vector-only control expression, total lysate. Lane 3: Vector-only control expression, soluble fraction. Lane 4: GFP-MO14 expression, total lysate. Lane 5: GFP-MO14 expression, soluble fraction. Lane 6: GST-MO14 expression, total lysate. Lane 7: GST-MO14 expression, soluble fraction. Lane 8: MBP-MO14 expression, total lysate. Lane 9: MBP-MO14 expression, soluble fraction. Lane 10: IM9-MO14 expression, total lysate. Lane 11: IM9-MO14 expression, soluble fraction. Lane 12: His-3C-MO14 expression, total lysate. Lane 13: His-3C-MO14 expression, soluble fraction. Lane 14: MO14 control expression, total lysate. Lane 15: MO14 control expression, soluble fraction.

The expression in Rosetta<sup>TM</sup>2 (DE3) pLysS cells was disappointing, and the only favourable expression levels came from the positive control of the MO14 wild-type protein. This would seem to confirm the explanation that the altered high quantity of non-native tRNAs present in this cell strain means that the organism is less able to express a gene that is designed to make use of the native genetic machinery. In BL21 cells, however, good insoluble yields were observed for GST, MBP and IM9 fusions, with lower yields for GFP and 3C. Soluble expression was more limited, with only IM9 (a solubility protein) and GST showing any soluble expression, however this is likely due to the increased size of the fusions over the MO14 gene alone.

### 3.4.1 Glutathione-S-transferase Purification

Given the good soluble expression of the GST-tagged MO14 in *E. coli* BL21, an attempt was made to purify by means of a GST affinity column. The GST tag consists of a glutathione-S-

transferase protein of approximately 26 kDa and the separation is achieved by the binding of this species to its substrate, glutathione. This molecule is attached to sepharose in order to produce the chromatographic column by which this technique is conducted. The GST-fusion protein was produced in *E. coli* BL21 cells, which were sonicated prior to conducting the purification. The soluble lysate was loaded onto a GST column, washed with buffer and eluted with glutathione, with the results analysed by SDS-PAGE, shown in Figure 3.21.

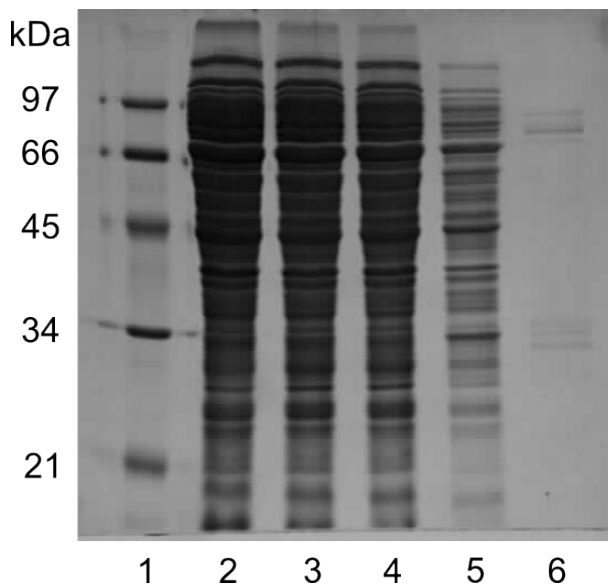


Figure 3.21: SDS-PAGE gel showing glutathione affinity purification of GST-COMO14. Lane 1: Low molecular weight marker (Biorad) with molecular weights given on the left in kiloDaltons. Lanes 2-4: Load samples. Lane 5: Non-binding fraction. Lane 6: Elution fraction.

The resultant purification of MO14 was relatively poor, with a large proportion of the enzyme not binding to the column. This is likely due to the poor binding affinity of the GST tag, which tends to require long cyclical loading on to the column at low temperatures to bind effectively. Additionally, we can again see the degradation that occurs in the majority of the purification strategies attempted for this protein.

### 3.5 Conclusions

The expression of wild-type MO14 was tested in the *E. coli* strains Rosetta<sup>TM</sup>2 (DE3) and Rosetta<sup>TM</sup>2 (DE3) pLysS and the pLysS strain selected for further use based on the largest production of soluble protein. Additionally, a codon-optimised version of this gene was designed and produced for comparative expression and purification alongside the native gene sequence. The expression of this codon-optimised strain was assessed in the *E. coli* strains Rosetta<sup>TM</sup>2 (DE3) pLysS and BL21, due to the difference in design features of these two strains. For the codon-optimised strain, the BL21 cells showed better expression than the Rosetta<sup>TM</sup>2 (DE3) pLysS. A wide range of column-based and column-free methods were attempted for use to purify MO14, with the largest focus on nickel IMAC systems, by means of a hexahistidine tag on the protein, however these were ultimately unsuccessful. The presence of an impurity that consistently co-eluted with MO14 was a large hindrance to the purification and proved difficult to remove by ion exchange chromatography, sepharose blue chromatography or hydrophobic interactions chromatography, all of which were attempted. The tendency of the protein to undergo degradation over time, especially when applied to a chromatography column, also proved to be an issue.

In future efforts toward the purification of this enzyme, the most promising route appears to be a combination of the column-free purification by means of calcium precipitation, in conjunction with a protease inhibitor. The inhibitor should prevent the large degradation observed for this purification method, which appears to be capable of removing the most consistent impurity. Should this course of action prove unsuccessful, several of the generated constructs may provide solutions to this purification or, alternatively, a combination of purification methods may prove successful subject to the time pressure of MO14 degradation.

## Chapter 4

# Biotransformations

### 4.1 Plasmid Preparation

To begin the project, stocks of the BVMO genes previously identified and cloned by Szolkowy<sup>118</sup> from *Rhodococcus jostii* sp. RHA1, in addition to CHMO<sub>Acineto</sub> for reference purposes, had to be generated to ensure consistency of material throughout the work to be conducted. These genes were available in the YSBLIC-3C plasmid and stocks were prepared using a plasmid miniprep kit, the results of which were analysed by restriction digestion using the enzymes NdeI and NcoI. This experiment was conducted in order to confirm that the plasmids were correctly transformed and that mutations are unlikely to have occurred, and additionally to confirm that the gene encoding the relevant enzyme is still present in the plasmid. The resulting agarose gel, shown in Figure 4.1, indicates that the transformation was successful, as the bands present are those that were predicted by previous work by Szolkowy; *i.e.* a vector band at approximately 5.5 kb and an appropriately-sized band for the enzyme-encoding gene.

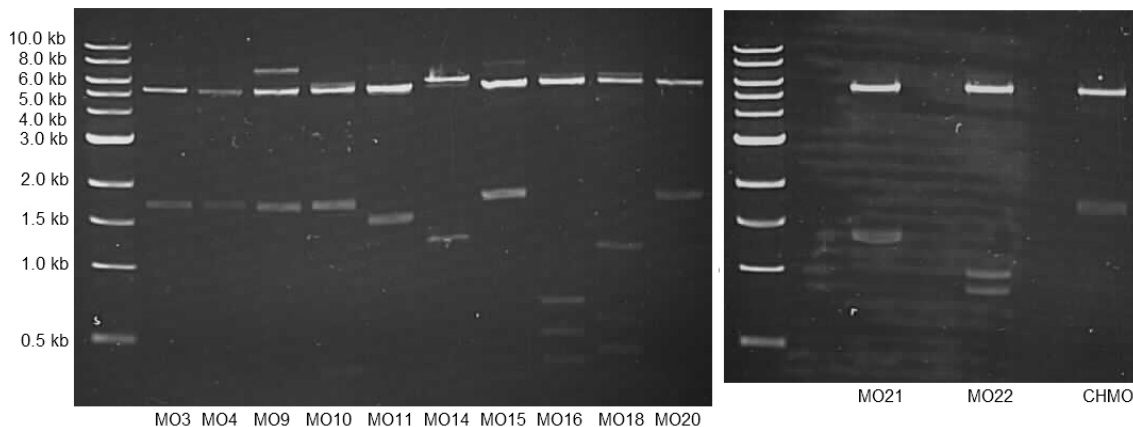


Figure 4.1: Agarose Gels Showing the Results of Restriction Digest of Plasmid DNA by Nde1 and Nco1

## 4.2 Ketone Biotransformations

As the main class of substrates for Baeyer-Villiger monooxygenases is ketones, the majority of the efforts involved the investigation and optimisation of the biotransformations of these compounds. Much of the work focusses on the exceptional capabilities of MO14 to convert substrates regio- and enantio-selectively, however the other BVMOs and BVMO-like enzymes from *R. jostii* are also assessed for their various catalytic abilities.

### 4.2.1 Cell Stock Production and Initial Biotransformations

The first course of action in conducting biotransformation experiments was the production of cell stocks. These were suspensions of Rosetta<sup>TM</sup>2 (DE3) *E. coli* cells that had been supplied with the relevant plasmids, grown in LB medium and frozen with glycerol at -80 °C. These cell stocks were intended to allow the screening of substrates against a large library of enzymes with relative ease, with twenty-three BVMOs available for study. Initial screening of the substrates involved addition of a solution of the chosen substrate to twenty-three 1 mL cell stocks, one for each BVMO. The reaction mixtures were then incubated at 30 °C with shaking and samples were taken after 2 h and after 24 h. The samples were extracted from the reaction mixture using ethyl acetate and analysed



by gas chromatography. The first ketone to be analysed using this method was bicyclo[3.2.0]hept-2-en-6-one (**1**), the structure of which is shown in Figure 4.2 in addition to the structure of the expected major product of the reaction, 2-oxabicyclo[3.3.0]oct-6-en-3-one (**2**).

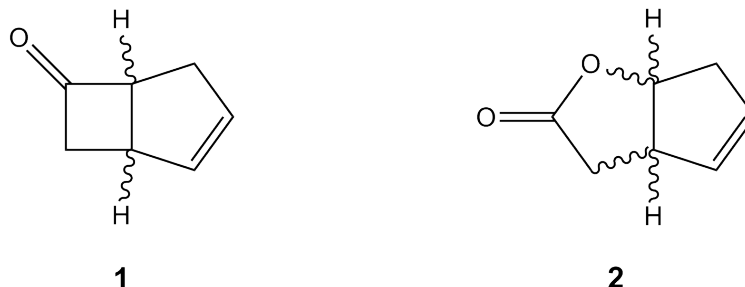


Figure 4.2: Bicyclo[3.2.0]hept-2-en-6-one, **1** and 2-oxabicyclo[3.3.0]oct-6-en-3-one, **2**

The BVMOs that showed most potential for converting this compound were MO3, MO4, MO10, MO11, MO20, MO21, and MO22; such a broad range of enzymes capable of transforming this substrate is to be expected as it represents the model substrate for testing of BVMOs. The GC traces for all bicyclo[3.2.0]hept-2-en-6-one transformations are shown in figure 4.3, with the substrate and expected major product labelled. Additional peaks consist of small amounts of impurities from the solvent or reactants, and some minor products; for example 3-oxabicyclo[3.3.0]oct-6-en-2-one.

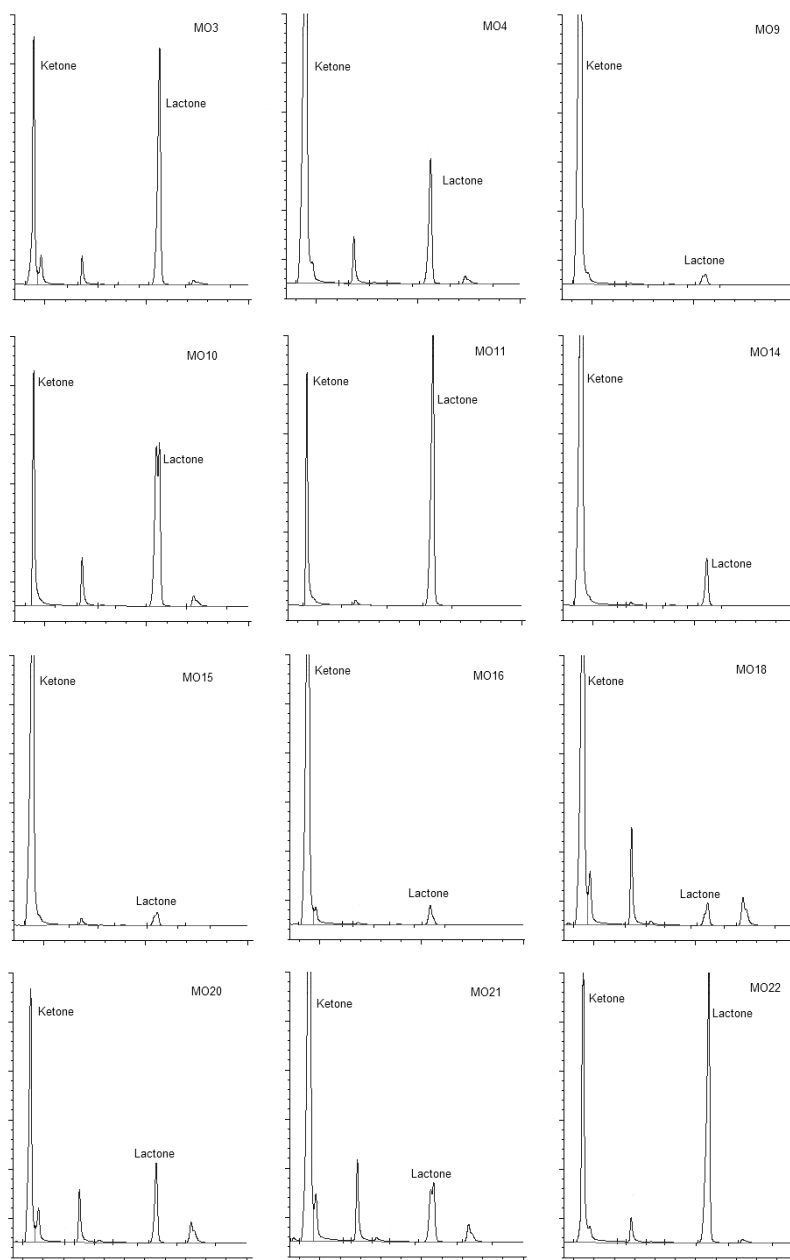


Figure 4.3: Gas Chromatograph Traces of bicyclo[3.2.0]hept-2-en-6-one Conversions to Lactone by Baeyer-Villiger Monooxygenases from *Rhodococcus jostii* in an achiral HP-5 column at 130 °C for 5 minutes. *x*-axes: GC Response (pA), *y*-axes: Time (min). Retention time of bicyclo[3.2.0]hept-2-en-6-one (Ketone) is 1.8 minutes and retention time of 2-oxabicyclo[3.3.0]oct-6-en-3-one (Lactone) is 3.1 minutes.

In an investigation targeted towards application to industrial processes, it is of interest to examine the capabilities of these enzymes to transform pharmaceutically relevant species. Rioz-Martinez *et al.*

*al.* demonstrated the capability of the BVMO 4-hydroxyacetophenone monooxygenase (HAPMO) to transform the substrates 1-indanone (**3**) and  $\alpha$ -tetralone (**4**) into their respective lactones, **5** and **6**.<sup>124</sup>

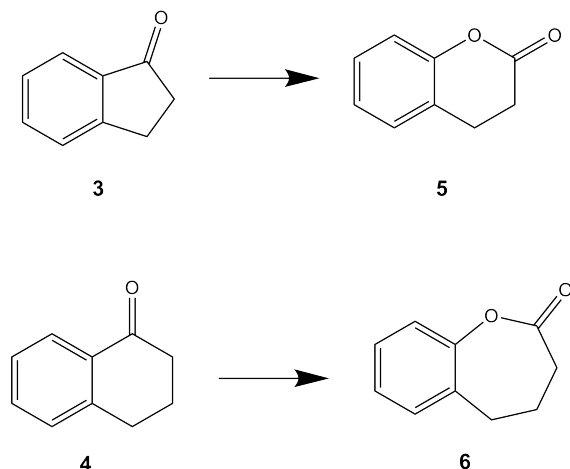


Figure 4.4: Structures of 1-indanone, **3**,  $\alpha$ -tetralone, **4** and their corresponding expected lactone products, **5** and **6**, respectively.

These substrates are of pharmaceutical interest owing to their similarity to building blocks of the anti-asthma agent, montelukast<sup>125</sup>, and a Baeyer-Villiger oxidation step would represent a convenient change to the synthetic route, avoiding the use of a Grignard reagent. HAPMO was able to conduct both Baeyer-Villiger oxidations in a 5 % solution of organic cosolvent and, in the case of 1-indanone, at a relatively high pH. In another example of BVMO engineering, they were also able to use a modified PAMO<sup>126</sup> to conduct a transformation of 1-indanone to produce the 3-oxa lactone to a yield of 79 %. These substrates are only somewhat soluble in water and therefore the ability of these BVMOs to conduct biotransformations in a biphasic system is very valuable.

Since these species are relevant due to both their pharmaceutical applicability and previous examples of Baeyer-Villiger oxidation, the library of BVMOs generated were assessed for their activity towards both **3** and **4**. 1 mL whole cell cultures were again mixed with substrate dissolved in EtOH and incubated for 24 h at 30 °C with shaking. The results were generally negative; shown in Fig-

ures 4.5 and 4.6 are the results that appeared to show some transformation of the substrates relative to standard GC analyses, however characterisation of these small quantities was not conducted due to the relatively minor ability of the tested BVMOs to perform these transformations.

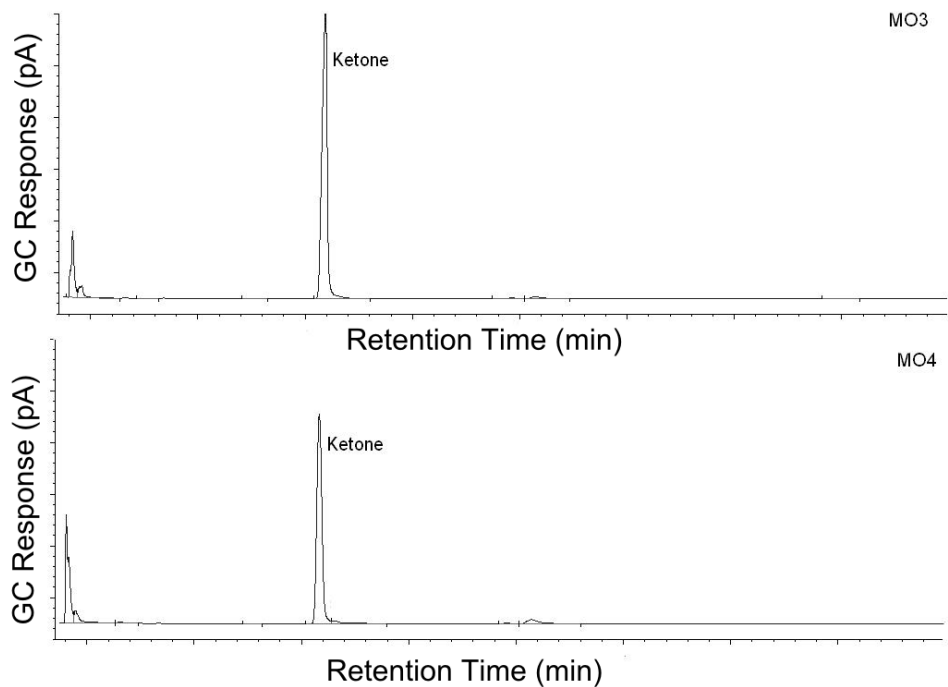


Figure 4.5: Gas Chromatograph Traces of 1-indanone transformation by MO3 and MO4.

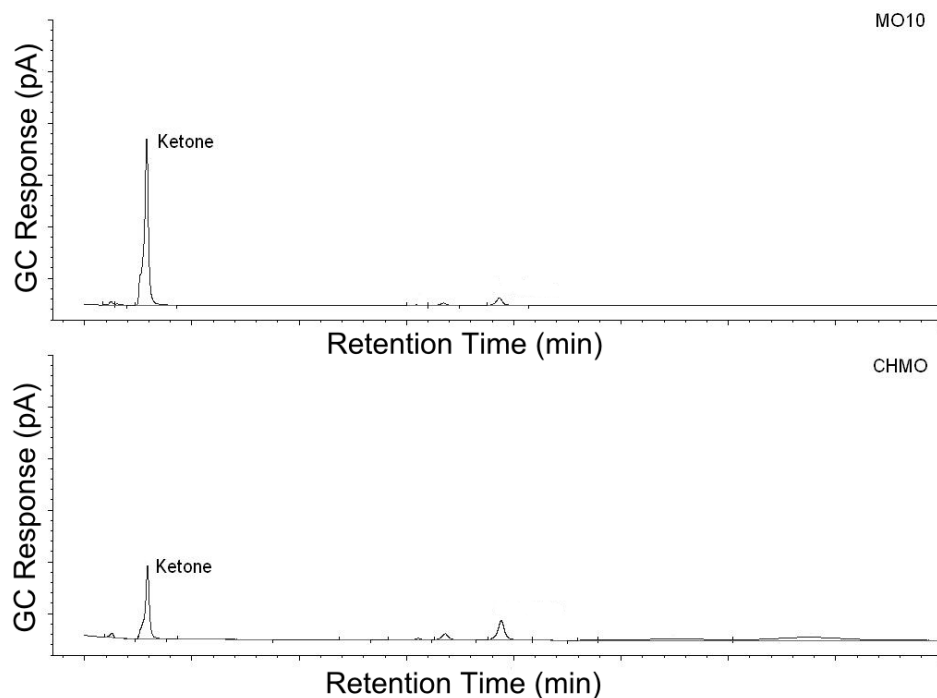


Figure 4.6: Gas Chromatograph Traces of  $\alpha$ -tetralone transformation by MO10 and CHMO<sub>Acineto</sub>.

#### 4.2.2 MO14 Biotransformation of Bicyclo[3.2.0]hept-2-en-6-one

Based on the disappointing results from the indanone and tetralone conversions, it was decided to focus on characterising the MO14 biotransformation of bicyclo[3.2.0]hept-2-en-6-one. This is of interest because MO14 transforms this substrate both enantio- and regio-selectively, uniquely among enzymes of its type. In order to characterise this transformation, the initial variable that was investigated was the cell density at which the reaction would be conducted. In general, it could be expected that the transformation of substrate would increase as the cell density rises; this would be due to the higher availability of biocatalyst to perform the reaction, *i.e.* more BVMO is produced and therefore more is available to conduct the reaction. In previous work, however, the increase in cell density appears to negatively affect the transformation.<sup>127</sup> These experiments showed the highest rate of transformation occurred with the lowest cell density, and indeed the increasing cell density showed a concurrent decrease in productivity. The suggestion therefore is that optimum

cell density derives from the oxygen demand of the system and flexibility to adjust other factors in the reaction. Although the specific aspects of the transformation conducted here differ significantly from the post-fermentation experiments conducted by Hilker *et. al.*, the results obtained inform the following experiments.

*E. coli* strain Rosetta<sup>TM</sup>2 (DE3) pLysS was transformed with the plasmid containing the gene encoding MO14 and cell stocks frozen at -80 °C in buffer R. Dilutions of these stocks were taken in order to discover the ideal optical density of cells containing the biotransformant at which to attempt the biotransformation by addition of the substrate to a 1 mL sample of cells, diluted to the appropriate cell density. The results are shown in Figure 4.7.

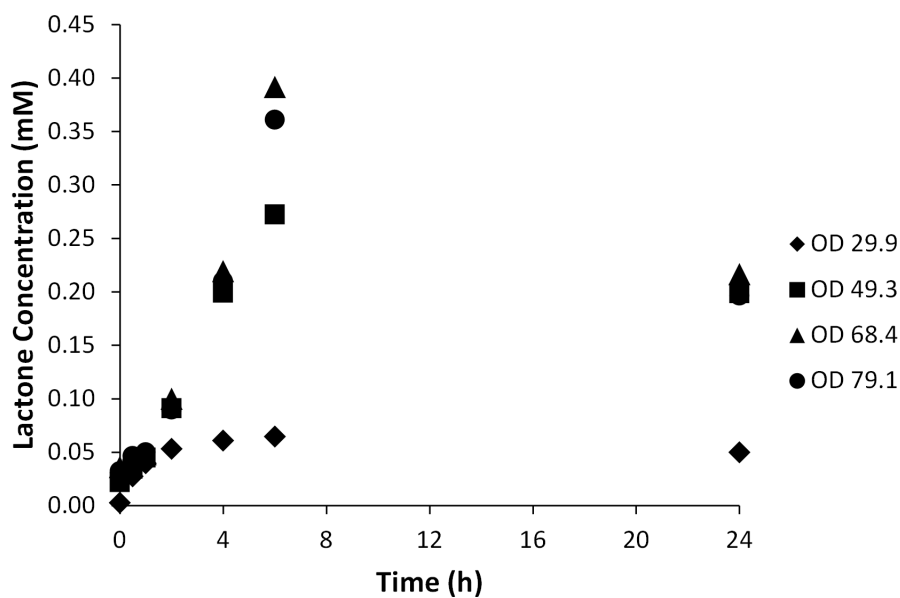


Figure 4.7: Conversion of *cis*-bicyclo[3.2.0]hept-2-en-6-one with change of cell density, measured by optical density at 600 nm, by *E. coli* Rosetta<sup>TM</sup>2 (DE3) pLysS cells expressing MO14.

As was expected based on similar experiments, we can observe from these results that increasing cell density improves the conversion, up to an upper limit. The steady increase in reaction rate is likely due to a greater amount of enzyme being present and available to perform the reaction as cell density increases. Once oxygen availability reaches a critical level, it begins to limit the

reaction and causes the drop that can be seen in the OD<sub>600</sub> 79.1 sample. Since the reactions were performed in 7 mL bijou vials, it seems likely that this limit would be reached relatively quickly as the headspace above the reaction, and therefore the available oxygen, is relatively small. This explanation for the decrease in conversion, being both easily explained and in concurrence with previous studies on these reactions, seems to be plausible here.

The second reaction attribute to be examined was the substrate concentration. Whole-cell work on BVMOs is often limited by the toxicity of the substrates used to the host organism<sup>128,129</sup>, with substrate concentrations optima of 0.2 - 0.4 g L<sup>-1</sup>. The most common method of overcoming this limitation is to use an *in situ* substrate feeding and product removal system, which allows for the optimum substrate concentration to be maintained.<sup>130,86</sup> It is of interest that this combined substrate feeding and product removal is necessary not only to maintain a low substrate concentration, but also to ensure that the product concentration does not reach inhibitory levels, as lactone concentrations above roughly 4 g L<sup>-1</sup> also have a deleterious effect on the transformations.<sup>127</sup> On the comparatively smaller scale of the reactions conducted here, an *in situ* process to maintain substrate and product levels is impractical and was therefore not considered.

The reactions were conducted as for the cell density experiments, however this time the optical density of cells was equal and a differing concentration of the substrate was added. The expected results would show an increase in product generation concurrent with the substrate concentration until the toxicity limit is reached and the product generation drops. This limit was expected to be approximately in line with previous observations in other research, *i.e.* between 0.2 g L<sup>-1</sup> and 0.4 g L<sup>-1</sup>, which corresponds to a molar concentration of approximately 2 to 4 mM. Shown in Figure 4.8 are the results observed for the substrate concentration optimisation experiment.

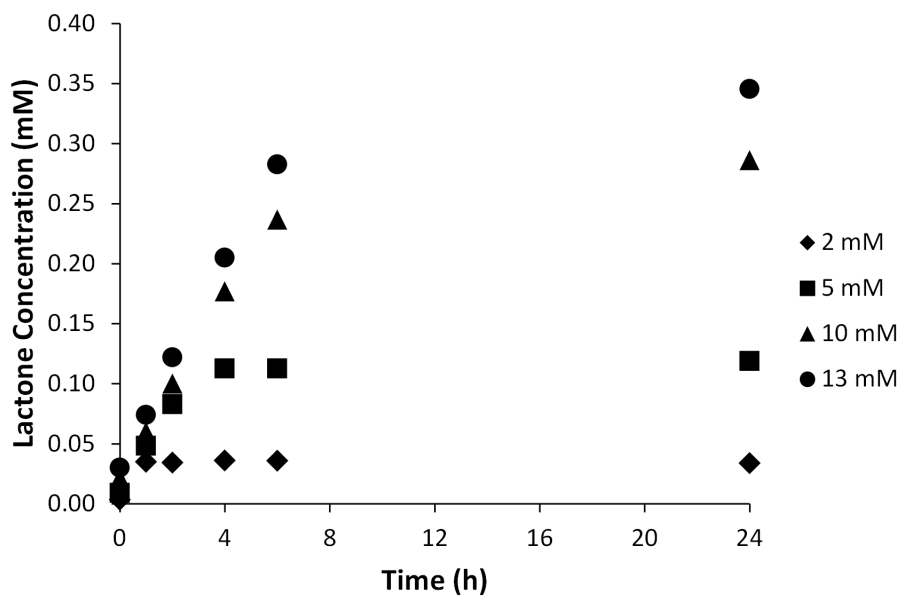


Figure 4.8: Conversion of *cis*-bicyclo[3.2.0]hept-2-en-6-one with change of substrate concentration, measured in mM, by *E. coli* Rosetta<sup>TM</sup>2 (DE3) pLysS cells expressing MO14.

In the substrate concentration results, we can see that there is a gradual increase in conversion with substrate concentration, owing to the greater occupation of enzyme active sites, as lower concentrations may not reach the  $K_M$  of the enzyme. Similarly, there is a reduction in conversion above 10 mM substrate, which can be explained as a saturation of enzyme active sites and the potentially damaging effects of the ketone on the *E. coli* cells. Interestingly, the substrate concentration does not appear to limit the transformation of this substrate even at the maximum concentration tested, 13 mM. This is over three times higher a concentration than the previously observed limitations and suggests either Rosetta<sup>TM</sup>2 (DE3) pLysS is a much more resilient strain of *E. coli* than those used in previous experiments or that MO14 confers extra stability to the host organism, perhaps by consuming the substrate before significant damage can occur.

When BVMO biotransformations are conducted with isolated enzymes, it is necessary to introduce a cofactor recycling system, as the NADPH is oxidised during the reaction and must be regenerated before another cycle can occur. Typically these cofactor systems consist of an enzyme



and substrate that will make use of the oxidised form of NADPH to conduct the reaction and occur much more quickly than the Baeyer-Villiger oxidation. For example, the G6P system involves glucose-6-phosphate dehydrogenase from *Leuconostoc mesenteroides* and glucose-6-phosphate itself. The dehydrogenase enzyme transfers a hydride from glucose-6-phosphate to NADP<sup>+</sup> and thus regenerates it.

In a whole-cell system, this addition is not necessary because most host organisms will possess an NADPH regeneration system within the cell. This regeneration system is generally required to maintain levels of NADPH for the host organisms' enzyme activity and means that a whole-cell approach is much simpler in terms of additives. In *E. coli*, the NADPH regeneration pathway depends on the presence of glucose<sup>131</sup> and is directly related to the growth of cells, rather than solely for the purpose of biotransformations. Efforts to improve the ability of *E. coli* to regenerate NADPH by modulating the relevant pathways therein have proved successful<sup>132</sup>, however in this case, simple addition of glucose to the cells was attempted in order to promote NADPH regeneration by the host organism to improve BVMO activity.

The biotransformations were conducted as before, with 1 mL of cell culture in a 7 mL bijou vial, to which was added glucose to a range of final percentages w/v. Substrate was added in solution in ethanol and samples taken and extracted with ethyl acetate over the course of the reaction, which was conducted at 30 °C with shaking for 24 h. The results were expected to show a minor increase in the rate of conversion of substrate, as NADPH regeneration is improved slightly, and are shown in Figure 4.9.

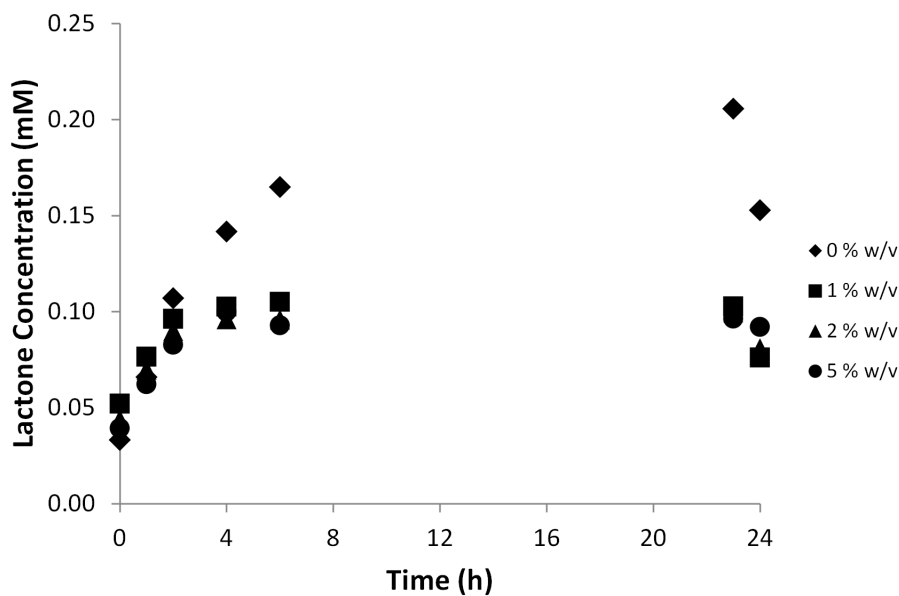


Figure 4.9: Conversion of *cis*-bicyclo[3.2.0]hept-2-en-6-one with change of glucose concentration, measured in % w/v, by *E. coli* Rosetta<sup>TM</sup>2 (DE3) pLysS cells expressing MO14.

The results show that, contrary to initial expectations, addition of glucose significantly reduces the ability of the bacteria to perform the reaction. The most likely cause of these results is that the presence of glucose influences the bacteria to invest energy in reproduction, rather than performing the reaction. This explanation would seem to agree with the knowledge that the NADPH regeneration pathway is tied to the growth of *E. coli* and therefore overstimulation thereof could trigger the bacteria to start the growth phase. On a larger scale, this could perhaps be avoided by ensuring that appropriate levels of other energy sources are available, allowing the glucose to be used for NADPH recovery. If necessary, the modification of the host organism by means of genetic manipulation could also prove to have beneficial effects, for example by modifying the host itself to contain a separate regeneration system, as seen for a number of biotransformations, including production of xylitol from xylose by a reductase enzyme and oxidation of *p*-chloroanisole by a cytochrome P450.<sup>132</sup>

The final optimisation investigated on this scale was the addition of  $\beta$ -cyclodextrin, which has

been reported to improve the activity of BVMOs.<sup>133</sup> Although the exact mechanism of this activity improvement has not been confirmed, it is suspected that the ability of cyclodextrins to sequester molecules may result in either assistance to the substrate in crossing the cell barrier or in the collection of the substrate away from cells, preventing toxic activity. It was therefore expected that the reaction would show a small increase in activity on addition of cyclodextrin and the results are shown in Figure 4.10, with the experiment conducted as for glucose concentration.

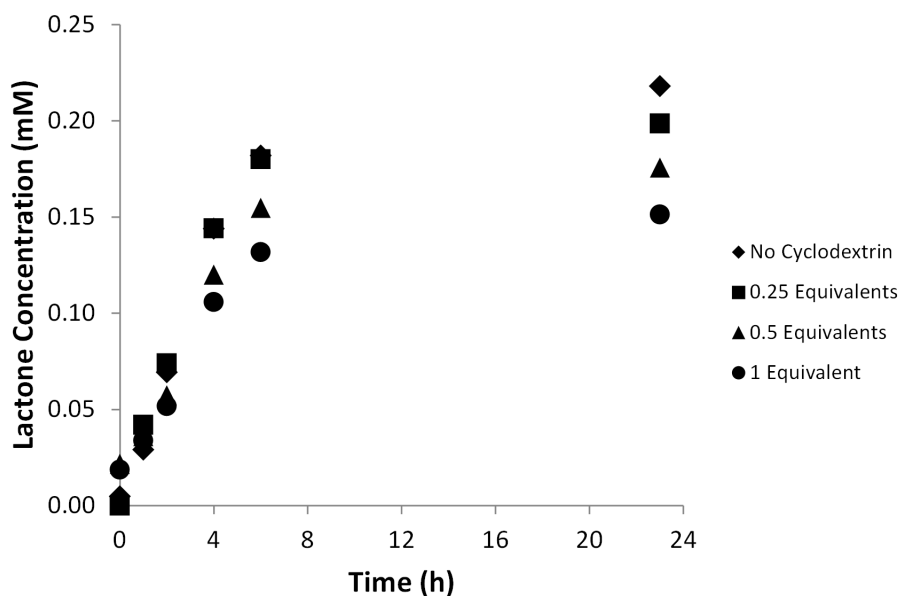


Figure 4.10: Conversion of *cis*-bicyclo[3.2.0]hept-2-en-6-one with change of cyclodextrin quantity, measured in molar equivalents to substrate, by *E. coli* Rosetta<sup>TM</sup>2 (DE3) pLysS cells expressing MO14.

In these results, there is clearly a decrease in the conversion when cyclodextrin is added. In the previous study that showed improvement to the conversion, a concentration of only 10 mol %, *i.e.* 0.1 equivalents was used, and it is possible that an amount this low may be the exact amount required to improve conversion by the means suggested, whereas the quantities used here result in the substrate being sequestered more thoroughly, to the point that there is no access to the BVMO.

These small-scale reactions are useful to determine a starting point for conducting a scale-up reaction that could then be used to inform industrial scale syntheses. As the conversion of bicyclo[3.2.0]hept-

2-ene-6-one is potentially relevant to prostaglandin synthesis, an investigation such as this allows the knowledge base to be increased without the requirement for significant investment. Clearly demonstrated is the need to carefully select a density of cells and a substrate concentration appropriate to the reaction, and two potentially useful additives have also been screened for their contribution to the activity of MO14.

### 4.3 MO14 Biotransformation of Sulfides

In addition to the Baeyer-Villiger reaction, the broad promiscuity in the substrates accepted by BVMOs permits the biotransformation of a number of other species. BVMOs have been observed to catalyse the transformations of boronic acids to phenols<sup>134</sup>, tertiary amines to N-oxides<sup>135</sup> and double bonds to epoxides<sup>136</sup>, but most commonly sulfides to sulfoxides.<sup>137,138,139</sup> These transformations are notable for sharing the high rate of enantioselectivity that they possess towards their traditional substrates with the sulfide targets, resulting in the formation of chiral sulfoxides, which are of key interest in organic synthesis owing to both their high stability and their utility as chiral auxiliaries in a number of reactions ranging from Diels-Alder cycloadditions in the form of a bis-sulfinylimidoamidine<sup>140</sup> to hydrogenations<sup>141</sup> and allylic substitutions.<sup>142</sup>

Of particular interest industrially is the pharmaceutical agent esomeprazole, which is the *S* enantiomer of omeprazole. Both of these species are used in the treatment of gastrointestinal ulcers with the single enantiomer claimed to be more effective than the racemic mixture.<sup>143</sup> These compounds act as a proton pump inhibitor and represent a key target for pharmaceutical investigation, as one of the top selling drugs in the US. One of the key steps in the synthesis of this species is the oxidation of a sulfide to the relevant sulfoxide<sup>144</sup> and the development of a new method to perform this transformation would represent a valuable step in this compound's production, as shown in Figure 4.11.

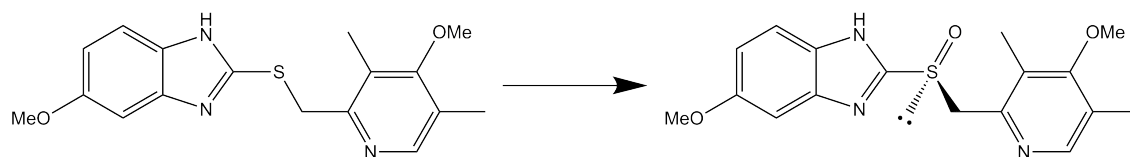


Figure 4.11: The desired asymmetric sulfoxidation in the synthesis of esomeprazole.

BVMO activity against sulfides has been known for over twenty-five years<sup>145</sup> and differs significantly from the mechanism by which ketone oxidation occurs; the sulfide biotransformation can be explained by a nucleophilic attack of the sulfur on the peroxyflavin species, which results in the addition of oxygen to the sulfide.<sup>146</sup> Much of this early work on BVMO oxidation of sulfides centred on CHMO<sub>Acinetobacter</sub>, due to the high promiscuity of this enzyme toward various targets. More recently, owing to the interest in chiral sulfoxides from a synthetic point of view, a number of other BVMOs have been assessed for their ability to convert sulfides and have also shown success, including PAMO<sup>147</sup> and HAPMO.<sup>148</sup> In some cases, the breadth of the activity of BVMOs can be a drawback in this chemistry, as the possibility for over-oxidation of the sulfoxide to the sulfone is present, as is observed for CHMO<sub>Acinetobacter</sub>,<sup>134</sup> and represents a significant challenge to sulfide oxidation in both synthetic organic chemistry and the adaptation of these enzymes to sulfoxide synthesis.

The ability of MO14 to convert a range of prochiral sulfides was therefore investigated. The first analysis of the activity used MO14 present *E. coli* Rosetta<sup>TM</sup>2 (DE3) pLysS cells expressing MO14 or CHMO<sub>Acinetobacter</sub>, in the same manner as the reaction with bicyclo[3.2.0]hept-2-en-6-one, *i.e.* 1 mL of cell culture to which the sulfide was added as a solution in ethanol. Very low conversions were achieved by this method, for which two explanations seem most likely: the substrate may be toxic to cells, resulting in the NADPH regeneration system no longer being viable and the reaction therefore ceasing; or the substrate may be unable to pass through the membrane of the cells, rendering it inaccessible to MO14.

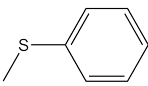
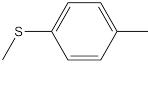
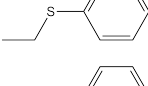
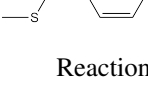
In general, previous work on BVMO sulfide oxidation has used isolated enzyme for study, how-

ever as previously discussed, the purification of MO14 has proven very challenging. Given the unavailability of purified MO14 enzyme, it was decided to conduct the experiment using crude cell lysate. The MO14 was expressed in *E. coli* Rosetta<sup>TM</sup>2 (DE3) pLysS cells, which were then lysed via sonication and the cell lysate extracted by high-speed centrifugation. The cell lysate was then combined with a glucose-6-phosphate NADPH-regeneration system and the sulfides added in ethanolic solution, before incubation at 30 °C with shaking for 24 h. The samples were then extracted with ethyl acetate and analysed by GC.

#### **4.3.1 Lower Functionality Sulfides**

The first category of sulfides examined were those with lower levels of functionality, *i.e.* those that possessed only carbon and hydrogen atoms besides the sulfur; using these substrates as an initial test allows the investigation of the effect of compound size and sulfide position on the conversion. Four sulfides were examined in this category: methyl phenyl sulfide as a 'base' sulfide from which to work; methyl p-tolyl sulfide to assess the effect of a small, hydrophobic para-substituent on the reaction; benzyl methyl sulfide and ethyl phenyl sulfide to test the effect of shifting the position of the sulfur atom along the hydrocarbon chain at the 1-position on the molecule. The results of these biotransformations are shown in Table 4.2.

Table 4.1: Low Functionality Sulfide Biotransformations by *E. coli* Rosetta<sup>TM</sup>2 (DE3) pLysS cells expressing MO14 or CHMO<sub>Acineto</sub>.

Sulfide	Structure	MO14 Yield	MO14 e.e.	CHMO Yield	CHMO e.e.	Lit. CHMO e.e. <sup>149</sup>
Methyl Phenyl Sulfide		26 %	85 % <i>S</i>	97 %	>99 % <i>R</i>	99 % <i>R</i>
Methyl <i>p</i> -tolyl Sulfide		66 %	>99 % <i>S</i>	Yes	43 % <i>S</i>	37 % <i>S</i>
Ethyl Phenyl Sulfide		66 %	>99 % <i>S</i>	Yes	8.9 % <i>R</i>	47 % <i>R</i>
Benzyl Methyl Sulfide		12 %	68 % <i>S</i>	97 %	22 % <i>R</i>	54 % <i>R</i>

Reactions conducted at 30 °C with shaking for 24 h.

### Methyl Phenyl Sulfide

The results for the transformation of methyl phenyl sulfide, or thioanisole, were relatively positive. The overall yield was fairly low, which would seem to indicate that this substrate is a poor fit for the active site of MO14. The e.e. of the transformation is fairly good at 85 %, and represents a favouring for one orientation of the substrate in the active site. The symmetric nature of this substrate would seem to indicate that the mechanism by which the enantioselectivity originates involves the attack of the molecule by the oxygen source from only one side, resulting in the majority enantiomer. This interaction cannot be completely directed, however, due to the presence of the minor enantiomer. The experiment conducted with CHMO<sub>Acineto</sub> shows a much higher yield and a very enantioselective reaction with this substrate, with almost complete conversion of the sulfide to the *R* sulfoxide, which makes this potentially a very useful reaction. The results compare favourably to the literature observed e.e. for CHMO<sub>Acineto</sub> on this substrate, with the results in agreement.

### Methyl *p*-Tolyl Sulfide

The conversion of methyl *p*-tolyl sulfide shows a marked improvement in both yield and e.e. from the previous methyl phenyl sulfide. The improved yield of the reaction may be a result of the

increased electron availability in the phenyl ring due to the +I effect of the methyl group. This effect is expected to be relatively minor, however, and it may also be the case that this methyl group causes the positioning of the substrate to be more favourable to the shape of the active site. The e.e. is also improved over that of methyl phenyl sulfide to represent a very enantioselective reaction, which may be again due to the closer localisation of the reaction centre to the relevant amino acid residues. These results are particularly impressive when compared to the reaction conducted by CHMO<sub>Acineto</sub>, which showed only a 43 % e.e. and this result was higher than the literature value for this transformation of only 35 %. This *S*-selective character of MO14 constitutes a trend observed throughout these experiments.

### **Ethyl Phenyl Sulfide**

The reaction of ethyl phenyl sulfide investigates the impact of adding the extra carbon atom to the other end of the molecule from methyl *p*-tolyl sulfide. Interestingly, the addition of this moiety in this location results in a very similar yield to the methyl *p*-tolyl sulfide and a similarly high e.e.. These observations are somewhat surprising, as the expectation would be that the extra length of the ethyl group at the sulfur would cause a different position of the substrate in the active site and therefore altered activity. It is possible that the same effect from increasing electron density near the sulfur atom results in stabilisation of a reaction intermediate and therefore increases the yield, however the similar increase in the e.e. is more difficult to explain. The extra bulk from the ethyl group, as well as the methyl group in the methyl *p*-tolyl sulfide experiment, may both result in the positioning of the phenyl group to result in a  $\pi$ -stacking interaction that localises the substrate in a manner that can increase the e.e.. This result again shows a significant improvement over the CHMO<sub>Acineto</sub> results, which themselves are very different from those observed in the literature. The difference in the conducted CHMO<sub>Acineto</sub> experiment from the previous research may result from a difference in the buffer solution used to resuspend the cells prior to sonication.



### **Benzyl Methyl Sulfide**

Benzyl methyl sulfide possesses a very similar structure to ethyl phenyl sulfide and a comparative experiment is therefore useful to inform the exact positioning of the sulfur atom for optimal conversion and enantiomeric selectivity. This sulfide shows a significant decrease in the conversion yield, which may be due to the shift of the sulfur atom one atom along the hydrocarbon chain disrupting the position of the reaction centre away from the catalytic site. Additionally, the enantiomeric excess is reduced, the explanation of which is less certain. It is possible that the free rotation of the molecule around an additional carbon atom may result in less specific conversion as both potential positions for conversion become accessible. The e.e. is still higher in absolute terms than the  $\text{CHMO}_{Acineto}$  result, which was observed in this experiment as 22 % but has been reported at 54 %. The higher e.e. for MO14 is only slight, however, and does not represent the ideal e.e. values that are obtained for other substrates in this work.

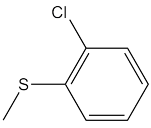
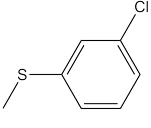
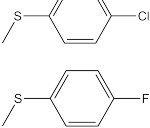
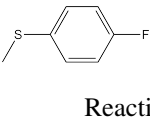
These low-functionality sulfides are very useful in determining further experiments to be conducted and seem to indicate that movement of the sulfur atom from adjacent to the phenyl ring has a deleterious effect on the reaction, hence it can be considered that the position of the phenyl ring is key to placing the sulfur atom in the correct position. This observation is concurrent with a  $\pi$ -stacking interaction for the phenyl ring with another aromatic moiety located in the active site; this would account for the requirement for accurate sulfur positioning. It also seems that additional electron density being pushed towards the sulfur atom has a positive effect on the reaction, perhaps stabilising a positively-charged intermediate, as is the case of catalysis of the traditional Baeyer-Villiger reaction when the Criegee intermediate is generated.

### **4.3.2 Halo-substituted Sulfides**

In order to further probe the activity of MO14 towards sulfides, a selection of halo-substituted thioanisoles was screened. This selection of experiments was designed to investigate the differing

effects of the same group in different positions around the phenyl ring and also to compare the effects of chloro- and fluoro- substitutions. Literature studies with CHMO<sub>Acineto</sub> indicate that the chloro-substituted substrates are not converted in a very selective manner, with e.e. values no higher than 51 %, whereas the fluoro-substituted thioanisole was converted to a very high degree of enantioselectivity reaching 93 % e.e. for the *S* enantiomer. The results of these experiments are shown in Table 4.3.

Table 4.2: Halo-Substituted Sulfide Biotransformations by *E. coli* Rosetta<sup>TM</sup>2 (DE3) pLysS cells expressing MO14 or CHMO<sub>Acineto</sub>.

Sulfide	Structure	MO14 Yield	MO14 e.e.	CHMO Yield	CHMO e.e.	Lit. CHMO e.e. <sup>149</sup>
2-Chlorothioanisole		28 %	>99 % <i>S</i>	Yes	53 % <i>R</i>	32 % <i>R</i>
3-Chlorothioanisole		74 %	>99 %	Yes	74 %	-
4-Chlorothioanisole		72 %	>99 % <i>S</i>	Yes	72 % <i>S</i>	51 % <i>S</i>
4-Fluorothioanisole		23 %	86 % <i>S</i>	99 %	84 % <i>R</i>	92 % <i>R</i>

Reactions conducted at 30 °C with shaking for 24 h.

## 2-Chlorothioanisole

The first halo-substituted compound tested was 2-chlorothioanisole, which possesses a chloro-group in the ortho position of the phenyl ring. The results for this compound are a similar conversion yield to the unsubstituted thioanisole transformation, with a much higher enantioselectivity for the *S* product. The chloro- group has a general negative inductive effect on the ring, reducing the overall electron density in the system, in addition to a very weakly positive mesomeric effect which is generally overcome by the strength of the inductive effect. This reduction in available electron density would, based on the previous results for lower electron density near the sulfur atom, lower the conversion. Additionally, it is possible that the steric bulk of the chlorine atom

may affect the ability of the enzyme to access the sulfur atom and conduct the biotransformation. It is notable that the e.e. is so high, and this may be a result of the bulk of the chloro- group preventing the rotation within the active site, which encourages the production of a single enantiomer. CHMO<sub>Acineto</sub> showed a reasonable ability to convert this substrate, although the enantiomeric excess reached was only 32 %, and preferred to conduct the *R*-selective reaction, which indicates that the active site in CHMO<sub>Acineto</sub> may be inverted with respect to the catalytic residues when compared to MO14.

### 3-Chlorothioanisole

3-Chlorothioanisole shifts the chloro- group into the *meta* position on the phenyl ring and should result in less steric hindrance of the enzyme, as the accessibility of the sulfur atom is markedly increased. A significant increase in the yield is observed and the high enantioselectivity observed for the 2-chloro derivative is maintained, which lends more credence to the theory that the chlorine atom is preventing rotation in the active site and raising e.e. values. The high conversion observed seems to disagree with lower electron density affecting the conversion negatively, as there is an improvement over the original thioanisole conversion. This may suggest that the prevention of rotation also helps to maintain the positioning of the sulfur atom close to the catalytic residues, the effect of which was obscured in the 2-chlorothioanisole experiment by the steric bulk of the chlorine atom being so close to the sulfur. Unfortunately, the specific enantiomer produced could not be identified, as the chiral GC responses of the enantiomers have not yet been identified, however the general preference for MO14 suggests that the *S* enantiomer is more likely to be favoured. The conversion performed by CHMO<sub>Acineto</sub> also shows a fairly high e.e., although not to the excellent level observed for MO14, and the literature is lacking a result for this transformation.

### 4-Chlorothioanisole

The *para*-substituted chlorothioanisole results are perhaps more complicated to explain than the previous two results. Since there is no asymmetry, it follows that the chloro group is unlikely to be

preventing the rotation of the substrate in the active site, yet this compound is still converted nearly three times as effectively as thioanisole itself. The explanation for this likely resembles that for methyl *p*-tolyl sulfide, in that the presence of a *para* substituent may result in better positioning of the substrate for conversion by the enzyme. The e.e. is again very high and demonstrates again the remarkable preference for this enzyme to transform these substrates in an *S* selective manner, well beyond the capabilities of CHMO<sub>Acineto</sub>. The values observed for the CHMO<sub>Acineto</sub> transformation of this substrate are themselves good in this context, but again are overshadowed by MO14, as are the literature results previously identified.

#### **4-Fluorothioanisole**

The final transformation in this category is that of 4-fluorothioanisole. This substrate possesses a similar group to the 4-chloro analog, but the size of the fluoro moiety is significantly smaller than the chloro equivalent. This decrease in size manifests in a drop in conversion to just 23 %, a significant drop compared to the chloro equivalent and suggests that the bulk of the previous group is directly related to the ability of the enzyme to convert it. A fluoro group is smaller than both the comparable methyl (as in methyl *p*-tolyl sulfide) and chloro (as in 4-chlorothioanisole) groups and the transformation conducted here is lower than both of these comparisons. Additionally, the e.e. decreases from the excellent values for other substituents in this position, both being >99 %, to a value of 86 %. This transformation retains the *S* selectivity previously seen across MO14 substrates but is nevertheless impaired by this particular substituent.

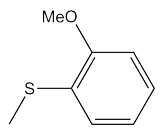
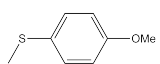
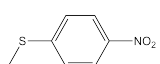
The halo-substituted thioanisoles tested assist in describing the nature of the active site present in MO14. The results for the *ortho* and *meta* substituted thioanisoles indicate that the prevention of rotation of the molecule by asymmetric design of substrate results in a high degree of enantioselectivity, and the 4-chloro and 4-fluoro thioanisole transformations, when compared to the previous results for thioanisole and methyl *p*-tolyl sulfide, demonstrate the improvement in conversion observed when a bulky group is added in the *para* position of the phenyl ring and also suggests that

this positioning can be related to the enantioselectivity of the transformation. The result for the 2-chlorothioanisole also indicates that steric hindrance of the sulfur reaction centre can significantly affect the conversion yield, but does not necessarily inhibit the enantioselectivity of the enzyme.

### 4.3.3 Bulky Substituents

To further investigate the observations from the halo-substituted thioanisoles, a range of bulky groups were examined for their effects on the reaction when present on the phenyl ring of thioanisole. Two thioanisole derivatives, with methoxy groups in the 2- and 4- positions were tested, to further assess the effects observed for 2- and 4- chlorothioanisoles, and also 4-nitrothioanisole, to assess electronic effects on this reactions. Methoxy-substituted compounds are generally transformed more effectively by CHMO<sub>Acineto</sub> than the equivalent chlorothioanisole, although the nitrothioanisole is not seen to be transformed by CHMO<sub>Acineto</sub>. Conversions and e.e. values for these experiments are displayed in Table 4.4.

Table 4.3: Bulky-Substituted Sulfide Biotransformations by *E. coli* Rosetta<sup>TM</sup>2 (DE3) pLysS cells expressing MO14 or CHMO<sub>Acineto</sub>.

Sulfide	Structure	MO14 Yield	MO14 e.e.	CHMO Yield	CHMO e.e.	Lit. CHMO e.e. <sup>149</sup>
2-Methoxythioanisole		16 %	>99 % <i>S</i>	63 %	70 % <i>R</i>	51 % <i>R</i>
4-Methoxythioanisole		25 %	3 %	97 %	23 %	51 % <i>S</i>
4-Nitrothioanisole		61 %	-	No	-	-

Reactions conducted at 30 °C with shaking for 24 h.

#### 2-Methoxythioanisole

The best comparison for 2-methoxythioanisole is the similarly structured 2-chlorothioanisole previously studied, and the methoxy derivative shows a further drop in conversion while maintaining the high enantioselectivity that is characteristic of these MO14 experiments. The low overall con-

version is perhaps explained by the same reasoning as the 2-chlorothioanisole, *i.e.* the steric bulk affects the ability of the enzyme to access the key sulfur atom; the expectation would be that this effect would be greater for a methoxy group than for a chloro group owing to the greater steric bulk possessed by the methoxy. The enantioselectivity is again high, which may also be explained similarly to 2-chlorothioanisole, in that the asymmetric nature of the compound prevents rotation, increasing e.e.. Whether the size of the substituent affects the degree of enantioselectivity or there is simply a size at which the reaction become very enantioselective is uncertain, as both the examined substituents in this position result in e.e.'s >99 %. The conversion conducted using CHMO<sub>Acineto</sub> reached a much higher conversion which suggests, along with similar results for benzyl methyl sulfide and 4-fluorothioanisole, that the active site pocket in CHMO<sub>Acineto</sub> is more accepting of larger substituents on the substrate. The enantioselectivity observed for CHMO<sub>Acineto</sub> is again good, but again lower and the opposite selectivity to that of MO14.

#### **4-Methoxythioanisole**

The *para*-substituted methoxythioanisole shows a reduced conversion of the substrate than that observed for 4-chlorothioanisole and the enantioselectivity is severely impaired. The negative effects observed here may indicate that there is an ideal size for *para* substituents on this species and that a methoxy group represents too large a moiety to allow the ideal placement of the molecule in the active site. The enantioselectivity especially is a large change from other results for this enzyme, hence the bulk of this group may result in the location of this substrate in a position in which free rotation is more easily achieved, limiting both the conversion and especially the enantiospecificity. CHMO<sub>Acineto</sub>, by comparison, shows a much higher conversion of the substrate and achieves an enantiomeric excess equal to the general pattern of values for this enzyme. This high conversion may indicate that the suspected size of the active site in CHMO<sub>Acineto</sub> can accommodate the extra steric bulk of a methoxy group in the *para* position of the phenyl ring.

#### 4-Nitrothioanisole

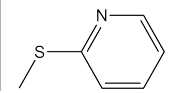
The results for the nitro derivative of thioanisole are somewhat peculiar when compared to the other results obtained. No literature value for the conversion of this substrate by CHMO<sub>Acineto</sub> exists and the experiment conducted also showed no conversion. The results for MO14 showed a surprisingly high level of conversion of the substrate, as the previous study of 4-methoxythioanisole would seem to indicate that there should be very little conversion of this substrate due to the large steric bulk of the nitro group. Regrettably, no chiral GC data could be obtained for this compound, hence it is suspected that the conversion value obtained represents an impurity in the sample rather than conversion by the enzyme.

These bulkier substrates demonstrate on a more extreme scale the observations previously made for the halo-substituted compounds. There is a clear preference to have no *ortho* substituent on the phenyl ring, to maintain accessibility of the sulfur atom to the catalytic residues. Additionally, there appears to be an ideal size for the *para* substituent to locate the substrate in the correct location while still allowing it to fit into the binding pocket of the enzyme.

#### 4.3.4 Heterocyclic Sulfides

The final sulfide tested was 2-methylthio pyridine. This substrate represents a heterocyclic sulfide, the transformation of which has previously been observed by CHMO<sub>Acineto</sub> and would be an interesting comparison for MO14, owing to the unique chemistry that these species possess. Conversion of heterocyclic species by BVMOs can often be completed at rates comparable to those observed for ideal substrates<sup>91</sup> and also can obtain relatively high enantioselectivities.<sup>149</sup> The results of this transformation are shown in Table 4.5.

Table 4.4: Heterocyclic Sulfide Biotransformation by *E. coli* Rosetta<sup>TM</sup>2 (DE3) pLysS cells expressing MO14 or CHMO<sub>Acineto</sub>.

Sulfide	Structure	MO14 Yield	MO14 e.e.	CHMO Yield	CHMO e.e.	Lit. CHMO e.e. <sup>149</sup>
2-Methylthiopyridine		2 %	24 % S	97 %	>99 % R	87 % R

Reactions conducted at 30 °C with shaking for 24 h.

### 2-Methylthiopyridine

It is clear from these results that this substrate is not very well accepted by MO14, even more so than the similar thioanisole. Since the sole difference between these two species is the nitrogen atom, it seems likely that any explanation of the inactivity must be related to this substitution. A nitrogen atom in the phenyl ring should increase the electron density present in the ring, which was thought to improve the reactivity, however this seems to have a negative effect on the conversion. It is possible that the lone pair present on the nitrogen may cause some inaccessibility of the sulfur atom to the enzyme, however the exact reason for this inactivity is unclear. CHMO<sub>Acineto</sub> shows significantly greater ability to convert this substrate than MO14, achieving 97 % conversion and an excellent e.e., which may be ascribed the active site in CHMO<sub>Acineto</sub> being ideal for cyclohexane rings and the presence of nitrogen in the pyridinyl ring may cause it to have more similar character to this ideal substrate.

Overall, MO14 shows excellent substrate scope for sulfides and is capable of producing a high level of enantioselectivity in most of these transformations. Particularly interesting is the preference for the production of *S* enantiomers of the products of these biotransformations. Certainly amongst BVMOs, MO14 demonstrated e.e. values that are generally more *S* selective than CHMO<sub>Acineto</sub>, which generally prefers *R* selectivity<sup>149</sup>; PAMO, which has no significant overall preference for enantioselectivity but shows high *S* character for simple phenyl sulfides<sup>147</sup> and HAPMO, which does show significant *S* selectivity for most substrates but a clear preference for *R* products for



benzyl sulfides.<sup>148</sup> Indeed, MO14 shows the potential to be considered one of the best *S*-selective sulfide biocatalysts, provided that further optimisation and characterisation with a wider range of prochiral sulfides and reactions conditions.

#### 4.4 Conclusions

*E. coli* Rosetta<sup>TM</sup>2 (DE3) pLysS cells were transformed by plasmids containing BVMO enzymes from *R. jostii* and experiments conducted to assess their activity towards 1-indanone and  $\alpha$ -tetralone. Poor activity was observed for these transformations and therefore further biotransformational investigations were continued with *E. coli* Rosetta<sup>TM</sup>2 (DE3) pLysS cells expressing the enzyme MO14, which had been shown to perform the transformation of bicyclo[3.2.0]hept-2-en-6-one with excellent regio- and enantio-selectivity. This transformation was studied for optimal conditions on the 1 mL culture scale, with the intention to inform larger scale biotransformations that are described later in this work. The effect of various organic solvents on the this reaction were also studied, with generally negative results, however the use of heptane may be tolerated sufficiently to be used for more organically soluble substrates. Sulfide biotransformations were also investigated, with generally excellent enantioselectivities being observed and the possibility of MO14 to be considered one of the most *S*-selective biocatalysts for sulfoxidation processes.



## 5.1 Method Development

Before beginning experiments on MO14 biotransformations on a larger scale, it was necessary to determine the conditions in which this would be attempted. The small scale experiments conducted with this enzyme and substrate have focussed on the use of resting cells, *i.e.* cells that have ceased to divide and are therefore more able to perform biotransformations. Indeed, the addition of glucose in the small scale experiments appeared to restart the growth of the cells performing this transformation, which had a significantly negative effect on the reaction. It may be that the effect of the reaction is time-based however, with the initial growth phase being particularly sensitive to substrate addition. The use of growing cells offers a number of advantages, not least the possibility of performing the reaction inside the growth media, rather than needing to resuspend the bacteria prior to biotransformation.

Growth on this scale requires a different approach to the shake-flask production of cells used to produce the small scale production. To better resemble the industrial production, it was decided to focus on a fermenter-based system for generation of the host cells, as this would offer the best opportunity to generate the ideal conditions for biotransformation. Fermenters allow significantly greater control of the growth conditions and, if necessary, would also permit the reaction to be conducted within the fermenter itself, meaning that both growing and resting cells are a possible course to be taken.

Analogous experiments have shown successful results using resting<sup>151,114</sup> cells, which often employ a substrate feeding and product removal process, allowing the issues of substrate and product inhibition of the reaction to be avoided, as both would be present only in safe concentrations. The development of such a system is beyond the scope of this work, which was limited to a 2 L fermentation scale and was unsuited to the use of the necessary resin-based techniques for this process. Growing cells have remained largely uninvestigated for Baeyer-Villiger biotransforma-

tions, however there is precedent in other oxygenase groups for this process resulting in successful transformations with high enantioselectivities.<sup>152</sup>

Resting cell biotransformations using CHMO<sub>Acineto</sub> to convert the model BVMO substrate bicyclo-[3.2.0]hept-2-en-6-one have been conducted on up to a 200 L pilot plant scale<sup>114</sup>, converting the substrate to a final concentration of 4.5 g L<sup>-1</sup>, which represents 900 g of product. Clearly, this process is capable of the scale up to industrial production, however limitations include substrate mixing and oxygen supply on a large scale. The 50 L scale offers perhaps a more efficient system, as higher concentrations of substrate are achievable, which may be due to the improved mixing of the substrate on a smaller scale.

Whereas resting cell biotransformations resemble the small scale biotransformations previously conducted in that the cells are grown either by shake-flask or fermenter, harvested and the biotransformation subsequently conducted, growing cell biotransformations involve the reaction taking place during the growth itself. This represents a much more streamlined and simply achieved transformations, as there is no middle step necessary to prepare the cells for the transformation. Previous studies have also shown BVMO activity of CHMO<sub>Acineto</sub> in growing cells to achieve transformations in excess of 95 % yield and e.e..<sup>153,154</sup> A comparison of CHMO<sub>Acineto</sub> and cyclopentanone monooxygenase from *Pseudomonas* NCIB 9872 (CPMO) shows good conversion and e.e. for CPMO under growing conditions as well.<sup>155</sup> As MO14 shows such good activity against the model BVMO substrate in cells, it was decided to assess the ability of this enzyme to conduct the reaction during a large-scale growth in fermentation conditions. The key factor to be ideally managed is oxygen availability, which is thought to have been a leading contributor to the inefficiency observed in the biotransformations conducted in 5 mL vials. In a fermentation system, oxygen concentration can be maintained at a constant level, which should allow the growth of a much higher cell density and therefore conversion.

In this way, it is hoped that a 'green' chemical process to generate the product can be developed. Here, an investigation of the fermentation-based biotransformation of bicyclo[3.2.0]hept-2-en-6-one by MO14 was conducted, with a view to the optimisation for potential scale-up to industrial use. Several fermentation experiments were conducted to assess the effects of a number of conditions: temperature, substrate concentration, codon-optimisation/bacterial strain optimisation and delayed addition of substrate.

## 5.2 Temperature

To ascertain the ideal temperature at which the fermentation should be conducted, a trial expression of MO14 at 16 °C, 30 °C and 37 °C was performed. The choices of temperature were based on a number of factors: 16 °C is the standard expression temperature used for MO14, as for previous experiments, and 37 °C was selected to investigate the possibility of not changing the temperature of the fermentation on induction of gene expression, which has previously shown to be an effective strategy<sup>113</sup>. The temperature of 30 °C was chosen to investigate a mid-point between the two temperatures tested, as previous work in this area<sup>133,156</sup> has used similar mid-point level temperatures and the investigation of the biotransformation at a raised temperature in a fermentation environment may provide results of interest that are not tied to the protein expression levels observed. The SDS-PAGE gel samples of these expressions are shown in Figure 5.2.

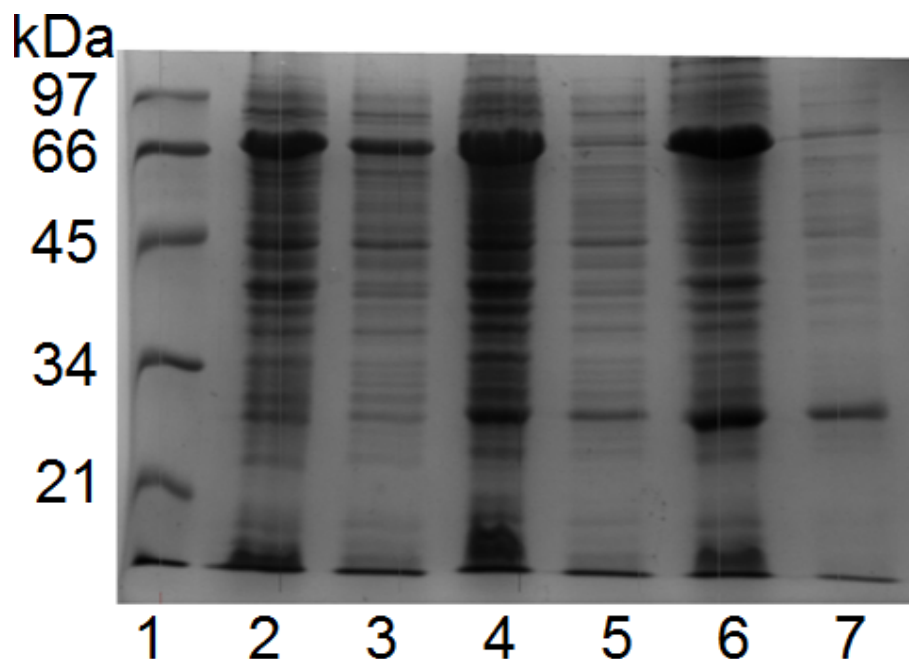


Figure 5.2: SDS-PAGE showing expression of native ro03437 gene in *E. coli* Rosetta™2 (DE3) pLysS strain at different temperatures. Lane 1: Low molecular weight Marker (Biorad) with molecular weights given on the left-hand side in kiloDaltons (kDa); Lane 2: Total cell fraction 16 °C; Lane 3 soluble cell fraction 16 °C; Lane 4: Total cell fraction 30 °C; Lane 5 soluble cell fraction 30 °C; Lane 6: Total cell fraction 37 °C; Lane 7 soluble cell fraction 37 °C.

The expression gel shows that the level of soluble protein at 37 °C was poor, which is likely due to the prevalence of higher energy misfolding of the protein being accessible at higher temperatures, and it was therefore decided to perform two fermentations to assess the effect of temperature: one at 16 °C and one at 30 °C, a more suitable expression temperature. Samples were taken at induction, and hourly over 24 h. The conversion of substrate to product was analysed by GC and graphs of the progression of conversion are shown in Figure 5.3.

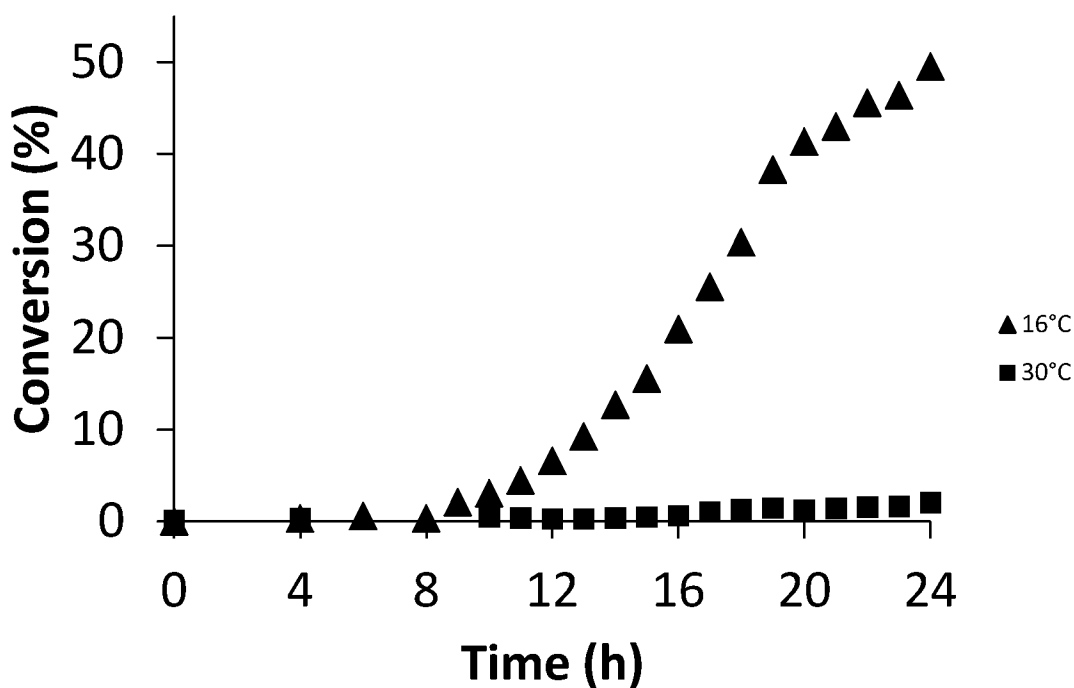


Figure 5.3: The conversion of bicyclo[3.2.0]hept-2-en-6-one over time by *E. coli* Rosetta<sup>TM</sup>2 (DE3) pLysS cells expressing wild-type MO14 at 16 °C and 30 °C. Substrate concentration of 0.5 g L<sup>-1</sup> added simultaneously with induction of gene expression.

The results suggest that the reaction significantly favours being run at a lower temperature, probably resulting from differences in protein folding. At high temperatures, less favourable folds can be obtained due to the increased thermal energy permitting access to higher energy folds. These folds may not allow the enzyme to perform the reaction as efficiently by, for example, changing the shape of the active site such that the substrate no longer binds effectively or by changing the shape of the NADPH or FAD binding sites. This result is interesting, however, as previous fermentation work on the same substrate using CHMO<sub>Acineto</sub> in resting *E. coli* cells by Woodley *et al.* has used 37 °C<sup>113</sup> and 30 °C<sup>156,127</sup>. Further characterisation of the fermentations was achieved by conducting a second fermentation at 16 °C and following the concentration of both ketone and lactone enantiomers over the course of the reaction, Figures 5.5 and 5.6, as well as the conversion overall, Figure 5.4.

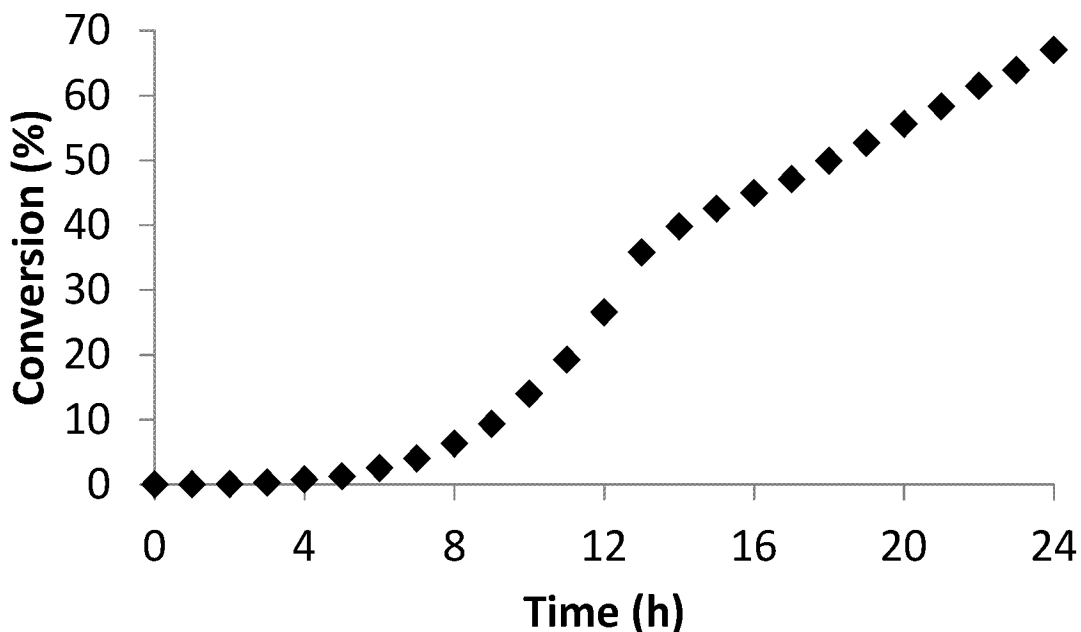


Figure 5.4: The conversion of bicyclo[3.2.0]hept-2-en-6-one over time by *E. coli* Rosetta<sup>TM</sup>2 (DE3) pLysS cells expressing wild-type MO14 at 16 °C. Substrate concentration of 0.5 g L<sup>-1</sup> added simultaneously with induction of gene expression.

In both fermentations, the initial exponential curve gives way to a linear curve after 19 h in the first fermentation and 14 h in the repeat. The enantiomeric analysis provides some more information on this phenomenon. We can see that the reaction possesses a biphasic character, where production of the (1*R*, 5*S*) enantiomer does not begin until the initial ketone substrate enantiomer has been almost completely consumed. The slow drop in the alternative ketone substrate enantiomer prior to this time is presumably due to evaporation from the system over time. This suggests that the (1*R*, 5*S*) ketone substrate has a significantly higher affinity for the MO14 active site than the (1*S*, 5*R*) ketone, which in turn suggests that the shape of the active site is more conducive to binding one enantiomer than the other. It is of great interest that the MO14 enzyme proves able to convert both enantiomers of the substrate, but that it only converts the (1*S*, 5*R*) once there is none of the preferred enantiomer remaining, as this suggests that MO14 could be used for production of either lactone enantiomer if the substrate were to be administered in an enantiomerically pure condition. Alternatively, if



sufficient control could be achieved over the fermentation, it may be possible to extract pure (1*S*, 5*R*) lactone product from a reaction initially then, once this conversion is complete, to follow by extracting the (1*R*, 5*S*) enantiomer from the same reaction; this would result in an increased atom efficiency of the reaction, as the undesired substrate/product is otherwise discarded.

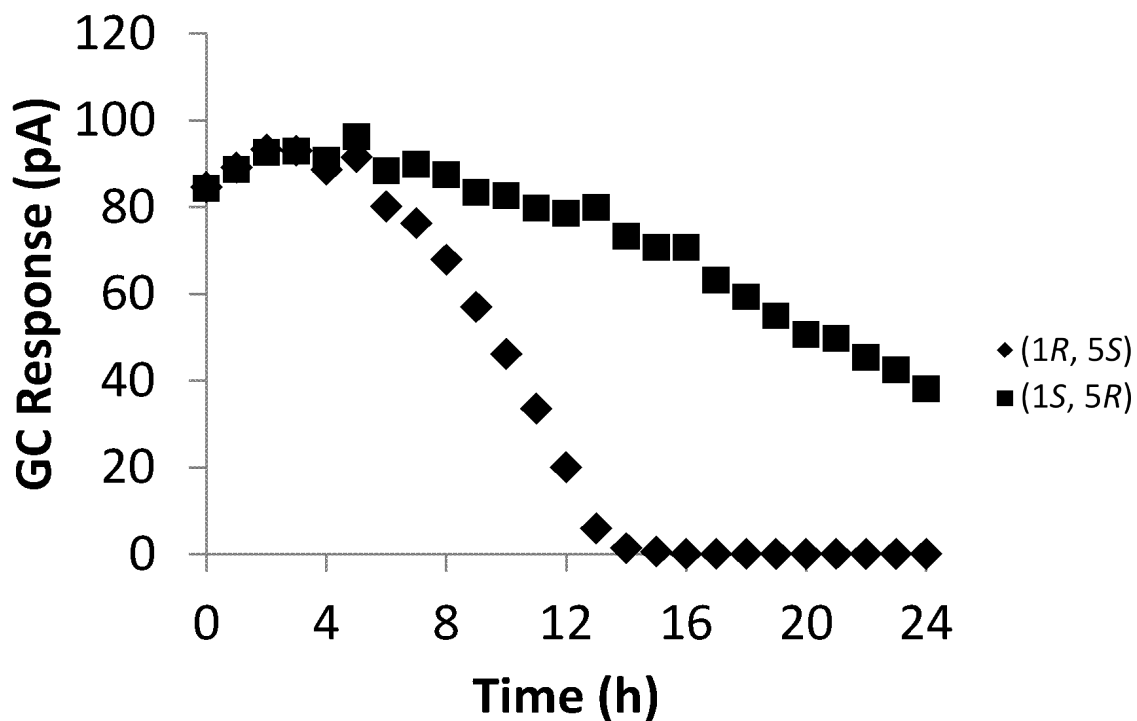


Figure 5.5: The ketone enantiomer levels during the fermentation experiment investigating the effect of temperature.

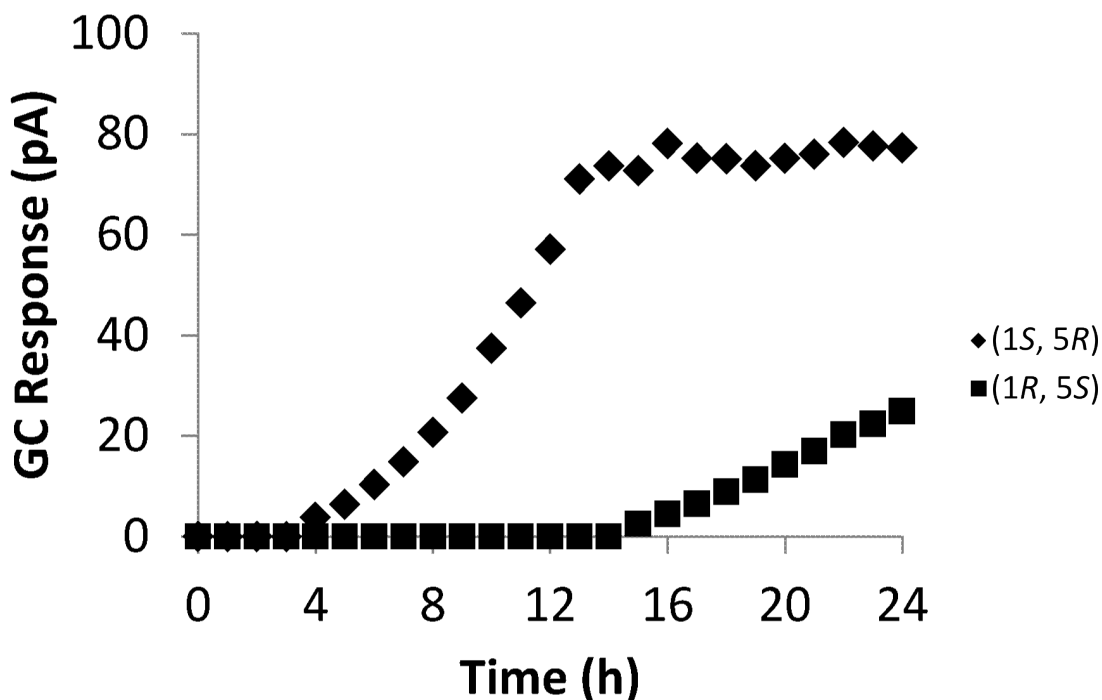


Figure 5.6: The lactone enantiomer levels during the fermentation experiment investigating the effect of temperature.

### 5.3 Substrate Concentration

Continuing in the vein of attempting to achieve maximum efficiency from this reaction, further optimisation of the conditions was undertaken. The activity of a number of enzymes is known to be inhibited by elevated concentrations of the substrate that they convert and it would be useful to know if this is the case for MO14. Also, if there is no deleterious effect on the rate of conversion, it is more favourable from an industrial standpoint to maximise the generation of product from one fermentation reaction. The effect expected, based on the previous laboratory-scale experiment, was that there would be an increase in the conversion observed up to 13 mM substrate, or 1.3 g L<sup>-1</sup>, and any further increase in concentration may result in the decrease in the rate of product generation.

Two fermentations were set up side-by-side: one at  $1 \text{ g L}^{-1}$  and one at  $2 \text{ g L}^{-1}$  substrate; both conducted at  $16 \text{ }^\circ\text{C}$ . This provides us with three data points from which to deduce a conclusion on the effect of substrate concentration, i.e.  $0.5 \text{ g L}^{-1}$  from the initial fermentation experiment and  $1.0 \text{ g L}^{-1}$  and  $2.0 \text{ g L}^{-1}$  from this experiment. Samples were taken hourly from one hour after induction to 16 h and a final sample at 24 h and the results are shown in Figure 5.7.

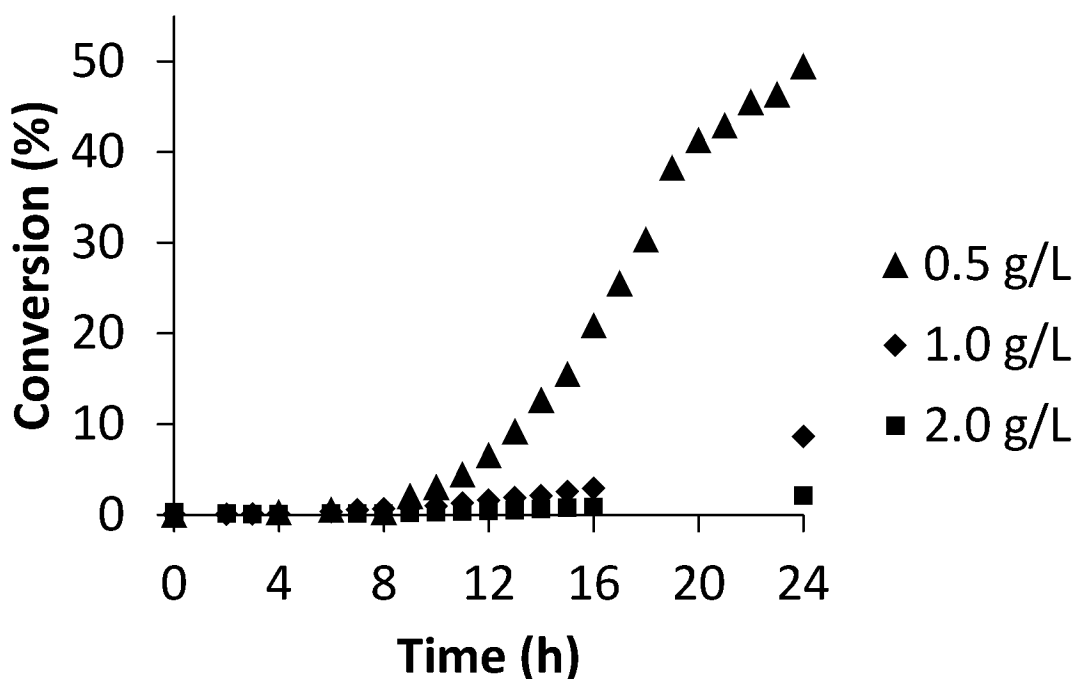


Figure 5.7: The conversion of bicyclo[3.2.0]hept-2-en-6-one over time by *E. coli* Rosetta<sup>TM</sup>2 (DE3) pLysS cells expressing wild-type MO14 at  $16 \text{ }^\circ\text{C}$ . Substrate concentration of  $0.5 \text{ g L}^{-1}$ ,  $1.0 \text{ g L}^{-1}$  or  $2.0 \text{ g L}^{-1}$  added simultaneously with induction of gene expression.

There is a clear and significant decrease in enzyme activity that is concurrent with the increasing concentration of the substrate. This is concurrent with observations of Top10 *E. coli* cells expressing CHMO<sub>Acinetobacter</sub>, where concentrations of the substrate greater than  $0.2\text{-}0.4 \text{ g L}^{-1}$  show toxicity effects.<sup>156,127</sup> The drop is almost exponential, with final product conversion for  $0.5 \text{ g L}^{-1}$  being 49 %,  $1 \text{ g L}^{-1}$  being 9 % and  $2 \text{ g L}^{-1}$  being 2 %.

This seems to indicate  $0.5 \text{ g L}^{-1}$  would be best concentration of substrate to use, but examination of the concentration of product gives quite different results. In this case,  $1 \text{ g/L}$  is the best concentration of substrate, with a product concentration of  $0.16 \text{ mM}$ , as compared to  $0.5 \text{ g L}^{-1}$  substrate ( $0.07 \text{ mM}$  product) and  $2 \text{ g L}^{-1}$  substrate ( $0.08 \text{ mM}$  product).

This raises more issues with conducting these fermentations industrially; for example, if the conversion has a theoretical maximum of  $50 \%$  product extraction from the reaction mixture becomes an issue. Also, the evidence from the earlier fermentations indicates that the opposite enantiomer of product will be produced when the initial substrate is completely consumed; in this case, enantiomer separation is a challenge that must be overcome. Finally, the issues in generating pure, easily extracted product challenge the efficiency of maximising yield as opposed to maximising conversion efficiency. This in turn raises questions about the 'green-ness' of the reaction if total yield is preferred over conversion efficiency.

## 5.4 Codon-Optimisation

Codon-optimisation of the MO14 gene should, in theory, lead to improved expression in the selected strain of bacteria. As previously considered, expression is routinely carried out in the *E. coli* Rosetta (TM) 2 (DE3) pLysS strain, which compensates for non-standard codons in the genetic sequence. This is accomplished by a modification of the genetics of the bacterium to contain additional tRNAs that can recognise the less common codons that are present. The codon-optimised MO14 expression after analysis by SDS-PAGE is shown in Figure 5.8, for comparison with the native MO14 expression.

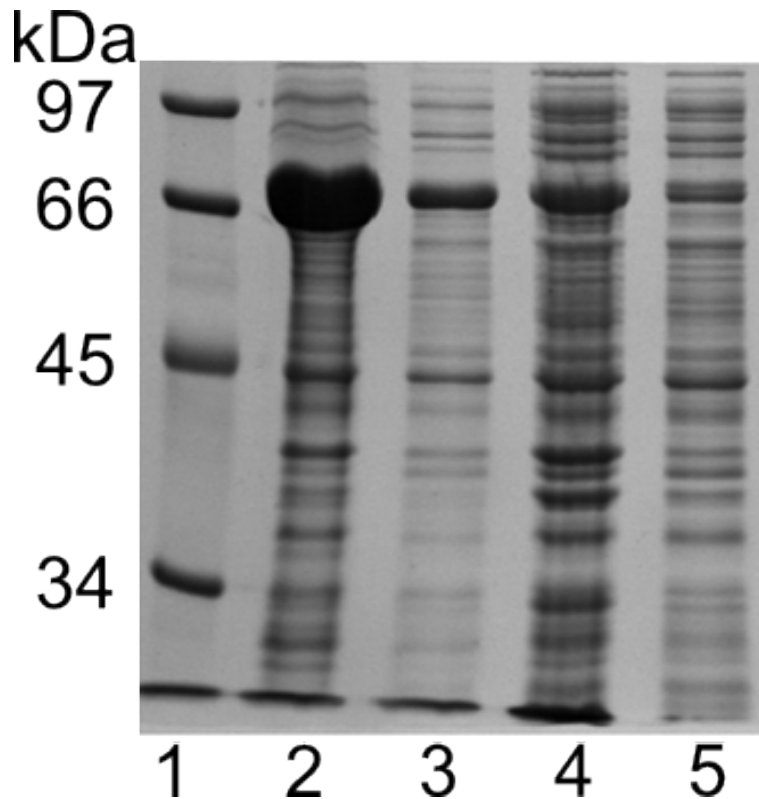


Figure 5.8: SDS-PAGE showing expression of native and codon-optimised ro03437 gene in *E. coli* Rosetta (TM) 2 (DE3) pLysS strain. Lane 1: Low molecular weight Marker (Biorad) with molecular weights given on the left-hand side in kiloDaltons (kDa); Lane 2: Native gene, total cell fraction 16 °C; Lane 3: Native gene: soluble cell fraction 16 °C; Lane 4: Codon-optimised gene, total cell fraction 16 °C; Lane 5: codon-optimised gene, soluble cell fraction 16 °C.

As the expression is comparable to the expression of native MO14, the experiment was undertaken. Codon optimisation takes effectively the opposite approach, wherein the genetic sequence of the MO14 gene is altered such that the codons used more closely match the distribution of mRNAs found in the *E. coli* genome. This theoretically has a similar effect to the bacterial strain alteration, *i.e.* the expression is improved by better ability of available mRNAs to recognise the gene sequence.

To investigate the difference in expression efficiency, the codon-optimised gene was expressed in *E. coli* BL21 cells, which do not have the increased level of rare codon mRNAs, hence will be a useful comparison for industrial purposes as to whether it is more useful to optimise the genetic

sequence or the bacterial strain. One fermentation was set up and conducted at 16 °C. This gives us two data points from which to work in determining the effect by comparison to the 16 °C temperature experiment. Samples were taken hourly from one hour after induction to 24 hours and the data plots are shown in Figure 5.9.

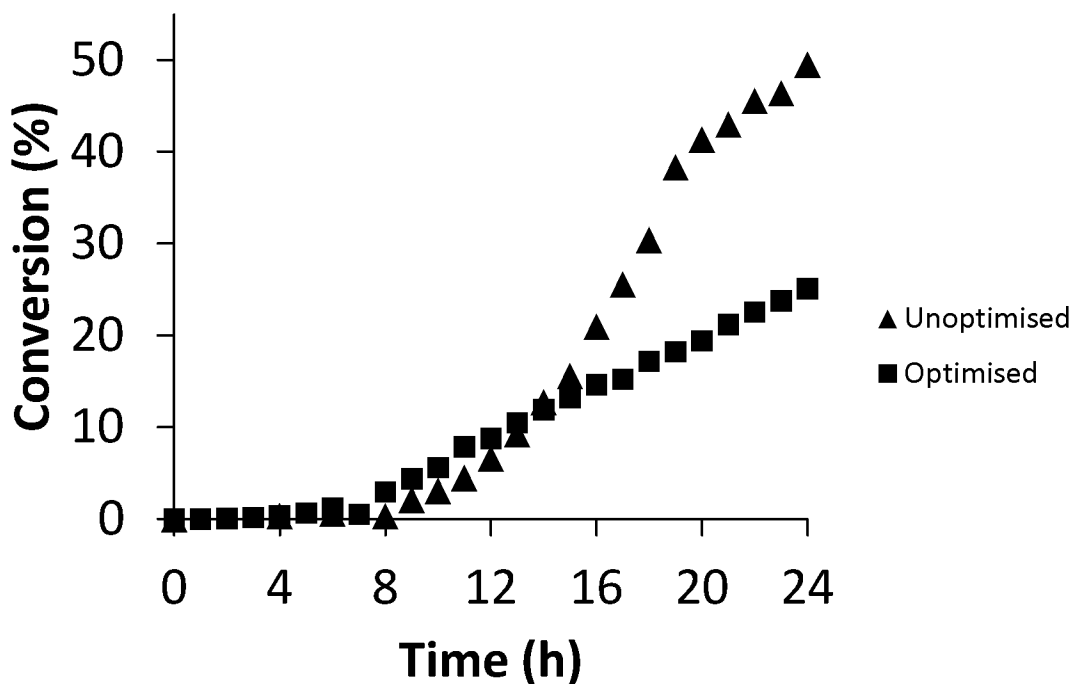


Figure 5.9: The conversion of bicyclo[3.2.0]hept-2-en-6-one over time by *E. coli* Rosetta™2 (DE3) pLysS cells expressing wild-type MO14 and *E. coli* BL21 cells expressing codon-optimised MO14, both at 16 °C. Substrate concentration of 0.5 g L<sup>-1</sup> added simultaneously with induction of gene expression.

From these data it is clear that the reaction reaches a higher level of conversion when the bacterial strain is optimised to make full use of the gene, as opposed to optimising the gene to make use of more common bacterial strains. Since we know that the enantioselectivity is sufficient in the unoptimised gene, an examination of the efficiency of this characteristic in the codon-optimised gene reaction would perhaps provide no significant new information. Nevertheless, shown in Figure 5.10 is the enantiomeric excess of ketone over time in the codon-optimised gene reaction. This shows that a gradual increase in the e.e. of the ketone is observed over the course of the reaction

as one enantiomer is preferred.

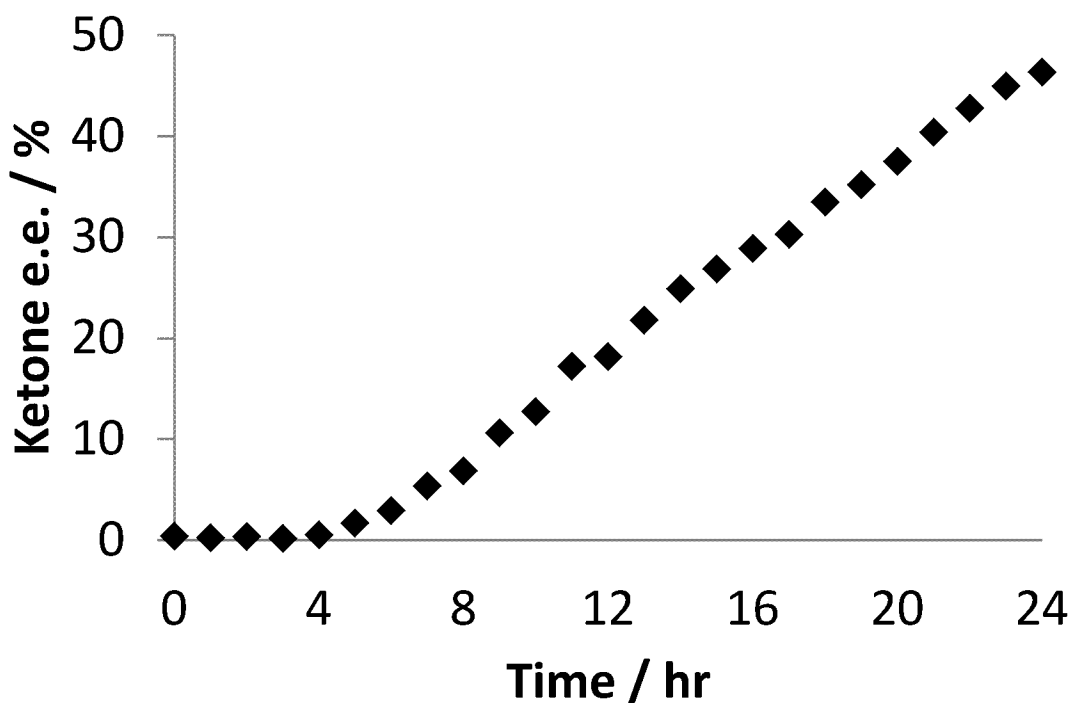


Figure 5.10: e.e. of ketone substrate during codon-optimised fermentation experiment.

## 5.5 Delay of Substrate Addition

There is a possibility that the bicyclo[3.2.0]hept-2-en-6-one substrate is toxic to the cells used in this fermentation, as substrates of this type have previously been observed to inhibit the growth of *E. coli* under fermentation conditions<sup>133</sup>; if this is the case, the simultaneous addition of substrate with induction may cause a decrease in the reaction's overall viability. If this is so, the toxic effect would kill the cells before they have the chance to produce any substantial amount of MO14 with which the reaction can proceed. The results observed for the fermentation conducted with control of substrate concentration also indicate that there is a strong effect on the reaction when the substrate concentration is increased, suggesting that the substrate inhibits the reaction.

Examining the reaction progression in the previous fermentation experiments, we can see that the rate of conversion before approximately eight hours have passed is fairly insignificant, hence the delay of substrate addition for any length of time within this initial window should not prove deleterious to the overall conversion. In order to minimise the disruption to the experiment, however, a one hour delay after induction of gene expression before addition of substrate was used. Samples were taken as before and the analysis shown in Figure 5.11.

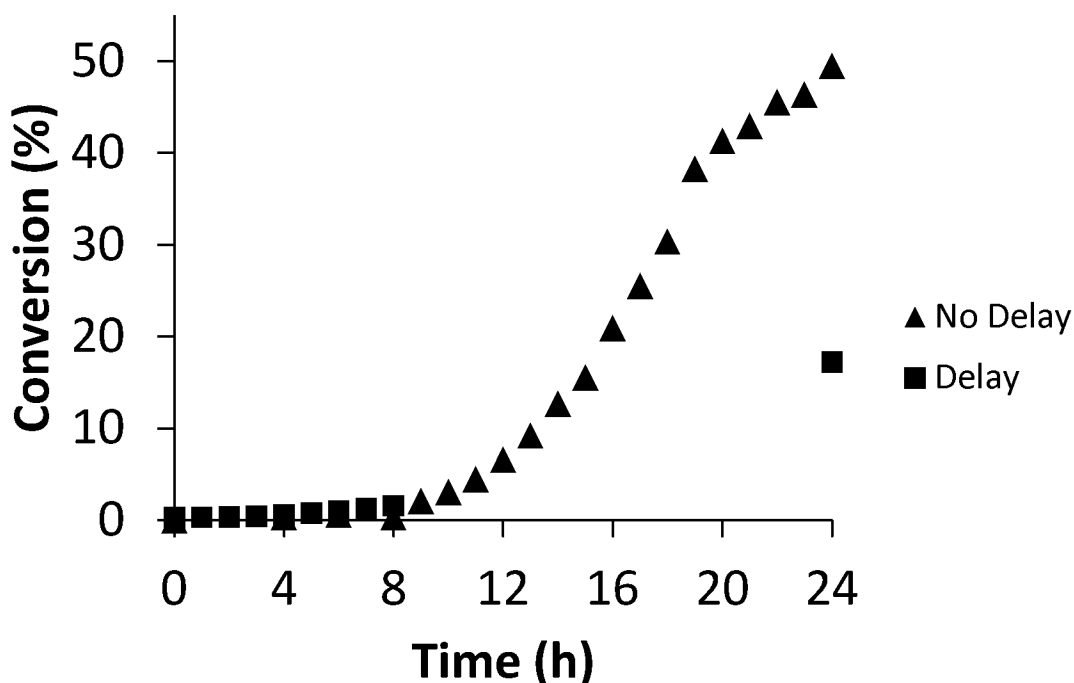


Figure 5.11: The conversion of bicyclo[3.2.0]hept-2-en-6-one over time by *E. coli* Rosetta™2 (DE3) pLysS cells expressing wild-type MO14 at 16 °C. Substrate concentration of 0.5 g L<sup>-1</sup> added simultaneously with induction of gene expression or after a one hour delay.

In this experiment, there is a clear preference for the substrate to be added alongside the induction of gene expression. This phenomenon is challenging to explain, as the expected result was that a delay would provide time for the protein to be produced, allowing the substrate to be consumed more rapidly and therefore its potential cytotoxic effect would be decreased. The substrate may not be cytotoxic, however, and the presence of the ketone during initial induction of gene expression



may in fact encourage the expression of MO14. The substrate not being cytotoxic is not necessarily surprising, as concentrations used are lower than those previously studied<sup>133</sup>; however the encouragement of gene expression is more challenging for which to suggest a cause.

There is precedent for gene expression to be triggered by substrate presence, as observed in the commonly used *lac* operon from *E. coli* and other enteric bacteria<sup>157</sup>; however there is no known genetic regulation inherent to the gene structure of MO14. The improved conversion observed therefore probably relies on physiological changes to the bacterium enacted by the substrate, for example increased permeability of the cell membrane permitting an increased diffusion of substrate into the cell and therefore increasing contact with MO14.

## 5.6 Conclusions

In summary, a number of fermentation reactions were conducted in an effort to optimise the enantioselective production of the (1*S*, 5*R*)-2-oxa lactone product from the Baeyer-Villiger oxidation of racemic bicyclo[3.2.0]hept-2-en-6-one. The variables investigated were temperature, substrate concentration, codon-optimisation, bacterial strain and delayed addition of substrate.

One of the main factors in deciding to conduct these fermentation reactions was the ability to control the oxygen level within the reaction media, however this control has also caused a further problem. In all of the fermentations conducted and as seen particularly in Figure 5.5, the volatility of the ketone substrate causes a substantial amount of ketone to be lost during the fermentation. This occurrence makes the progress of the reaction difficult to track accurately and the measurements taken to be pessimistic with regard to potential overall conversion of the ketone. In order to improve this situation, a reduced oxygen saturation could be employed, however oxygen saturation lower than 30 % can be deleterious to growth of the bacteria in the fermentation. Alternatively, the addition of glucose could be revisited; in the resting phase, it was found that addition of glucose

had a negative effect on the transformation of the substrate, however in growing cells, this would likely not be a problem and has previously been shown to have a positive effect on a similar BVMO fermentation biotransformation.<sup>133</sup>

A second issue that has been brought to attention by these experiments is the problem of product removal. Although no investigation of this challenge has been conducted in this work, the possibility of using substrate immobilised on a resin has been developed and seems to offer a simple solution to extraction of the product once conversion is complete.<sup>133,88</sup> This may also help to solve the most important issue observed in these fermentations - the low overall product yield, which reached a maximum yield of only  $0.2 \text{ g L}^{-1}$ , which is still a long way short of the necessary levels of conversion needed to move to industrial scale.

The clear comparison for this process is the kilogram-scale conversion of the same substrate by CHMO<sub>Acineto</sub>, although this enzyme is not regioselective and produces a single enantiomer of each of the two regioisomers of product, the (1*S*, 5*R*)-2-oxa and the (1*R*, 5*S*)-3-oxa.<sup>151</sup> This fermentation was conducted on a the 50 L scale and raises an interesting question as to how one would proceed to decide on a route to produce this 2-oxa lactone enantioselectively. MO14 offers a method to retain the (1*S*, 5*R*) ketone enantiomer, however the sheer level of production achieved with CHMO<sub>Acineto</sub> makes this a more obvious method for producing the 2-oxa lactone derivative. MO14 also shows some ability to produce the (1*R*, 5*S*) lactone, however CHMO<sub>Acineto</sub> is also amenable to mutation for selectivity and stereoselectivity switching has previously been shown to be possible in oxygenase enzymes.<sup>158</sup>

## Chapter 6

# Mutations

In the previous sections, the excellent regio- and enantio- selectivity observed in MO14 has been the key characteristic that justifies the investigation of this BVMO. In order to probe the nature of the enantio- and regio-selectivity observed in the biotransformation of bicyclo[3.2.0]hept-2-en-6-one by MO14, an examination of the active site was conducted, in the hope that it would provide information as to the origin of these selectivities. By conducting genetic mutations of the enzyme, it may be possible to obtain information about the active site of MO14 and identify potential key residues for changing the specificity.

### 6.1 Target Selection

Previous work has indicated that the Group II BVMOs MO9, MO14 and MO15 all exhibit a preference toward the enantioselective transformation of the (1*R*, 5*S*) enantiomer, with MO14 showing additional regioselectivity, producing exclusively the (1*S*, 5*R*)-2-oxa lactone, whereas MO15 produces the (1*S*, 5*R*)-2-oxa lactone and the (1*S*, 5*R*)-3-oxa lactone in roughly equal amounts, with a low level of the (1*R*, 5*S*)-3-oxa lactone also produced.<sup>115</sup> Investigations of the sequences of MO14 and MO15 show a 50 % identical sequence and 67 % strong similarity overall.

Currently there is no structure solved for MO14 or MO15, which makes the investigation of the active sites of these two enzymes more challenging. A homology search was therefore performed using the PhyRE web service; this service takes the amino acid sequence of a protein, conducts a structure prediction and then searches for other proteins with similar structures and uses these to inform a further structural prediction of the submitted sequence.<sup>121</sup>

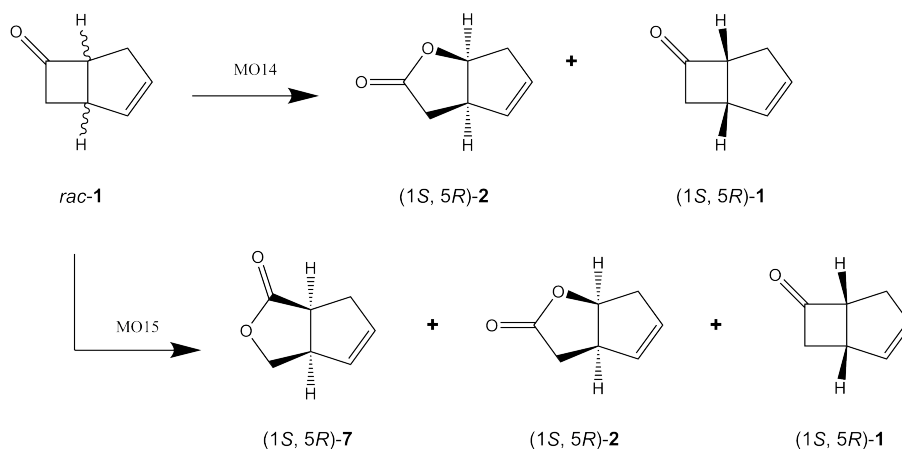


Figure 6.1: The biotransformations of bicyclo[3.2.0]hept-2-en-6-one catalysed by MO14 and MO15.

For both MO14 and MO15, the closest match was PAMO, a BVMO for which a structure has been previously published and the structures generated are shown in Figures 6.2 and 6.3. As both of these structures are based on PAMO, the high similarity to the PAMO structure is necessarily the case, however these simulated structures can suggest answers to a number of questions. Both structures show two expected domains present in BVMOs, the FAD-binding domain and the NADPH-binding domain and it seems likely that the active site for these enzymes is present at the same location between the two domains.

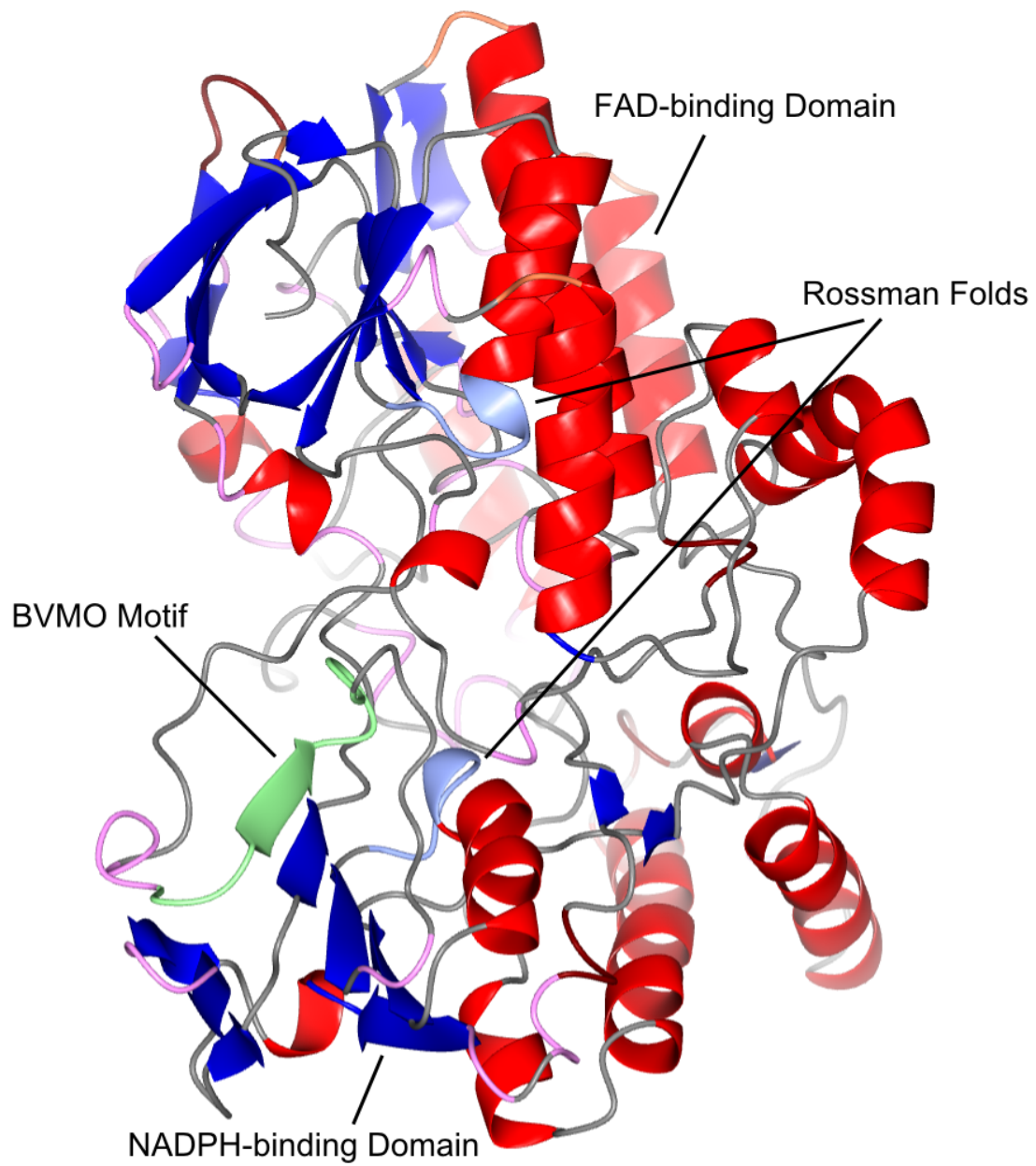


Figure 6.2: The predicted structure for MO14 based on homology with PAMO.

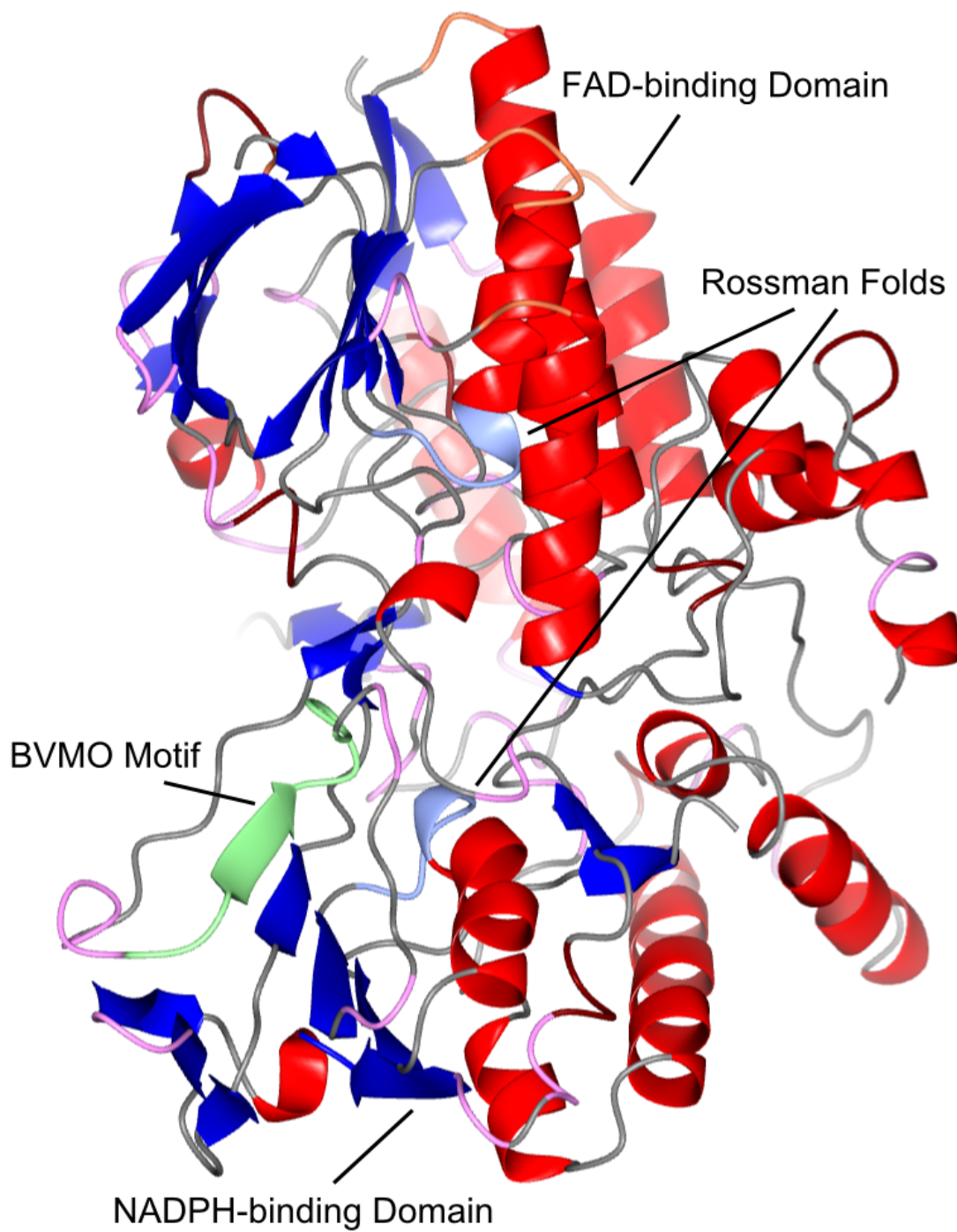


Figure 6.3: The predicted structure for MO15 based on homology with PAMO.

Given how similar MO14 and MO15 are, the possibility exists for an investigation into the origin

of the regio-selectivity observed in MO14 over MO15 from only a small number of amino acid residues. The examination in Table 6.1 shows the amino acid residues present at sites within 9 Å of the C4 $\alpha$  atom of the FAD moiety, as identified in the PAMO structure, with the intention of selecting mutations targeted at the differing residues between the two genes. These residues should represent the active site in these enzymes, which would lead to the identification of differing residues between the two enzymes that may be responsible for the difference in selectivities.

The residues revealed to differ between the two genes are MO14-Ile60 (PAMO-Ile67, MO15-Val67) and MO14-Pro441 (PAMO-Leu447, MO15-Val447), with all other residues within the area being identical. The mutants therefore selected to be generated were the Ile60Val and Pro441Val mutants of MO14, as well as the double mutant (DM) Ile60Val/Pro441Val, in addition to the corresponding reciprocal mutants in MO15.

Table 6.1: Comparison of residues within 9 Å of the FAD moiety when sequences are aligned with the solved PAMO structure.<sup>81</sup> The numbers are amino acid positions in PAMO.

Enzyme	26	55	65	66	67	72	96	153	200	337	441	442	445	446	447
PAMO	F	W	C	D	I	Y	I	L	Q	R	S	A	N	M	L
MO14	F	W	C	D	I	Y	I	L	Q	R	S	V	N	M	P
MO15	F	W	C	D	V	Y	I	L	Q	R	S	V	N	M	V

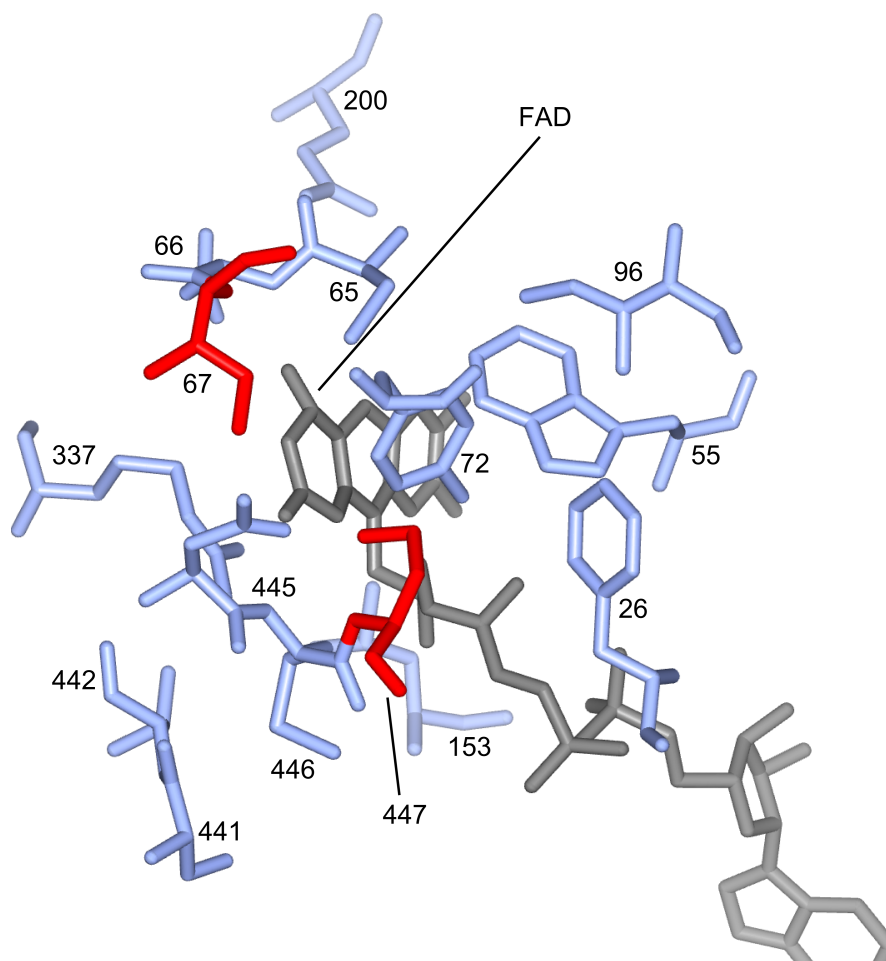


Figure 6.4: Representation of amino acid residues within 9 Å of the C4 $\alpha$  atom of the FAD moiety. The amino acid residues are shown in blue, with the selected mutation targets highlighted in red. FAD is shown in grey.

MO14 and 15 also share significant homology with the BVMO, CHMO<sub>Rhod</sub> and an alignment of MO14 with this enzyme was also conducted using PhyRE. Shown in Figure 6.5 are the selected



mutants, however in this structure only the P441V mutant appears to reside within the active site. Depending on the specific folds observed for MO14 and MO15, it may be that one or both of these enzymes will not have a significant effect; as even between two high similarity matches the structure of the active site and the residues therein vary significantly.

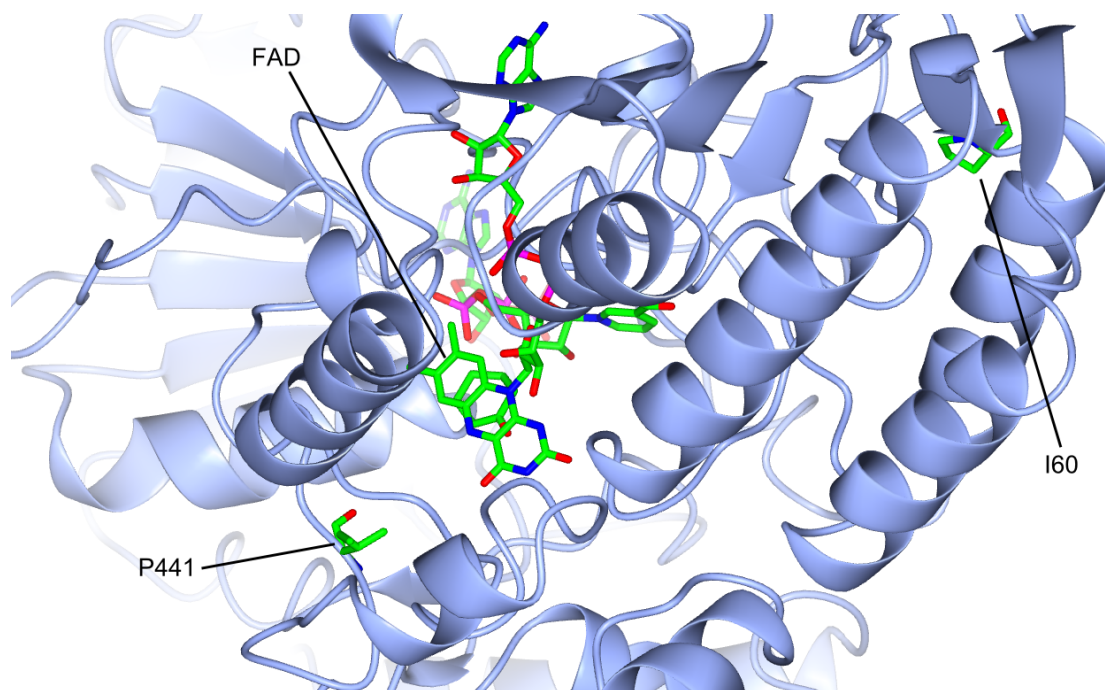


Figure 6.5: The predicted structure for MO14 based on homology with  $CHMO_{Rhod}$ , FAD cofactor and mutation target residues displayed in colouration by atom.

Previously, similar mutants to those proposed here have been generated in PAMO,<sup>159,160</sup> which allows a facile comparison in terms of the effect on the biotransformation being conducted. Both the I67T and S441A mutations for PAMO, which compare to the position I60 and P441 in MO14, resulted in a significant decrease in the regioselectivity of PAMO, which is the anticipated result of the mutations in MO14.

## 6.2 Mutant Generation

In order to generate these mutants, site-directed mutagenesis was performed. This technique involves the design of primers, short sequences of DNA, with small mis-matches in their genetic code that result in the desired mutation. These primers bind to the native sequence during a PCR, as shown in Figure 6.6, and the replication of DNA continues from this mismatched primer to produce large quantities of the new gene sequence. This allows the rapid and selective generation of the desired mutations.

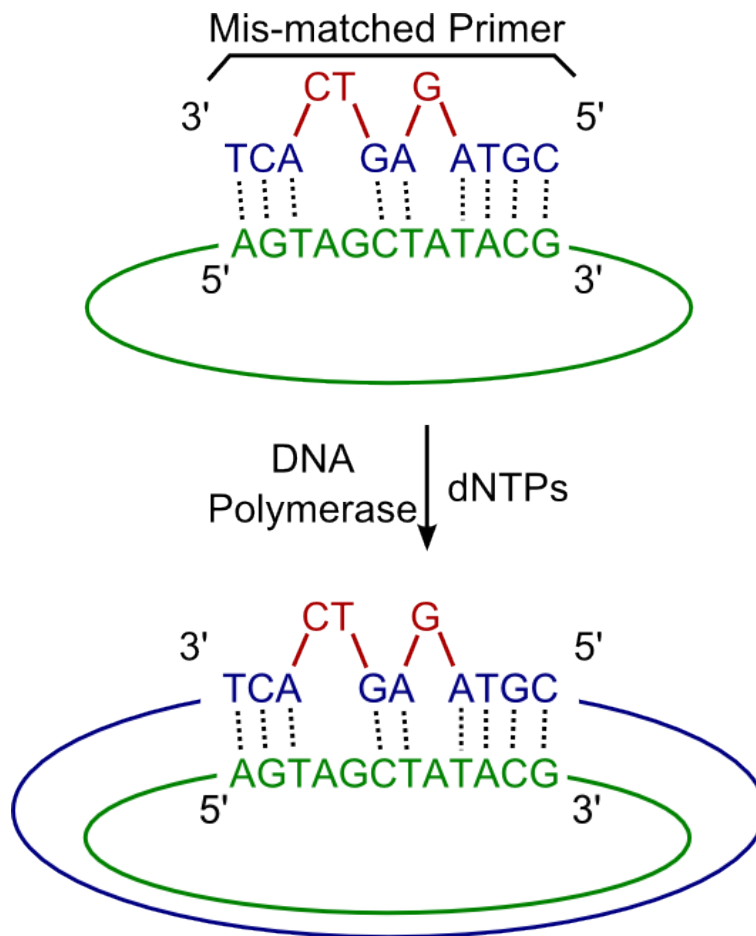


Figure 6.6: An example of site-directed mutagenesis.

The mutagenesis was performed and the six desired mutations produced and the successful generation confirmed by sequence analysis. Prior to conducting a complete biotransformation test of the

mutants capabilities, the effect of mutation on the expression levels of the mutated genes had to be investigated. *E. coli* Rosetta<sup>TM</sup>2 (DE3) pLysS cells were transformed by the YSBLIC-3C plasmid containing the mutated genes, which were expressed as described in the methodology for Chapter 3. The expression was analysed by SDS-PAGE, shown in Figure 6.7.

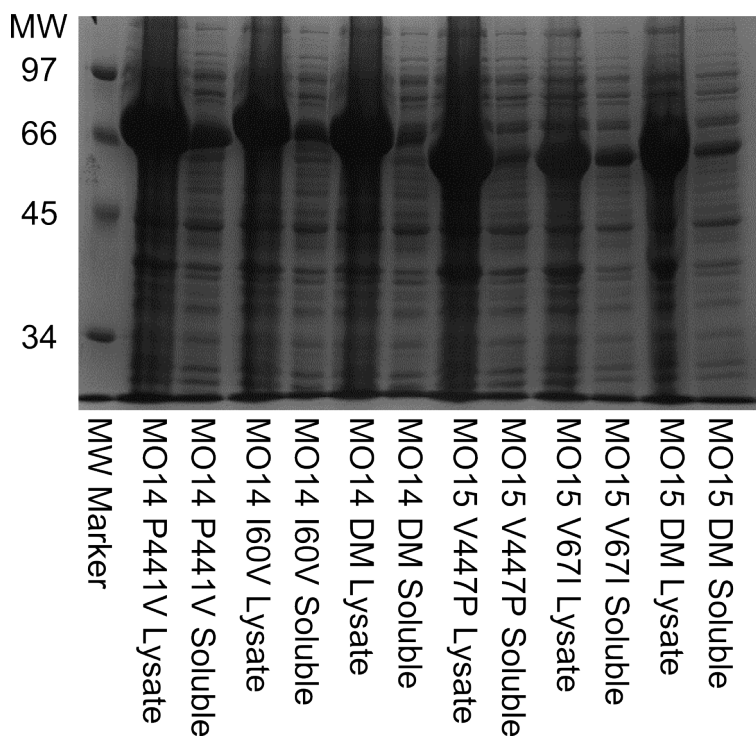


Figure 6.7: SDS-PAGE analysis of mutant expression.

All of the mutants show good expression, with very large bands visible in the total lysate samples. The soluble expression is only a small proportion of the overall expression, however this has previously been observed for the wild-type proteins and is therefore acceptable. It was not anticipated that a large effect on the level of protein expression would be observed, as the bacterial strain selected compensates for unusual codons that may have been chosen for the mutants. The soluble expression was not expected to change significantly either, as the location of these mutations was in the active site of the enzyme, well away from any contact with the solute. Since the protein mutants were expressed successfully, biotransformations could be conducted with these mutants.

## 6.3 Biotransformations

*E. coli* Rosetta<sup>TM</sup>2 (DE3) pLysS cells containing plasmids encoding the mutant BVMOs were grown in 2 L shake flasks and protein production induced by addition of IPTG. The whole cell samples were then pelleted and resuspended in buffer, while the lysate samples were pelleted, resuspended and sonicated. Biotransformations were conducted in 7 mL bijoux vials, with bicyclo[3.2.0]hept-2-en-6-one added in an ethanol solution to 1 mL of cell solution or cell lysate. The samples were extracted with ethyl acetate and analysed by gas chromatography as described in the methodology for Chapter 4; results are shown in Table 6.2.

Table 6.2: Biotransformations of MO14 and MO15 mutants.

Mutant	GC Response (pA) for (1 <i>S</i> , 5 <i>R</i> )- <b>2</b>	GC Response (pA) for (1 <i>R</i> , 5 <i>S</i> )- <b>2</b>	GC Response (pA) for <b>7</b>	% r.e.	% e.e.
MO14 Native Cells	42.2	2.2	1.7	92.6	90.1
MO14 Native Lysate	21.7	-	-	>99	>99
MO14 P441V Cells	85.6	-	1.4	96.8	>99
MO14 P441V Lysate	111.3	2.8	1.6	97.2	95.1
MO14 I60V Cells	45.7	-	-	>99	>99
MO14 I60V Lysate	60.6	-	-	>99	>99
MO14 DM Cells	15.2	-	-	>99	>99
MO14 DM Lysate	6.6	1.4	-	>99	65.0
MO15 Native Cells	61.4	8.7	42.9	24.1	75.2
MO15 Native Lysate	57.9	9.0	41.5	23.4	73.1
MO15 V447P Cells	22.0	2.0	9.6	42.9	83.3
MO15 V447P Lysate	22.1	2.1	9.5	43.6	82.6
MO15 V67I Cells	18.0	1.5	9.4	34.9	84.6
MO15 V67I Lysate	72.6	5.4	38.4	34.0	86.21
MO15 DM Cells	16.9	-	6.1	47.0	>99
MO15 DM Lysate	23.0	1.4	8.3	49.2	88.5

### 6.3.1 Native Cells

The native cell transformations serve as a guide by which to judge the activity and selectivity of the generated mutants. MO14 shows the exceptional regio- and enantio-selectivity for which it is of interest, with somewhat higher excesses observed in the lysate than in the whole cell transformation. MO15 also displays adequate enantioselectivity, but a distinctly lower regioselectivity than

MO14, and it is this characteristic of the biotransformation in which we expect to see the greatest improvement.

### 6.3.2 MO14 P441V and MO15 V447P

The mutation of the proline residue in position 441 of MO14 to a valine in the cell-based transformation results in a modest increase in the regioselectivity and enantioselectivity observed, however due to the small change, this may be merely a margin of error rather than a significant difference in the conversion preference of the enzyme. In the cell lysate transformation, we see a decrease in both regio- and enantioselectivity compared to the native enzyme, which again is small and not necessarily indicative of a mutation-related change.

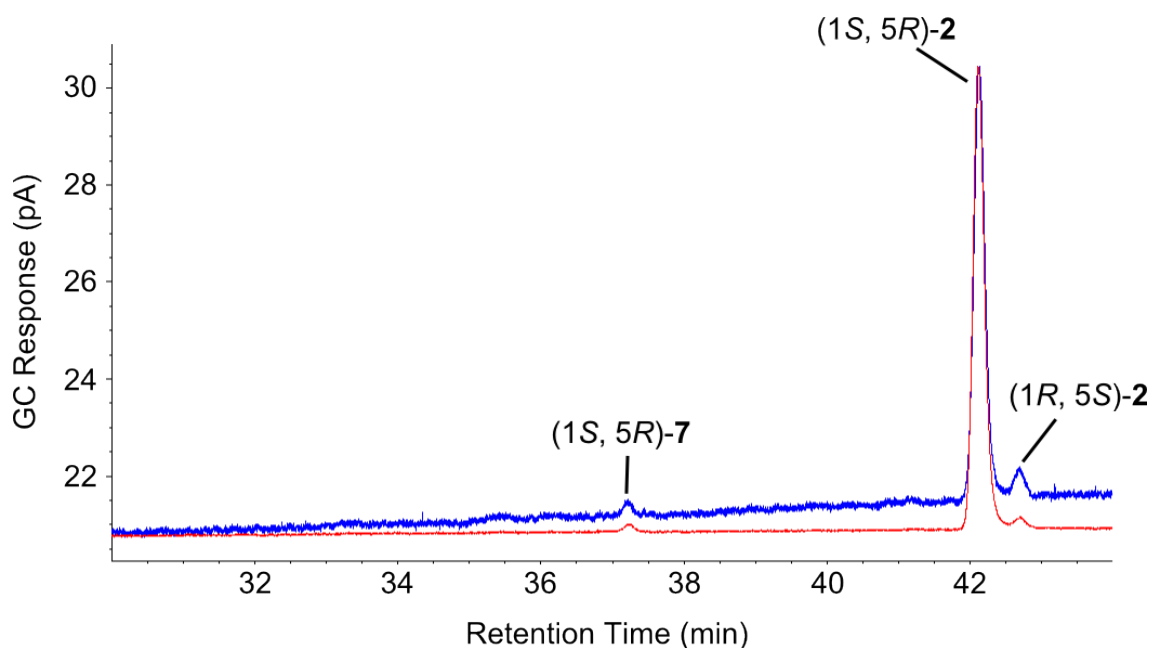


Figure 6.8: GC traces for products of the transformation of bicyclo[3.2.0]hept-2-en-6-one by *E. coli* Rosetta<sup>TM</sup>2 (DE3) pLysS cells expressing native MO14 (blue) and the MO14-P441V mutant (red).

The reciprocal change in MO15, from a valine to a proline, would therefore be expected to show a similarly negligible change in regioselectivity, however the actual observation is a marked increase in regiomer excess in both the whole cell transformation and the cell lysate transformation. The difference between the whole cell transformation and the cell lysate transformation is minimal, and

this is a clear sign that the alteration of this residue is linked to the regioselectivity of MO15, although the lack of change in MO14 is curious, a doubling of regiomer excess is a very significant result.

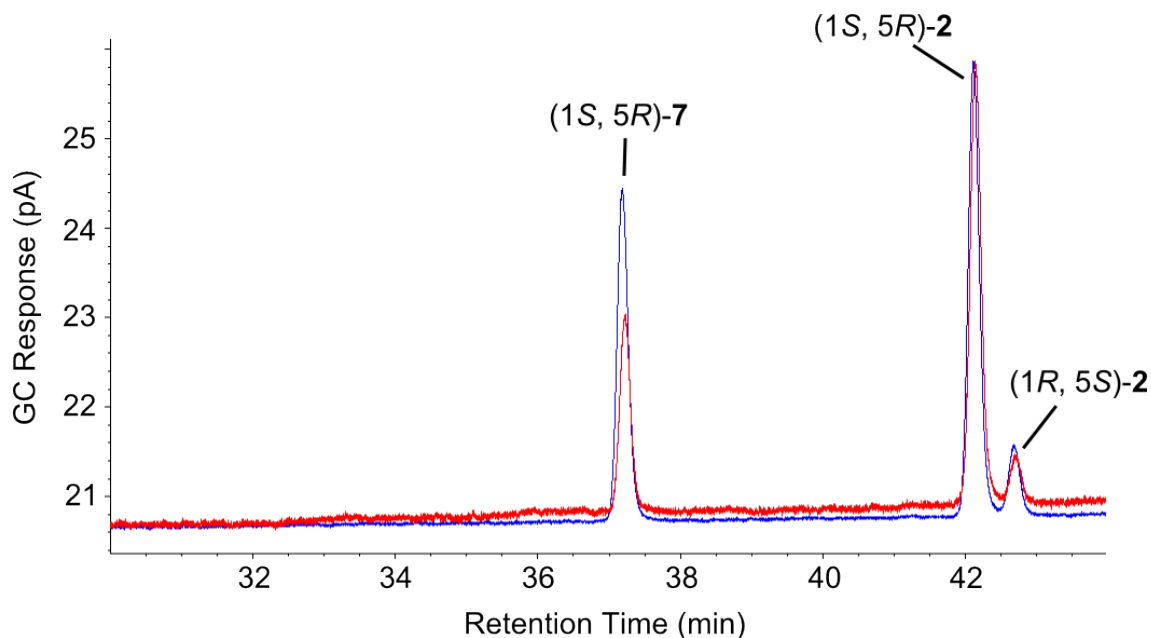


Figure 6.9: GC traces for products of the transformation of bicyclo[3.2.0]hept-2-en-6-one by *E. coli* Rosetta<sup>TM</sup>2 (DE3) pLysS cells expressing native MO15 (blue) and the MO15-V447P mutant (red).

### 6.3.3 MO14 I60V and MO15 V67I

The second differing residue in the projected active site for MO14 and MO15 is the isoleucine residue in position 60 for MO14. Based on the lack of alteration observed in MO14 from the first mutant assessed, it was anticipated that this residue would show a large difference in the regiomer excess, as it represents the only other residue that differentiates these two enzymes. It appears, however, that the mutation from isoleucine to valine has no observable effect on the regioselectivity of MO14 in either whole cell biotransformations or in cell lysate transformations. This would seem to indicate that the change in selectivity comes about either by means of the combined mutations working collaboratively or another mechanism more complicated than simply the effects of amino acid residues near the suggested active site.

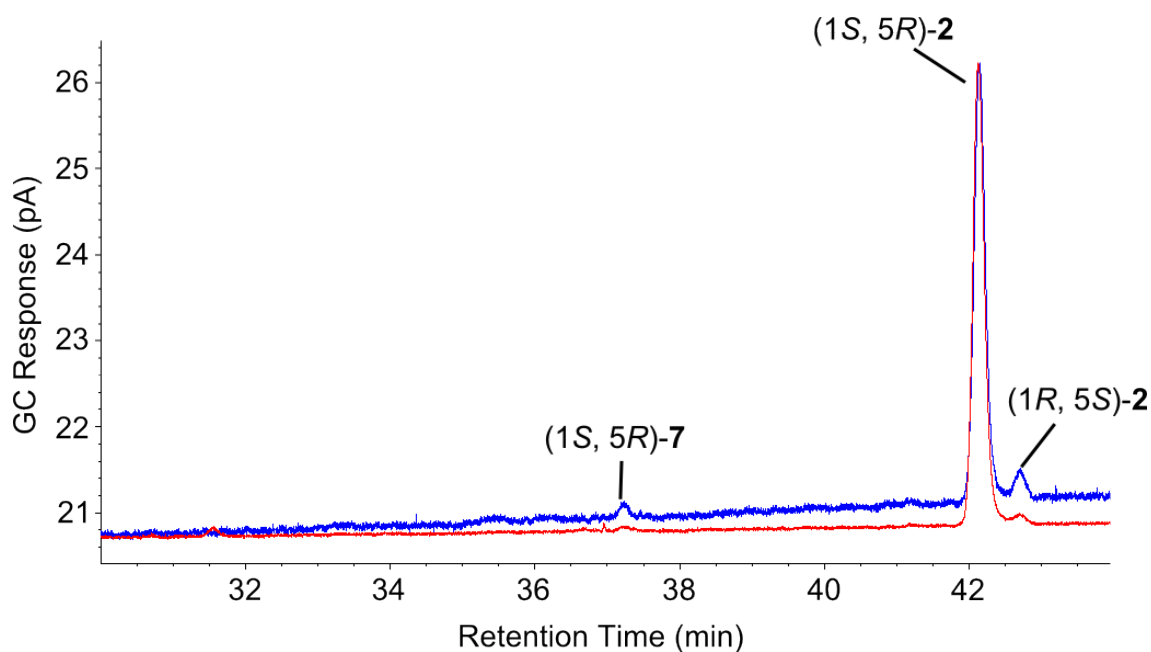


Figure 6.10: GC traces for products of the transformation of bicyclo[3.2.0]hept-2-en-6-one by *E. coli* Rosetta<sup>TM</sup>2 (DE3) pLysS cells expressing native MO14 (blue) and the MO14-I60V mutant (red).

In MO15, the reciprocal mutant again shows an increase in regio- and enantioselectivity. Both whole cell and cell lysate biotransformations show an increase in regiomer excess of approximately 10 %, which again is in contrast to the MO14 result. This increase is more minor than the result for the V447P mutation, however this again represents a significant increase in selectivity and suggests that, although the overall excellent regioselectivity observed for MO14 cannot be easily deleted by means of mutations, it is possible to induce a greater degree of regioselectivity by making these simple alterations to MO15. The suggestion therefore is that the regioselectivity of MO14 arises from a combination of relevant amino acid residues and the overall fold of the enzyme and that MO15 maintains a similar enough fold to MO14 to benefit from the mutation of the differing residues without being close enough in shape that the regioselectivity can be elevated to MO14-like levels.

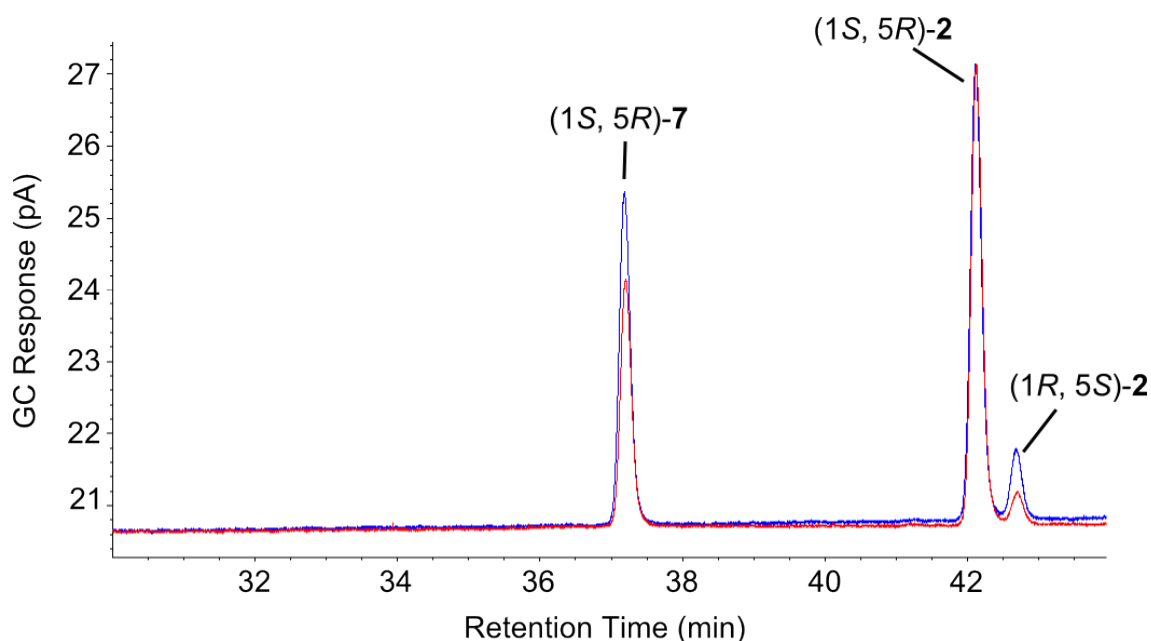


Figure 6.11: GC traces for products of the transformation of bicyclo[3.2.0]hept-2-en-6-one by *E. coli* Rosetta<sup>TM</sup>2 (DE3) pLysS cells expressing native MO15 (blue) and the MO15-V67I mutant (red).

### 6.3.4 Double Mutants

In order to fully confirm that the excellent selectivity of MO14 arises from more than simple residues differences the double mutant was generated, which should result in the region within 9 Å of the bound FAD being identical in environment to the same region in MO15. We again observe no deviance from the native protein in regioselectivity for either transformation, however there is a loss of enantioselectivity observed in the cell lysate biotransformation. Although the GC signals observed for both enantiomers of the 2-oxa lactone are very low, which may cause the actual results to be more minor than the % e.e. would suggest due to potential errors, the possibility that mutating these two residues results in a loss of enantioselectivity is interesting and might suggest that the regio- and enantioselectivity of these enzymes are linked.



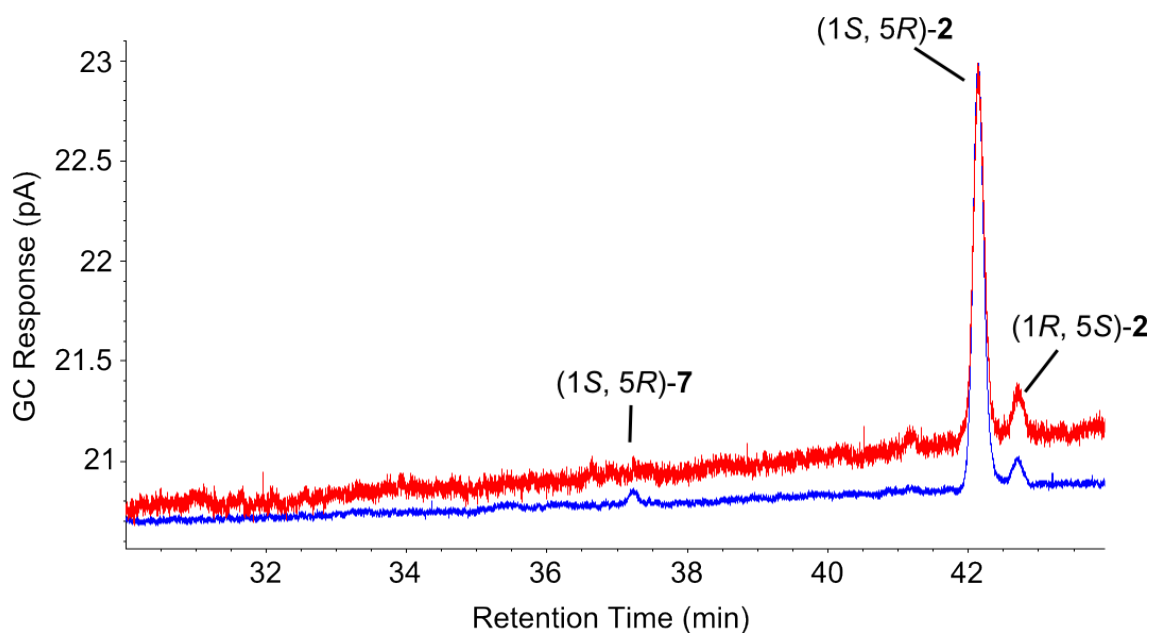


Figure 6.12: GC traces for products of the transformation of bicyclo[3.2.0]hept-2-en-6-one by *E. coli* Rosetta<sup>TM</sup>2 (DE3) pLysS cells expressing native MO14 (blue) and the MO14-P441V-I60V double mutant (red).

MO15 shows an additive effect between the two mutations, resulting in a regiomer excess of approximately 25 %, indicating that these two mutations can act in parallel to increase the selectivity of this enzyme. It is interesting that the regioselectivity is not absolute, as the active site should now be identical to that of MO14, however this would seem to confirm the theory that the selectivity originates from a more diverse combination of effects than simply the relevant amino acid residues. Also observed is again an increase in enantioselectivity, with the whole cell biotransformation reaching an enantiomeric excess equal to MO14, which lends credence to the suggestion that these residues are responsible for mediating enantio- as well as regioselectivity.

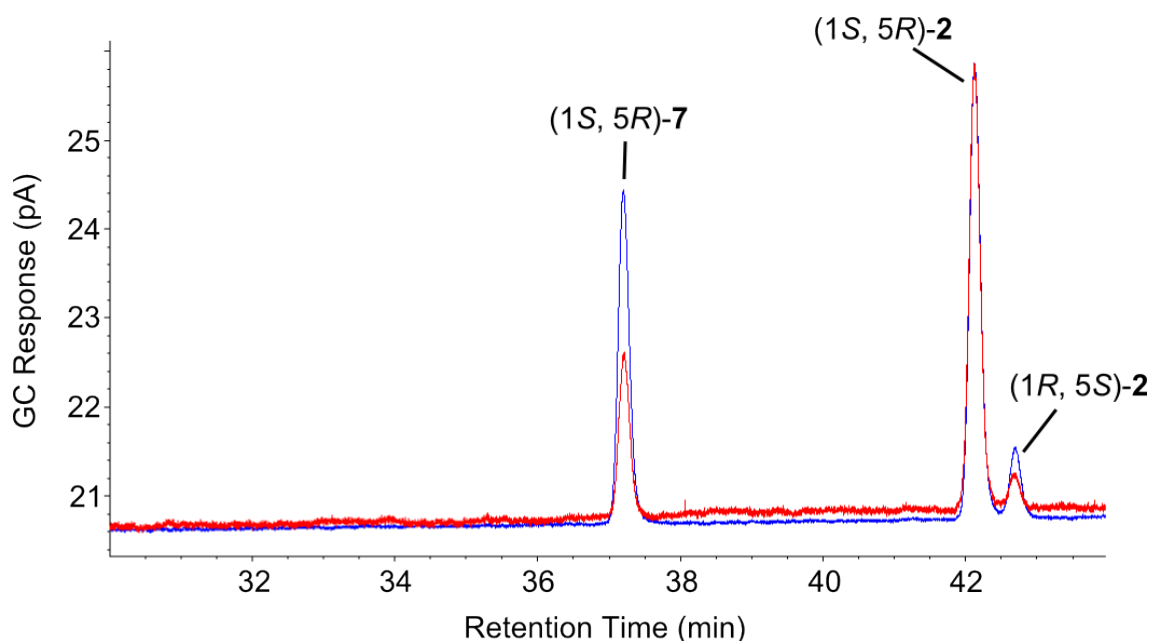


Figure 6.13: GC traces for products of the transformation of bicyclo[3.2.0]hept-2-en-6-one by *E. coli* Rosetta<sup>TM</sup>2 (DE3) pLysS cells expressing native MO15 (blue) and the MO15-V447P-V67I double mutant (red).

## 6.4 Conclusions

The results are somewhat surprising, as the overall similarity between the active sites of MO14 and MO15 would seem to indicate that the difference in regioselectivities observed between the two enzymes may be mediated by these two amino acid residues. This work instead reveals that, although some level of control over the regioselectivity derives from this area, there is a significant lack regioselectivity that persists in the mutated MO15 enzyme. The area that is being targeted has previously been investigated by means of targeted mutagenesis<sup>159</sup> and both mutations examined here have previously been studied in PAMO.<sup>160</sup> In that case, it was observed that the mutation of I67 to threonine or S441 to alanine led to a drop in regioselectivity from the initially observed ratio of 3:1 2-oxa:3:oxa lactone to a roughly 1:1 ratio. Since S441, or its equivalent, is present in both MO14 and MO15 we can draw the conclusion that regioselectivity in BVMOs can arise from a variety of amino acid residues and positions and the failure to generate a regioselective MO15 mutant reinforces this theory. It also appears that the mutated residues are in some way linked

to the enantioselectivity of the enzyme, as the enantiomeric excess in the product of the MO15 biotransformation showed an increase of 20+ %, reaching an excellent level of selectivity. Finally, this work demonstrates that a more in-depth approach is needed for the further characterisation and modelling of active sites in these enzymes, as this will allow for more targeted mutations of BVMOs to suit the desired functionality.

# Chapter 7

## Conclusions

### 7.1 Conclusions

The expression of MO14 was tested in a number of strains based upon the *E. coli* organism and the soluble expression levels assessed for the selection of an ideal strain. The greatest generation of soluble MO14 occurred when the strain *E. coli* Rosetta<sup>TM</sup>2 (DE3) pLysS was used.

Attempts were made to purify MO14 by means of IMAC, using the N-terminal histidine tag present in the YSBLIC-3C plasmid. These efforts proved unsuccessful, hence a C-terminally tagged construct was produced, as the N-terminus is potentially buried, preventing access to the binding site. This, too, proved unsuccessful, leading to the use of other techniques.

A variety of column-based purifications were tested, including ion exchange chromatography, sepharose blue affinity chromatography and hydrophobic interaction chromatography, all meeting with little success. Ammonium sulfate precipitation was also examined as a pre-purification step to remove a large amount of impurity present in the cell lysate. There is evidence that application to a column induces the proteolysis of MO14, and a degradation experiment over 24 hours seems to indicate that this is correct.

A column-free purification of MO14 by means of protein fusion with a 17-fold repeat of a calcium-binding domain led to the generation of a mostly impurity-free sample of protein, however this appears to result in significant protein degradation. This degradation may, however, be of the tag rather than MO14, hence cleavage of the tag may result in pure MO14.

A codon-optimised version of this gene was designed and produced for comparative expression and purification alongside the native gene sequence and the best expression strain also selected for this genetic sequence. Following this, a range of purification constructs were generated for MO14 and the expressions of these constructs tested in two strains of *E. coli*. The best expressing construct was used in a purification attempt by means of glutathione affinity chromatography, however this resulted in poor binding to the column.

*E. coli* Rosetta<sup>TM</sup>2 (DE3) pLysS cells were transformed by plasmids containing a selection BVMO enzymes from *R. jostii* sp. RHA1, as well as CHMO<sub>Acineto</sub> and experiments conducted to assess their activity towards 1-indanone and  $\alpha$ -tetralone, which are industrially relevant substrates. Poor activity was observed for these transformations and therefore further biotransformational investigations were continued with *E. coli* Rosetta<sup>TM</sup>2 (DE3) pLysS cells expressing the enzyme MO14, which had been shown to perform the transformation of bicyclo[3.2.0]hept-2-en-6-one with excellent regio- and enantio-selectivity.

This transformation was studied for potential indicators as to optimal conditions on the 1 mL culture scale, including work towards the optimisation of cell density, substrate concentration and two additives;  $\beta$ -cyclodextrin and glucose. These experiments revealed that the two additives had a deleterious effect on the transformation; cell density optimum was an OD<sub>600</sub> of approximately 70; and substrate concentration optimum was approximately 10 mM. These data were used to inform larger scale experiments conducted later in the project.

The effect of various organic solvents on the this reaction were also studied, with generally negative results, however the use of heptane may be tolerated sufficiently to be used for more organically soluble substrates. Also interesting was the effect of DMSO on the reaction, which significantly increased yield as the expense of selectivity.

A broad selection of prochiral sulfide biotransformations were also investigated, with generally excellent enantioselectivities being observed and the possibility of MO14 to be considered one of the most *S*-selective biocatalysts for sulfoxidation processes. The sulfide biotransformations also provide an insight into the structure of the MO14 active site, with the effects of specific functional groups on the activity towards thioanisole derivatives having significant effects on the conversion and enantioselectivity.

A number of fermentation reactions were conducted in an effort to optimise the enantioselective production of the (1*S*, 5*R*)-2-oxa lactone product from the Baeyer-Villiger oxidation of racemic bicyclo[3.2.0]hept-2-en-6-one. The variables investigated were temperature, substrate concentration, codon-optimisation/bacterial strain and delayed addition of substrate.

The fermentation reaction reaches the highest % conversion yield at 16°C and a substrate concentration of 0.5 g L<sup>-1</sup>, however a higher overall amount of product can be generated by the use of 1.0 g L<sup>-1</sup> substrate. The use of a codon-optimised gene in a non-optimised bacterial strain does not show an improvement over the native protein in *E. coli* Rosetta<sup>TM</sup>2 (DE3) pLysS and delayed substrate addition also shows no improvement over simultaneous addition of IPTG and substrate.

The volatility of the ketone substrate poses an issue to these experiments as it makes the progress of the reaction difficult to track accurately and the measurements taken to be pessimistic with regard to potential overall conversion of the ketone. Previous work in this area mostly relies on a

substrate feeding process to overcome this issue, as well as the toxicity of the substrate to the host organism.

Mutants of MO14 and MO15 were generated to investigate the origin of the exception selectivity demonstrated by MO14. MO14 and MO15 differ by only two residues in the active site, when modelled to a structure of PAMO. The results are somewhat surprising as, although some level of control over the regioselectivity derives from the two amino acids, there is a significant lack of regioselectivity that persists in the mutated MO15 enzyme.

Previously investigations of this area of PAMO observed that the mutation of these residues led to a drop in regioselectivity from the initially observed ratio of 3:1 2-oxa:3-oxa lactone to a roughly 1:1 ratio. We can draw the conclusion that regioselectivity in BVMOs can arise from a variety of amino acid residues and positions and the failure to generate a regioselective MO15 mutant reinforces this theory. It also appears that the mutated residues are in some way linked to the enantioselectivity of the enzyme, as the enantiomeric excess in the product of the MO15 biotransformation showed an increase of 20+

## **7.2 Further Work**

The purification of MO14 is expected to be achieved by means of the column-free purification attempted, combined with a protease inhibitor. It is anticipated that this purification, following cleavage of the calcium-binding tag, would result in the generation of pure MO14, suitable for crystallisation studies. Failing this outcome, a number of the generated constructs remain unexpressed solubly and may represent potential targets for purification. Finally, a combination of purification methods may present a successful route to purification, however the time pressure of MO14 degradation may affect this pathway.

A broader study of the sulfide activity of MO14 would provide both more potential industrial targets and a greater understanding of the active site by examination of more varied thioanisole derivatives. These efforts could particularly focus on the synthesis of esomeprazole, which represents a potentially very valuable synthetic route in industrial chemistry. A similar study of a broad range of ketones could also be of use, as these would allow a facile comparison to the activities of other BVMOs and could confirm the status of MO14 as perhaps the most *S*-selective enzyme for ketone and sulfide oxidations.

Continued study of the fermentation of MO14 could result in more fine-tuned optimisation of reaction conditions. Additionally, the investigation of a substrate feeding and product removal system is of worth due to both the inhibitory effects of substrate and product and the issues observed with evaporation of substrate. The scale of the reaction could also be increased to more closely resemble the scale of industrial processes.

Finally, the further mutation of MO14 could be conducted in a similar manner to that conducted for CHMO<sub>Rhod</sub> to improve the physical characteristics of the enzyme. Alternatively, a wider range of mutants could be conducted, assessing the impact of all amino acids near the FAD and NADPH cofactors, rather than only those near the suspected active site. This wider examination may reveal other amino acids that affect the selectivity observed for this enzyme. Following the determination of a structure of MO14, the selection of amino acid targets for mutation would be much simpler and may permit the designed alteration of MO14 activity.



## Appendix

### Native MO14 Sequence

ATGTCAAAGACCATTTCTGCCGACGTCGACGTCGTCGTCGTCGGGTGCCGG  
ATTCGCCGGCCTCTACGCCCTGCGCAAGCTGCGCGACACGATGAAGCTGT  
CGACACGGGTGTTTGAAGCCGGCTCGGAGGTCGGCGGCACCTGGTTCTGG  
AATCGCTATCCGGGTGCCCGCTGCGACATCGAGAGCGTCCACTATTCTGA  
CTCGTTCGACGAGGATCTGCAGCAGGAATGGCAGTGGAGTGAGCGGTTCG  
CCGGACAGCCGGAGATCCTCCGCTACCTCGAACACGTCGCCGACCGCTTC  
GACCTGCGCAAAGACATCACGTTGACACCCGCGTGGTCGGCGTGCACTG  
GGACGACGAGAAGTTCGGTGTGGACGGTCCGCACCGACGACGGCGCCGTCG  
TGCGCAGCCGGTACTTCATCTCGGGGGCAGGCAACCTGTCGGTGCCGAAG  
ACGCCGGAGTTCGGCGGTATCGACAAGTTCGCGGGCGAGGTGCTGCTCAC  
CGGCAACTGGCCACGTGAGGGCGCCGACTTCACCGGCAAGAGGGTGGCCG  
TGATCGGGACCGGGGCCAGCGGCATCCAGGCCATCCCGTTCATCGCCGAG  
GACGCCGCCGAAGTGGTGGTCTTCCAGCGCACCCCCAACTTCGCGACCCC  
TCTCGGCAACGGTCCGATGGACCCGAACGAATTGGCGGACATCAAGAGCA  
ACTATGCGGACGTGCGGACCGCGGCCCGCAACCACTTCTCGGCGTCCCG  
TTCAATCAGGTGCAGCCGTCCGCGCTCGCCGTCGACGCCGAGGAGCGCCG  
CCGCACGTTTCGACGAGCGCTGGAACGCCGGCGGGTTCCGGTTGTTTCATCG  
ACTCCTACCAGGACATCCTGTTTCGACAAGAAGGCCAACGACACGATCGCC  
GACTACATCCGCGACCGGATCCACGAGCGGGTGCAGGACCCGGCGAAGGC  
CGCGACGCTGGCGCCGACGGGCTACGCGTACGGCACCAAGCGTCCCCCGC  
TCGAGACCAACTACTACGAGGCGTTCAACCGCGACTCGGTGAGTGTCGTC  
GACGTGAAGTCCACGCCGATCGACGAGATCACGCCGACCGGAGTCCGGGT  
CGGTGACCGCGTCTACGAGGTCGACACCATCGTCCTCGCAACCGGATTCG  
ACGCGATGACCGGTCCGTTGATGGCCATGGACATCCGCGGTTCGGGGCGGT

TTGCCGTTGGCCGAGAAGTGGGAGCACGGACCCAGGACCTACCTCGGCAT  
CATGGTCAACGAGTTCCCCAACCTGTTCCCTCATCACGGGACCGCAGTCGC  
CGTCGGTGCTCTACAACATGCCACTCGCCATCGAGGACCACGTCTGACTTC  
GCGACCGACGCGATCGACTACCTGGACCGACGCGACCTCGACGTCATCGA  
GCCCACCGCGCAGGCCGAAAGCGATTGGGGTGCCTTGACCAACGAGATCG  
CCGACCAGACCCTGCTGCCGGAGACGAACTCGTGGTACATGGGCGCGAAC  
ATTCCCGGCAAGCCTCGTGCCTGCATGGTCTACCTCGGCGGCGCCCCAC  
CTACCGGGCGACGTGCGACGAGGTAGTGGCAGGCGGCTACTCCGGTTTCG  
CGCTACCCGGGCGGAGGCCCGCGCGGCCTCCACCGTGTCTGA

**Codon-Optimised MO14 Sequence**

ATGAGCAAACCATTAGCGCAGATGTTGATGTTGTTGTGGTTGGTGCAGG  
TTTTGCAGGTCTGTATGCACTGCGTAAACTGCGTGATACCATGAAACTGA  
GCACCCGTGTTTTTTGAAGCAGGTAGCGAAGTTGGTGGCACCTGGTTTTGG  
AATCGTTATCCGGGTGCACGTTGTGATATTGAAAGCGTTCATTATAGCTA  
CAGCTTCGATGAAGATCTGCAGCAAGAATGGCAGTGGTCAGAACGTTTTG  
CCGGTCAGCCGGAAATTCTGCGTTATCTGGAACATGTTGCCGATCGTTTT  
GATCTGCGTAAAGATATTACCTTTGATACCCGTGTTGTTGGTGTTCATTG  
GGATGATGAAAATAGCGTTTGGACCGTTCGTACCGATGATGGTGCAGTTG  
TTCGTAGCCGTTATTTTCATTAGCGGTGCAGGTAATCTGAGCGTTCCGAAA  
ACACCGGAATTTGGTGGTATTGATAATTTTCGTGGTGAAGTTCTGCTGAC  
CGGTAATTGGCCTCGTGAAGGTGCAGATTTACCCGGTAAACGTGTTGCAG  
TTATTGGTACAGGTGCAAGCGGTATTCAGGCAATCCGTTTATTGCAGAA  
GATGCAGCCGAACTGGTTGTTTTTCAGCGTACCCCGAATTTTGCAACACC  
GCTGGGTAATGGTCCGATGGATCCGAATGAACTGGCAGATATCAAAAGCA  
ATTATGCCGATGTGCGTACCGCAGCACGTAATCATTTTTCTGGGTGTTCCG  
TTAATCAGGTTTCAGCCGAGCGCACTGGCAGTTGATGCAGAAGAACGTCG

TCGCACCTTTGATGAACGTTGGAATGCCGGTGGTTTTTCGTCTGTTTATTG  
ATAGCTACCAGGACATCCTGTTTCGACAAAAAGCAAATGATACCATTGCC  
GATTATATCCGCGATCGTATTCATGAACGTGTTTCAGGATCCGGCAAAGC  
AGCAACCCTGGCACCGACCGGTTATGCATATGGCACCAAACGTCCGCCTC  
TGGAACCAACTATTATGAAGCATTTAATCGTGATAGCGTGAGCGTTGTT  
GATGTGAAAAGCACCCCGATTGATGAAATTACCCCGACCGGTGTTTCGTGT  
TGGTGATCGTGTTTATGAAGTGGATAACAATTGTTCTGGCAACCGGTTTTG  
ATGCAATGACCGGTCCGCTGATGGCAATGGATATTCGTGGTCGTGGTGGT  
CTGCCGCTGGCAGAAAAATGGGAACATGGTCCGCGTACCTATCTGGGTAT  
TATGGTTAATGAATTTCCGAACCTGTTTCTGATTACAGGTCCGCAGAGCC  
CGAGCGTTCTGTATAATATGCCTCTGGCAATTGAAGATCATGTGGATTTT  
GCCACCGATGCCATTGATTATCTGGATCGTCGTGATCTGGATGTTATTGA  
ACCGACCGCACAGGCAGAAAGCGATTGGGGTGCACTGACCAATGAAATTG  
CAGATCAGACCCTGCTGCCGGAAACCAATAGCTGGTATATGGGTGCAAAT  
ATTCCGGGTAAACCGCGTGCATGTATGGTTTATCTGGGTGGTGCACCGAC  
CTATCGTGCAACCTGTGATGAAGTTGTTGCGGGTGGTTATAGCGGTTTTG  
CCCTGACCCGTGCCGAAGCACGTGCAGCAAGCACCGTTAGCTAA

# List of Abbreviations

<b>AEBSF:</b>	4-(2-Aminoethyl)benzenesulfonyl fluoride
<b>ADP:</b>	Adenosine diphosphate
<b>Ala:</b>	Alanine
<b>Arg:</b>	Arginine
<b>Asp:</b>	Aspartic acid
<b>Asn:</b>	Asparagine
<b>BVMO:</b>	Baeyer-Villiger monooxygenase
<b>C:</b>	Cysteine
<b>CHMO<sub>Acineto</sub>:</b>	Cyclohexanone monooxygenase from <i>Acinetobacter calcoaceticus</i> NCIMB 9871
<b>CHMO<sub>Rhod</sub>:</b>	Cyclohexanone monooxygenase from <i>Rhodococcus</i> sp. HI-31
<b>COMO14:</b>	Codon-optimised MO14
<b>CPMO:</b>	Cyclopentanone monooxygenase from <i>Pseudomonas</i> NCIB 9872
<b>Cys:</b>	Cysteine
<b>D:</b>	Aspartic acid
<b>DMSO:</b>	Dimethylsulfoxide
<b>EDTA:</b>	Ethylenediaminetetraacetic acid
<b>EGTA:</b>	Ethylene glycol tetraacetic acid
<b><i>E. coli</i>:</b>	<i>Escherichia coli</i>
<b>F:</b>	Phenylalanine
<b>DNA:</b>	Deoxyribonucleic acid
<b>FAD:</b>	Flavin adenine dinucleotide
<b>FPLC:</b>	Fast protein liquid chromatography
<b>FMN:</b>	Flavin mononucleotide
<b>FMO:</b>	Flavin-containing monooxygenase
<b>GC:</b>	Gas chromatography
<b>GFP:</b>	Green fluorescent protein
<b>Gln:</b>	Glutamine
<b>Gly:</b>	Glycine
<b>GST:</b>	Glutathione-S-transferase
<b>HAPMO:</b>	4-hydroxyacetophenone monooxygenase from <i>Pseudomonas fluorescens</i> ACB
<b>His:</b>	Histidine

<b>I:</b>	Isoleucine
<b>Ile:</b>	Isoleucine
<b>IMAC:</b>	Immobilised metal affinity chromatography
<b>IPTG:</b>	Isopropyl- $\beta$ -D-1-thiogalactopyranoside
<b>LB:</b>	Luria-Bertani
<b>LC-MS:</b>	Liquid chromatography mass spectrometry
<b>Leu:</b>	Leucine
<b>MBP:</b>	Maltose binding protein
<b>mCPBA:</b>	meta-Chloroperbenzoic acid
<b>Met:</b>	Methionine
<b>N:</b>	Asparagine
<b>NADP<sup>+</sup>:</b>	Nicotinamide adenine dinucleotide phosphate, positively charged
<b>NAD(P)H:</b>	Nicotinamide adenine dinucleotide (phosphate)
<b>NMO:</b>	N-hydroxylating monooxygenase
<b>OD<sub>600</sub>:</b>	Optical density at a wavelength of 600 nm
<b>P:</b>	Proline
<b>PAMO:</b>	Phenylacetone monooxygenase from <i>Thermobifida fusca</i>
<b>PBA:</b>	Perbenzoic acid
<b>PCR:</b>	Polymerase chain reaction
<b>Phe:</b>	Phenylalanine
<b>Q:</b>	Glutamine
<b>R:</b>	Arginine
<b><i>R. jostii</i>:</b>	<i>Rhodococcus jostii</i>
<b>RNA:</b>	Ribonucleic acid
<b>SDS-PAGE:</b>	Sodium dodecyl sulfate - Polyacrylamide gel electrophoresis
<b>Ser:</b>	Serine
<b>TAE:</b>	Tris acetate EDTA
<b><i>t</i>-Bu:</b>	<i>tert</i> -butyl
<b>TEMED:</b>	Tetramethylethylenediamine
<b>Tris:</b>	Tris(hydroxymethyl)aminomethane
<b>tRNA:</b>	Transfer ribonucleic acid
<b>Tyr:</b>	Tyrosine
<b>UV:</b>	Ultraviolet
<b>V:</b>	Valine
<b>Val:</b>	Valine
<b>W:</b>	Tryptophan
<b>Y:</b>	Tyrosine

# Bibliography

- [1] A. von Baeyer, V. Villiger, *Ber. Dtsch. Chem. Ges.* **1899**, 32, 3625–3633.
- [2] H. Caro, *Angew. Chem.* **1898**, 11, 845–846.
- [3] A. von Baeyer, V. Villiger, *Ber. Dtsch. Chem. Ges.* **1900**, 33, 124–126.
- [4] A. Werner, A. Piguet, *Ber. Dtsch. Chem. Ges.* **1904**, 37, 4295–4315.
- [5] G. Wittig, G. Pieper, *Ber. Dtsch. Chem. Ges.* **1940**, 73, 295–297.
- [6] R. Criegee, *Liebigs Ann. Chem.* **1949**, 565, 7–21.
- [7] R. Criegee, *Justus Liebigs Ann. Chem.* **1948**, 560, 127–135.
- [8] W. Doering, E. Dorfman, *J. Am. Chem. Soc.* **1953**, 75, 5595–5598.
- [9] W. Doering, L. Speers, *J. Am. Chem. Soc.* **1950**, 72, 5515–5518.
- [10] P. Deslongchamps, *Stereoelectronic Effects in Organic Chemistry*, Pergamon Press, Oxford, **1983**, p. 313.
- [11] R. Noyori, T. Sato, H. Kobayashi, *Tetrahedron Lett.* **1980**, 21, 2569–2572.
- [12] C. M. Crudden, A. C. Chen, L. A. Calhoun, *Angew. Chem. Int. Ed.* **2000**, 39, 2851–2855.
- [13] R. B. Turner, *J. Am. Chem. Soc.* **1950**, 72, 878–882.
- [14] T. F. Gallagher, T. H. Kritchevsky, *J. Am. Chem. Soc.* **1950**, 72, 882–885.

- [15] K. Mislow, J. Brenner, *J. Am. Chem. Soc.* **1953**, *75*, 2318–2322.
- [16] J. A. Berson, S. Suzuki, *J. Am. Chem. Soc.* **1959**, *81*, 4088–4094.
- [17] J. D. Rozzell Jr., S. A. Benner, *J. Org. Chem.* **1983**, *48*, 1190–1193.
- [18] M. F. Hawthorne, W. D. Emmons, K. S. McCallum, *J. Am. Chem. Soc.* **1958**, *80*, 6393–6398.
- [19] S. L. Friess, A. H. Soloway, *J. Am. Chem. Soc.* **1951**, *73*, 3968–3972.
- [20] M. F. Hawthorne, W. D. Emmons, *J. Am. Chem. Soc.* **1958**, *80*, 6398–6404.
- [21] T. Mitsunashi, H. Miyadera, O. Simamura, *J. Chem. Soc. Chem. Commun.* **1970**, 1301–1302.
- [22] B. W. Palmer, A. Fry, *J. Am. Chem. Soc.* **1970**, *92*, 2580–2581.
- [23] M. Renz, B. Meunier, *Eur. J. Org. Chem.* **1999**, 737–750.
- [24] G. R. Krow, *Comprehensive Organic Synthesis*, Pergamon Press, Oxford, **1991**, pp. 671–688.
- [25] J. K. Whitesell, R. S. Matthews, A. M. Helbling, *J. Org. Chem.* **1978**, *43*, 784–786.
- [26] J. F. Goodman, P. Robson, E. R. Wilson, *Trans. Faraday Soc.* **1962**, *58*, 1846–1851.
- [27] S. L. Friess, *J. Am. Chem. Soc.* **1949**, *71*, 2571–2575.
- [28] J. Boeseken, J. S. P. Blumberger, *Recl. Trav. Chim. Pay-B.* **1925**, *40*, 90–95.
- [29] A. Rassat, G. Ourisson, *Bull. Soc. Chim. Fr.* **1959**, 1133–1136.
- [30] W. F. Sager, A. Duckworth, *J. Am. Chem. Soc.* **1955**, *77*, 188–190.
- [31] S. L. Friess, N. Farnham, *J. Am. Chem. Soc.* **1950**, *72*, 5518–5521.
- [32] M. D. T. Frisone, F. Pinna, G. Strukul, *Organometallics* **1993**, *12*, 148–156.
- [33] K. Pignat, J. Vallotto, F. Pinna, G. Strukul, *Organometallics* **2000**, *19*, 5160–5167.

- [34] F. Velazquez, H. F. Olivo, *Org. Lett.* **2000**, *2*, 1931–1933.
- [35] R. Göttlich, K. Yamakoshi, H. Sasai, M. Shibasaki, *Synlett* **1997**, 971–973.
- [36] G.-J. ten Brink, I. W. C. E. Arends, R. A. Sheldon, *Chem. Rev.* **2004**, *104*, 4105–4123.
- [37] A. Berkessel, M. R. M. Andreae, H. Schmickler, J. Lex, *Angew. Chem. Int. Ed.* **2002**, *41*, 4481–4484.
- [38] M. J. Bogdanowicz, T. Ambelang, B. M. Trost, *Tetrahedron Lett.* **1973**, *12*, 923–926.
- [39] B. M. Trost, M. J. Bogdanowicz, *J. Am. Chem. Soc.* **1973**, 5311–5321.
- [40] G. Strukul, *Angew. Chem. Int. Ed.* **1998**, *37*, 1199–1209.
- [41] P. A. Grieco, G. F. Majetich, Y. Ohfuné, *J. Am. Chem. Soc.* **1982**, *104*, 4226–4233.
- [42] A. Corma, L. T. Nemeth, M. Renz, S. Valencia, *Nature* **2001**, *412*, 423–425.
- [43] T. Yamada, T. Takai, O. Rhode, T. Mukaiyama, *Chem. Lett.* **1991**, 1–4.
- [44] S.-I. Murahashi, *Angew. Chem. Int. Ed.* **1995**, *34*, 2443–2465.
- [45] C. Bolm, G. Schlinghoff, F. Bienewald, *J. Mol. Catal.* **1997**, *117*, 347–350.
- [46] C. Bolm, G. Schlinghoff, K. Weickhardt, *Angew. Chem. Int. Ed. Engl.* **1994**, *33*, 1848–1849.
- [47] T. Kanger, K. Kriis, A. Paju, T. Pehk, M. Lopp, *Tetrahedron: Asymmetry* **1998**, *9*, 4475–4482.
- [48] A. Gusso, C. Baccin, F. Pinna, G. Strukul, *Organometallics* **1994**, *13*, 3442–3451.
- [49] C. Paneghetti, R. Gavagnin, F. Pinna, G. Strukul, *Organometallics* **1999**, *18*, 5057–5065.
- [50] C. Bolm, O. Beckmann, *Chirality* **2000**, *12*, 523–525.
- [51] K. Mikami, M. N. Islam, M. Yamanaka, Y. Itoh, M. Shinoda, K. Kubo, *Tetrahedron Lett.* **2004**, *45*, 3681–3683.



- [52] T. Uchida, T. Katsuki, *Tetrahedron Lett.* **2001**, *41*, 6911–6914.
- [53] K. Ito, A. Ishii, T. Kuroda, T. Katsuki, *Synlett* **2003**, 643–646.
- [54] A. Yoshida, X. Hao, J. Nishikido, *J. Green Chem.* **2003**, *5*, 554–557.
- [55] C. Bolm, G. Schlinghoff, *J. Chem. Soc. Chem. Commun.* **1995**, *12*, 1247–1248.
- [56] S. Xu, Z. Wang, X. Zhang, X. Zhang, K. Ding, *Angew. Chem. Int. Ed.* **2008**, *47*, 2840–2843.
- [57] R. T. Aplin, R. P. K. Chan, T. G. Halsall, *J. Chem. Soc. (C)* **1969**, *17*, 2322–2327.
- [58] F. Kazmierczak, P. Helquist, *J. Org. Chem.* **1989**, *54*, 3988–3992.
- [59] R. Robinson, L. H. Smith, *J. Chem. Soc.* **1937**, 371–374.
- [60] P. D. Bartlett, C. H. Stauffer, *J. Am. Chem. Soc.* **1935**, *57*, 2580–2583.
- [61] Y. Tsuda, T. Tanno, A. Ukai, K. Isobe, *Tetrahedron Lett.* **1971**, *12*, 2009–2012.
- [62] G. B. Payne, C. W. Smith, *J. Org. Chem.* **1957**, *32*, 1680–1682.
- [63] G. E. Turfitt, *Biochem. J.* **1948**, *42*, 376–383.
- [64] A. I. Laskin, P. Grabowich, C. L. Meyers, J. Fried, *J. Med. Chem.* **1964**, *7*, 406–409.
- [65] J. Fried, R. W. Thoma, A. Klingsberg, *J. Am. Chem. Soc.* **1953**, *75*, 5768–5765.
- [66] D. H. Peterson, S. H. Eppstein, P. D. Meister, H. C. Murray, H. M. Leigh, A. Weingtraub, L. M. Reineke, *J. Am. Chem. Soc.* **1953**, *75*, 5768–5769.
- [67] G. S. Fonken, H. C. Murray, L. M. Reineke, *J. Am. Chem. Soc.* **1960**, *82*, 5507–5508.
- [68] K. Carlström, *Acta Chem. Scand.* **1973**, *27*, 1622–1628.
- [69] J. M. Urbanczyk, J. Soloducho, A. Zabza, G. Sodano, A. Grassi, *J. Basic Microbiol.* **1993**, *33*, 141–146.
- [70] M. J. van der Werf, A. M. Boot, *Microbiology* **2000**, *146*, 1129–1141.

- [71] C. A. Townsend, S. B. Christensen, S. G. Davis, *J. Am. Chem. Soc.* **1982**, *104*, 6154–6155.
- [72] J. L. C. Wright, T. Hu, J. L. McLachlan, J. Needham, J. A. Walter, *J. Am. Chem. Soc.* **1996**, *118*, 8757–8758.
- [73] S. Damtoft, H. Franzyk, S. R. Jensen, *Phytochemistry* **1995**, *40*, 773–784.
- [74] M. W. Fraaije, N. M. Kamerbeek, W. J. H. van Berkel, D. B. Janssen, *FEBS Lett.* **2002**, *518*, 43–47.
- [75] D. M. Ziegler, *Trends Pharmacol. Sci.* **1990**, *11*, 321–324.
- [76] M. Stehr, H. Diekmann, L. Smau, O. Seth, S. Ghisla, M. Singh, P. Macheroux, *Trends Biochem. Sci.* **1998**, *23*, 56–57.
- [77] S. F. Altschul, T. L. Madden, A. A. Schäffer, Z. Zhang, W. Miller, D. J. Lipman, *Nucleic Acids Res.* **1997**, *25*, 3389–3402.
- [78] N. A. Donoghue, D. B. Norris, P. W. Trudgill, *Eur. J. Biochem.* **1976**, *63*, 175–192.
- [79] D. Sheng, D. P. Ballou, V. Massey, *Biochemistry* **2001**, *40*, 11156–11167.
- [80] J. M. Schwab, *J. Am. Chem. Soc.* **1981**, *103*, 1876–1878.
- [81] E. Malito, A. Alfieri, M. W. Fraaije, A. Mattevi, *Proc. Natl. Acad. Sci. USA* **2004**, *101*, 13157–13162.
- [82] I. A. Mirza, B. J. Yachnin, S. Wang, S. Grosse, H. Bergeron, A. Imura, H. Iwaki, Y. Hasegawa, P. C. K. Lau, A. M. Berghuis, *J. Am. Chem. Soc.* **2009**, *131*, 8848–8854.
- [83] N. A. Donoghue, P. W. Trudgill, *Eur. J. Biochem.* **1975**, *60*, 1–7.
- [84] D. R. Kelly, C. J. Knowles, J. G. Mahdi, I. N. Taylor, M. A. Wright, *Tetrahedron: Asymmetry* **1996**, *7*, 365–368.
- [85] J. D. Stewart, K. W. Reed, C. A. Martinez, J. Zhu, G. Chen, M. M. Kayser, *J. Am. Chem. Soc.* **1998**, *120*, 3541–3548.

- [86] H. D. Simpson, V. Alphand, R. Furstoss, *J. Mol. Catal. B Enzym.* **2001**, *16*, 101–108.
- [87] M. J. Taschner, D. J. Black, *J. Am. Chem. Soc.* **1988**, *110*, 6892–6893.
- [88] I. Hilker, M. C. Gutierrez, R. Furstoss, J. Ward, R. Wohlgemuth, V. Alphand, *Nature Protocols* **2008**, *3*, 546–554.
- [89] J. D. Stewart, K. W. Reed, C. A. Martinez, J. Zhu, G. Chen, M. M. Kayser, *J. Org. Chem.* **1996**, *61*, 7652–7653.
- [90] M. M. Kayser, G. Chen, J. D. Stewart, *J. Org. Chem.* **1998**, *63*, 7103–7106.
- [91] N. M. Kamerbeek, A. J. J. Olsthoorn, M. W. Fraaije, D. B. Janssen, *Appl. Environ. Microbiol.* **2003**, *69*, 419–426.
- [92] D. Bonsor, S. F. Butz, J. Solomons, S. Grant, I. J. S. Fairlamb, M. J. Fogg, G. Grogan, *Org. Biomol. Chem.* **2006**, *4*, 1252–1260.
- [93] M. D. Mihovilovic, F. Rudroff, B. Groetzl, P. Kapitan, R. Snajdrova, J. Rydz, R. Mach, *Angew. Chem. Int. Ed.* **2005**, *44*, 3609–3613.
- [94] M. D. Mihovilovic, B. Muller, P. Stanetty, *Eur. J. Org. Chem.* **2002**, 3711–3730.
- [95] V. Alphand, R. Furstoss, *J. Org. Chem.* **1992**, *57*, 1306–1309.
- [96] M. W. Fraaije, J. Wu, D. P. H. M. Heuts, E. W. van Hellemond, J. H. Lutje Spelberg, D. B. Janssen, *Appl. Microbiol. Biotechnol.* **2005**, *66*, 393–400.
- [97] F. Secundo, S. Fialá, M. W. Fraaije, G. de Gonzalo, M. Meli, F. Zambianchi, G. Ottolina, *Biotechnol. Bioeng.* **2011**, *108*, 491–499.
- [98] S. Wu, J. P. Acevedo, M. T. Reetz, *Proc. Natl. Acad. Sci. USA* **2010**, *107*, 2775–2780.
- [99] F. Schulz, F. Leca, F. Hollmann, M. Reetz, *Beilstein J. Org. Chem.* **2005**, *1*, year.
- [100] D. J. Opperman, M. T. Reetz, *ChemBiochem* **2010**, *11*, 2589–2596.

- [101] P. Chaiyen, M. W. Fraaije, A. Mattevi, *Trends Biochem. Sci.* **2012**, *37*, 373–380.
- [102] J. R. Cherry, M. H. Lamsa, P. Scheider, J. Vind, A. Svendsen, A. Jones, P. A. H., *Nat. Biotechnol.* **1999**, *17*, 379–384.
- [103] S.-S. Ju, L.-L. Lin, H. R. Chien, W.-H. Hsu, *FEMS Microbiol. Lett.* **2000**, *186*, 215–219.
- [104] L. J. Perry, R. Wetzel, *Protein Eng.* **1987**, *1*, 101–105.
- [105] B. Morawski, S. Quan, F. H. Arnold, *Biotechnol. Bioeng.* **2001**, *76*, 99–107.
- [106] K. H. Oh, S. H. Nam, H. S. Kim, *Protein Eng.* **2002**, *15*, 689–695.
- [107] D. J. Bougioukou, S. Kille, A. Taglieber, M. T. Reetz, *Adv. Synth. Catal.* **2009**, *351*, 3287–3305.
- [108] T. W. Johannes, R. D. Woodyer, H. Zhao, *Biotechnol. Bioeng.* **2006**, *96*, 18–26.
- [109] N. Oberleitner, C. Peters, F. Rudroff, U. T. Bornscheuer, M. D. Mihovilovic, *J. Biotechnol.* **2014**, *in press*, year.
- [110] K. S. Atia, *Radiat. Phys. Chem.* **2004**, *73*, 91–99.
- [111] S. Staudt, U. T. Bornscheuer, U. Menyes, W. Hummel, H. Gröger, *Enzyme Microb. Technol.* **2013**, *53*, 288–292.
- [112] V. Alphand, A. Archelas, R. Furstoss, *Tetrahedron Lett.* **1989**, *30*, 3663–3664.
- [113] S. D. Doig, H. Simpson, V. Alphand, R. Furstoss, J. M. Woodley, *Enzyme Microb. Technol.* **2003**, *32*, 347–355.
- [114] C. V. F. Baldwin, R. Wohlgemuth, J. M. Woodley, *Org. Process Res. Dev.* **2008**, *12*, 660–665.
- [115] C. Szolkowy, L. Eltis, N. Bruce, G. Grogan, *ChemBioChem* **2009**, *10*, 1208.
- [116] C. Smith, *Nat. Methods* **2005**, *2*, 71–77.

- [117] E. Padan, C. Hunte, H. Reilander, *Membrane Protein Purification and Crystallization: A Practical Guide*, Academic Press, **2003**.
- [118] C. Szolkowy, PhD thesis, Department of Chemistry, University of York, **2009**.
- [119] V. Gaberc-Porekar, V. Menart, *J. Biochem. Biophys. Methods* **2001**, *49*, 335–360.
- [120] J. A. Bornhorst, J. J. Falke, *Methods Enzymol.* **2000**, *326*, 245–254.
- [121] L. A. Kelley, M. J. E. Sternberg, *Nature Protocols* **2009**, *4*, 363–371.
- [122] S. T. Thompson, K. H. Cass, E. Stellwagen, *Proc. Natl. Acad. Sci. USA* **1975**, *72*, 669–672.
- [123] O. Shur, K. Dooley, M. Blenner, M. Baltimore, S. Banta, *Biotechniques* **2013**, *54*, 197–206.
- [124] A. Rioz-Martinez, G. de Gonzalo, D. E. Torres Pazmiño, M. W. Fraaije, V. Gotor, *Eur. J. Org. Chem.* **2009**, *15*, 2526–2532.
- [125] Z. Zhao, H. Wang, Z. Wang, **2012**.
- [126] D. E. Torres Pazmiño, R. Snajdrova, D. V. Rial, M. D. Mihovilovic, M. W. Fraaije, *Adv. Synth. Catal.* **2007**, *349*, 1361–1368.
- [127] I. Hilker, C. Baldwin, V. Alphand, R. Furstoss, J. Woodley, R. Wohlgemuth, *Biotechnol. Bioeng.* **2006**, *93*, 1138–1144.
- [128] S. D. Doig, P. J. Avenell, P. A. Bird, P. Gallati, K. S. Lander, K. S. Lye, R. Wohlgemuth, J. M. Woodley, *Biotechnol. Prog.* **2002**, *18*, 1039–1046.
- [129] V. Alphand, G. Carrea, R. Wohlgemuth, R. Furstoss, J. M. Woodley, *Trends Biotechnol.* **2003**, *21*, 318–323.
- [130] I. Hilker, M. Gutiérrez, V. Alphand, R. Wohlgemuth, R. Furstoss, *Org. Lett.* **2004**, *6*, 1955–1958.
- [131] U. Sauer, F. Canonaco, S. Heri, A. Perrenoud, E. Fischer, *J. Biol. Chem.* **2004**, *279*, 6613–6619.

- [132] W.-H. Lee, M.-D. Kim, Y.-S. Jin, J.-H. Seo, *Appl. Microbiol. Biotechnol.* **2013**, *97*, 2761–2772.
- [133] F. Rudroff, V. Alpand, R. Furstoss, M. D. Mihovilovic, *Organic Process Research and Development* **2006**, *10*, 599–604.
- [134] P. Branchaud, C. T. Walsh, *J. Am. Chem. Soc.* **1985**, *107*, 2153–2161.
- [135] G. Ottolina, S. Bianchi, B. Belloni, G. Carrea, B. Danieli, *Tetrahedron Lett.* **1999**, *40*, 8483–8485.
- [136] S. Colonna, N. Gaggero, G. Carrea, G. Ottolina, P. Pasta, F. Zambianchi, *Tetrahedron Lett.* **2002**, *43*, 1797–1799.
- [137] G. Chen, M. M. Kayser, M. D. Mihovilovic, M. E. Mrstik, C. A. Martinez, J. D. Stewart, *New J. Chem.* **1999**, *23*, 827–832.
- [138] S. Colonna, N. Gaggero, G. Carrea, P. Pasta, *Chem. Commun.* **1998**, 415–416.
- [139] P. Pasta, G. Carrea, H. L. Holland, S. Dallavalle, *Tetrahedron: Asymmetry* **1995**, *6*, 933–936.
- [140] T. D. Owens, F. J. Hollander, A. G. Oliver, J. A. Ellman, *J. Am. Chem. Soc.* **2001**, *123*, 1539–1540.
- [141] P. Kvintovics, B. R. James, B. Heil, *J. Chem. Soc. Chem. Commun.* **1986**, *24*, 1810–1811.
- [142] I. Fernandez, N. Khiar, *Chem. Rev.* **2003**, *103*, 3651–3705.
- [143] J. E. Richter, P. J. Kahrilas, J. Johanson, P. Maton, J. R. Breiter, C. Hwang, V. Marino, B. Hamelin, J. G. Levine, E. S. Investigators, *Am. J. Gastroenterol.* **2001**, *96*, 656–665.
- [144] S. G. Bangalore, R. N. Kankan, S. L. Pathi, D. R. Rao, **2010**.
- [145] C. T. Walsh, Y.-C. J. Chen, *Angew. Chem. Int. Ed. Engl.* **1988**, *27*, 333–343.
- [146] C. C. Ryerson, D. P. Ballou, C. Walsh, *Biochemistry* **1982**, *21*, 2644–2655.

- [147] G. de Gonzalo, D. E. Torres Pazmiño, G. Ottolina, M. W. Fraaije, G. Carrea, *Tetrahedron: Asymmetry* **2005**, *16*, 3077–3083.
- [148] G. de Gonzalo, D. E. Torres Pazmiño, G. Ottolina, M. W. Fraaije, G. Carrea, *Tetrahedron: Asymmetry* **2006**, *17*, 130–135.
- [149] G. Carrea, B. Redigolo, S. Riva, S. Colonna, N. Gaggero, E. Battistel, D. Bianchi, *Tetrahedron: Asymmetry* **1992**, *3*, 1063–1068.
- [150] Various, *Asymmetric Catalysis on Industrial Scale: Challenges, Approaches and Solutions*, Wiley-VCH, **2011**.
- [151] I. Hilker, R. Wohlgemuth, V. Alphand, R. Furstoss, *Biotechnol. Bioeng.* **2005**, *92*, 702–710.
- [152] Z. Li, H. J. Feiten, D. Chang, W. A. Duetz, J. B. van Beilen, B. Witholt, *J. Org. Chem.* **2001**, *66*, 8424–8430.
- [153] C. M. Clouthier, M. M. Kayser, *J. Mol. Catal. B: Enzym.* **2007**, *46*, 32–36.
- [154] M. M. Kayser, C. M. Clouthier, *J. Org. Chem.* **2006**, *71*, 8424–8430.
- [155] S. Wang, M. M. Kayser, H. Iwaki, P. C. K. Lau, *J. Mol. Catal. B: Enzym.* **2003**, *22*, 211–218.
- [156] S. D. Doig, P. J. Avenell, P. A. Bird, P. Gallati, K. S. Lander, G. J. Lye, R. Wohlgemuth, J. M. Woodley, *Biotechnol. Bioeng.* **2006**, *18*, 1039–1046.
- [157] B. Müller-Hill, H. V. Rickenberg, K. Wallenfels, *Journal of Molecular Biology* **1964**, *10*, 303–318.
- [158] H. Venkataraman, S. B. Beer, L. A. Bergen, N. van Essen, D. P. Geerke, N. P. Vermeulen, J. N. Commandeur, *Chembiochem* **2012**, *13*, 520–523.
- [159] M. T. Reetz, S. Wu, *J. Am. Chem. Soc.* **2009**, *131*, 15424.
- [160] H. M. Dudek, G. de Gonzalo, D. E. Torres Pazmiño, S. P., L. S. Wyrwicz, L. Rychlewski, M. W. Fraaije, *Appl. Environ. Microbiol.* **2011**, *77*, 5730–5738.